



Norwegian University of
Science and Technology

Absorber for concentrating solar heat collectors

Trygve Stansberg Veslum

Master of Science in Product Design and Manufacturing

Submission date: July 2011

Supervisor: Ole Jørgen Nydal, EPT

Survey of absorbers for small scale concentrating solar systems

Department of Energy and Process Engineering
Norwegian University of Science and Technology

Master Thesis 2011

Trygve Stansberg Veslum



NTNU
**Norwegian University of
Science and Technology**

MASTEROPPGAVE

for

Student Trygve Veslum

Våren 2011

Absorbator for konsentrerende solvarme

Absorber for concentrating solar heat collectors

Bakgrunn

En målsetning med et løpende prosjekt på konsentrerende solfangere er å lagre varme ved høy temperatur (over 200 grader). I et samarbeidsprosjekt med 5 Afrikanske universitet undersøker vi flere konsept for innfangning, transport og lagring av varme. Det enkleste systemet er basert på oppvarming av luft i fokuspunktet, transport av den oppvarmede luften som deponerer varmen i et stein lager. Dette er ment å være en enkel teknisk løsning, som skulle være tilpasset produksjons- og bruksforholdene i Afrikanske omgivelser.

Det er en utfordring å lage en absorbator som gir en effektiv varmeovergang til luften. I en tidligere prosjektoppgave ble det utført forsøk med en absorbator der et varmeelement erstattet solstrålene. Det er mulig å gjøre for overflate absorbatorer, men ikke for volumetriske absorbatorer, som er den foretrukne løsningen for luftsystemer.

Det er viktig å utføre systematiske forsøk med forskjellige typer absorbatorer. EPT laboratoriene inkluderer en kunstig sol (en rekke lamper monterte på en bevegelig rampe). Denne kan utnyttes, evt. modifiseres til bruk for absorbatorstudier og for undersøkelser av kontrollmetoder for viften som skal drive luften til varmelageret.

Mål

Målsetningen er å komme fram til en absorbator som er enkel og robust og som gir en tilstrekkelig effektivitet for bruk i et småskala konsentrerende solenergi system med varmelager.

Oppgaven bearbeides ut fra følgende punkter

1. Utarbeiding av et testoppsett som kan brukes for sammenligning av forskjellige absorbatorer (kunstig sol, vifteløsning, temperaturmålinger)
2. Utforming og konstruksjon av absorbatorer
3. Forsøksarbeid for sammenligning av absorbatorer
4. Rapportering i MSc oppgave, med forslag til teknisk løsning for en prototyp solovn med varmelager

Belastningen på prosjektet utgjør 50% (11,25 studiepoeng dersom kandidaten har valgt 3 tema), eller 67 % (15 studiepoeng dersom kandidaten har valgt 2 tema) av fordypningsemnet.

En fremdriftsplan (*Planlagte aktiviteter med tidsplan for fremdrift*) for hele oppgaven skal forelegges faglærer/veileder(e) for kommentarer innen 14 dager etter utlevering av oppgaveteksten.

Besvarelsen redigeres mest mulig som en forskningsrapport med innholdsfortegnelse, et sammendrag på norsk, konklusjon, litteraturliste, etc. Ved utarbeidelsen av teksten skal kandidaten legge vekt på å gjøre teksten oversiktlig og velskrevet. Med henblikk på lesing av besvarelsen er det viktig at de nødvendige henvisninger for korresponderende steder i tekst, tabeller og figurer anføres på begge steder. Ved bedømmelsen legges det stor vekt på at resultatene er grundig bearbeidet, og at de oppstilles tabellarisk og/eller grafisk på en oversiktlig måte og diskuteres utførlig.

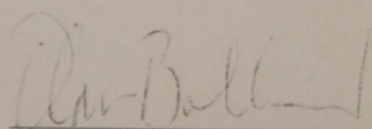
I henhold til "Utfyllende regler til studieforskriften for teknologistudiet/sivilingeniørstudiet" ved NTNU § 20, forbeholder instituttet seg retten til å benytte alle resultater i undervisnings- og forskningsformål, samt til publikasjoner.

Det forutsettes at kandidaten på eget initiativ etablerer et tilfredsstillende kontaktforhold med faglærer og veileder(e).

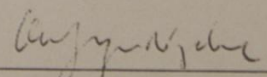
Sluttrapport for oppgaven skal leveres innbundet i 3 komplette eksemplarer med et "løsblad" med konsentrert sammendrag med forfatternavn og oppgavetittel for eventuell referering i tidsskrifter (maksimalt én maskinskrevet side med dobbel linjeavstand. Ytterligere kopier av rapporten til evt. medveileder(e)/kontaktpersoner skal avtales med, og evt. leveres direkte til, de respektive. Til faglærer/instituttet innleveres også en komplett kopi på CD-ROM i Word-format eller tilsvarende.

Sluttrapporten skal innleveres til Instituttet *innen 14. juni*.

Institutt for energi- og prosesseteknikk, 10 Januar 2010



Olav Bolland
Instituttleder



Ole Jørgen Nydal
Faglærer

Medveiledere/kontaktpersoner: Habtamu Bayera (PhD), Jørgen Løvseth (Emeritus)

Abstract

Open volumetric absorbers have been tested and evaluated with the objective to determine their ability to heat air for small scale concentrating solar systems, more exactly a solar oven where a stove is heated up by a rock bed storage provided with air above 220°C. The absorbers were tested in terms of different size, shape and material. Heating up air to the target temperature has been a challenge for years, but was achieved with good margin with an experimental setup based on the flaws of previous test setups.

At a concentration factor of 300 and a parabolic dish aperture area of 1.07 m², steady state air temperatures at 300°C were achieved with a stainless steel fiber mesh absorber and a silicon carbide honeycomb absorber which has been exposed for extensively testing in solar towers. The air temperatures were achieved at a flow rate of 1.96*10⁻³ kg/s, and as the flow rate was increased the air temperature decreased. At increased flow rate the absorber temperature was reduced and caused less radiation and convection loss which resulted in increased heat transfer between absorber and air. Efficiency defined as air energy increase through absorber divided by the normal direct solar irradiance ranges between 50 % and 80 %, where the efficiency peaked at the highest flow rate employed during the tests.

The greatest average air temperature measured was 350°C which was achieved by employment of the honeycomb absorber at a concentration factor of 600 and a mass flow of 1.5*10⁻³ kg/s.

Sammendrag

Volumetriske absorbatører har blitt testet og evaluert med sikte på å bestemme deres evne til å varme opp luft for småskala konsentrerende systemer, nærmere sagt en solovn, som er varmet opp ved hjelp av sola. Solovnen består av et steinlager som lagrer varme ved høye temperaturer der varmen kommer fra luft som er varmet opp til over 220 °C gjennom en porøs matte, nærmere bestemt en absorlator, som sitter i fokuspunktet til en reflekterende parabol.

Forskjellige absorbatører i form av ulike størrelser, geometrier og materialer har blitt testet og evaluert i denne rapporten. Å varme opp luft til ønsket temperatur har vært en utfordring i mange år, men målet om å nå 220 °C ble oppnådd med god margin i et eksperimentelt oppsett basert på manglene ved forrige generasjons testoppsett.

Ved en konsentrasjonsfaktor på 300 og et reflekterende solfangerareal på 1,07 m² ble stabile verdier på rundt 300 °C oppnådd med både en fiberabsorlator av stålull og en 4 cm tjukk absorlator av rekrystallisert silisiumkarbid. Sistnevnte materiale har tidligere blitt utsatt for grundig testing i høykonsentrerende soltårn for generering av elektrisk energi, og en kan derfor konkludere med at dette materialet egner seg for solovnen. Temperaturen på 300 °C ble oppnådd ved en massestrøm på 1.96*10⁻³ kg/s, men man kan observere en reduksjon av lufttemperaturen ved oppjustering av massestrømmen. Til tross for temperaturfall ved økt massestrøm øker varmeinnholdet i lufta i og med at absorbatøren blir utsatt for en økende kjøling og derfor får redusert varmetapet i form av konveksjon og stråling. Virkningsgraden, som er definert som varmeøkning i lufta delt på energien i direkte solstråling som treffer reflektoren, nådde verdier på mellom 50 % og 80 % der sistnevnte virkningsgrad fant sted ved relativ høy massestrøm.

Den høyeste registrerte lufttemperaturen som holdt seg over tid var 350 °C og ble oppnådd med silisiumkarbidabsorbatøren der konsentrasjonsfaktoren lå på ca 600. Massestrømmen i dette tilfellet var 1.5*10⁻³ kg/s.

Preface

This thesis is the result of the undersigned's Master Thesis at the Norwegian University of Science and Technology (NTNU) in the spring semester of 2011. This thesis was offered by the Department of Energy and Process Engineering in relation with a network project on small scale solar concentrating systems established in 2006 based on the initiatives from Professor Jørgen Løvseth, Department of Physics at NTNU.

The program is based on earlier projects on concentrating solar energy systems in Mozambique and South Africa. Its aim is to mobilize research collaboration between universities in Africa on thermal energy systems for rural communities.

The purpose of the research is to develop a concentrating solar energy system where the heat is stored and can be provided for cooking and water heating anytime. The main objective of this report is to present a survey based on testing and evaluation of available types of absorbers suitable for the concentrating solar system.

NTNU Gløshaugen, Trondheim
29.07.2011

Stud. Techn. Trygve Stansberg Veslum

Acknowledgements

The student gratefully acknowledges the helpful advice and support of Professor Ole Jørgen Nydal. PhD candidate Habtamu Madessa Bayera should be thanked for taking the time to help with experiments and report writing.

The experiments presented in this report could not have been carried out without the help given by the laboratory personnel, more specifically Martin Bustadmo and Paul Svendsen in particular, at the Department of Energy and Process Engineering.

Contents

1	Introduction	1
2	Objective	3
3	Air based absorbers for concentrated solar systems	3
3.1	<i>Volumetric absorber</i>	4
3.2	<i>Finned absorber</i>	6
3.3	<i>Cavity receiver</i>	7
3.4	<i>Small scale system demands</i>	8
4	Experimental work	9
4.1	<i>Test objective</i>	9
4.2	<i>Test Setup 1</i>	9
4.2.1	Overview of Test Setup 1	9
4.2.2	Test setup 1 components	10
4.2.3	Lamp	11
4.2.4	Temperature measurement and logging	11
4.2.5	Air fan	11
4.2.6	Air velocity meter	12
4.2.7	Steel pipe and pipe rack	12
4.3	<i>Investigated absorbers Test Setup 1</i>	13
4.3.1	Test setup 1 receiver and absorber materials	13
4.3.2	Testing procedure for absorbers - Test Setup 1	15
4.3.3	Flat fiber mesh absorber	17
4.3.4	Testing of flat fiber mesh absorber	17
4.3.5	Concave fiber mesh absorber	18
4.3.6	3D fiber mesh absorber – large	18
4.3.7	3D fiber mesh absorber – small	19
4.3.8	Flat honeycomb absorber	19
4.4	<i>Test Setup 2</i>	21
4.4.1	Replacement of reflective film	22
4.4.2	Constructing dish support	22
4.4.3	Tracking system	23
4.4.4	Receiver rack	23
4.4.5	Other	24
4.5	<i>Investigated absorbers Test Setup 2</i>	24
4.5.1	Test Setup 2 receivers and absorber materials	24
4.5.2	Testing procedure	25
4.5.3	70 mm SiC honeycomb absorber	28
4.5.4	70 mm fiber absorber	29
4.5.5	50 mm SiC honeycomb absorber	29
4.5.6	40 mm SiC honeycomb absorber	30
4.5.7	40 mm SiC foam absorber.	30

5	Results and discussion	33
5.1	<i>Example Test Setup 1 – 70 mm fiber absorber at 1.5 m/s</i>	33
5.2	<i>Comparing absorber shapes – Test Setup 1</i>	34
5.3	<i>Comparison between indoor and outdoor testing</i>	36
5.4	<i>Example Test Setup 2 – 50 mm honeycomb at 2 m/s</i>	38
5.5	<i>Comparison of different air velocities – Test Setup 2</i>	38
5.6	<i>Comparison of different concentration factors – Test Setup 2</i>	41
5.7	<i>Fiber versus honeycomb</i>	43
5.8	<i>Absorber wear</i>	44
5.9	<i>Heat losses during testing</i>	45
6	Conclusion	48
7	Appendix A	51
7.1	<i>Test Setup 1</i>	51
7.1.1	Flat 70 mm fiber absorber	51
7.1.2	Concave 70 mm fiber absorber	53
7.1.3	Concave 70 mm fiber absorber with different thickness – 1,0 m/s	54
7.1.4	50 mm 3D fiber absorber	56
7.1.5	80 mm 3D fiber absorber	58
7.1.6	70 mm honeycomb absorber	59
7.2	<i>Test Setup 2</i>	60
7.2.1	40 mm foam absorber	60
7.2.2	40 mm honeycomb absorber	60
7.2.3	50 mm flat honeycomb absorber	62
7.2.4	70 mm flat honeycomb absorber	63
7.2.5	70 mm fiber absorber	65
8	Appendix B	67
8.1.1	Calculations for Q and η	67

1 Introduction

In off-grid areas such as rural villages and hamlets the lack of electricity often makes heat-required cooking a challenge. Typical solutions replacing electricity for cooking purposes could be gas stoves, liquid fuel stoves or wood stoves. In certain parts of Africa fire wood covers more than 50 % of total energy consumption[1]. For Mozambique, this number exceeds 80 %. Since wood exists in limited amounts, deforestation can occur and in worst case affect the health of the local community. In Sudan, the growth-rate of the forests is smaller than the consumption, leading to an annually 5 % decrease of the forest area according to Schwarzer [9] . Also, fire wood is not necessarily available for free. In larger communities the supply of firewood is a problem which leads to high transportation costs, thus making it expensive for families to cook.

One way to reduce the consumption of bio mass can be an alternative energy source for cooking. A non-polluting and clean way to cook is by utilizing the solar rays directly, using a solar cooker. The first solar cookers were commissioned by Napoleon in 1860, where parabolic reflectors were used to concentrate solar radiation to a cooking pot placed in the focus point [10]. Today, this working principle is still used for a wide range of applications, from solar cooking to power generation. Regarding costs, the solar cooker is free to use, meaning the money spent on fire wood could be used to buy food and medications. However, some geographical locations are more suited for solar exploitation than other. The solar irradiation varies with geographical location on earth, due to degree of latitude and climate. According to Figure 1 most parts of Africa are suited for solar installations, having an annually mean irradiance approaching 270 W/m² in certain parts of the continent.

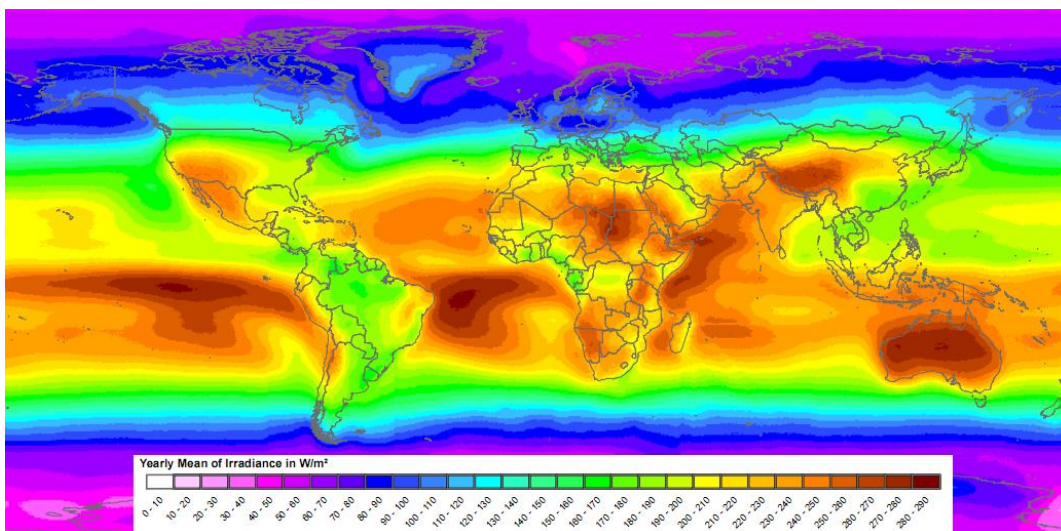


Figure 1 - Yearly mean irradiance at earth, showing a great potential for solar cookers at the African continent [4].

There are several sorts of solar cookers. Their common features are the ability to reflect the solar rays in a way which is supposed to directly heat up a vessel or pan containing the food to be cooked. However, if the thermal energy is transported from the focus point and stored, the heat can be used any time during day or night. This system is a so called solar oven developed at NTNU, Department of physics with Professor Jørgen Løvseth as initiator.

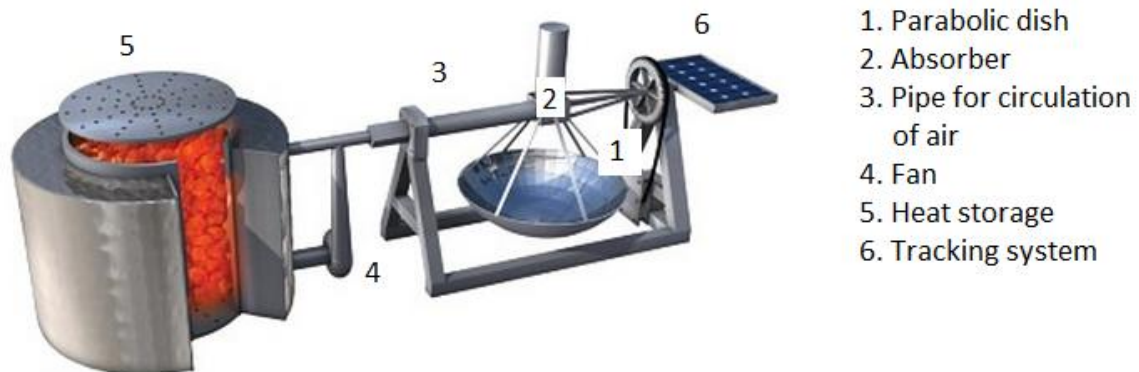


Figure 2 - The solar oven developed and constructed at NTNU [1].

In distinct from a direct solar cooker which normally only works as a reflector, the solar oven transports the heat collected in the focal point into the heat storage with air as heating medium. The concept of the solar oven is shown in Figure 2. A solar oven similar to this one has earlier been constructed and employed for testing at NTNU.

The rays are reflected in the parabolic dish and heats up the absorber, from where the heat is removed by circulating air at atmospheric pressure which is transported to the heat storage. The air is circulated by a fan which can be powered by energy from a solar cell or a small scale Stirling engine. The heat storage consists of rocks and is insulated in order to maintain the heat at a minimum temperature of 220 °C which is sufficient for cooking. The heat can be used after removing an insulating top lid at the top of the heat storage. In order to maintain the focus point at the absorber during heat loading, the solar oven is equipped with a tracking system which either can be driven by weight driven clockwork or be powered by a solar cell. In order to implement the solar oven to rural communities, it has to be robust, simple and reliable. Thus, the solar oven should mainly consist of parts which are obtainable locally in case of damage when spare parts are needed. Some of the components which are crucial for the solar oven to work satisfactory and still under investigation is the tracking system, heating medium, absorber and heat storage.

2 Objective

The performance of the solar oven in terms of temperature level in the heat storage depends on several components. The tracking system must follow the sun path correctly, the parabolic reflector must provide for the solar rays to hit the absorber and the air out of the absorber has to be heated up to a sufficient temperature level.

One of the main challenges is to absorb the radiant energy and convert it into thermal energy, which is done by the absorber. As the absorber is irradiated, the air flowing through it must be heated up to a temperature level above 220 °C. Thus, an efficient heat transfer to the air is crucial for the solar oven to operate as required. So far, air based absorbers tested for the solar oven have until yet not met the requirements of heating the air sufficiently, making it essential to put further investigation on air-based absorbers for the solar oven.

The objective of this work is to test and optimize absorbers to be used in a prototype concentrating system for air based heat collection and storage. This involves a survey of available types of absorbers. Establishment of an experimental test setup must be carried out to perform experimental comparison and optimization of available absorbers.

3 Air based absorbers for concentrated solar systems

There are several requirements for a solar absorber to work efficiently:

- Absorb the radiant energy in the concentrated sunlight to a highest possible degree. This means no transmission must occur, neither reflection.
- Emissance of infrared radiation should be kept at lowest possible level.
- The absorber must sustain thermal stresses created by large temperature gradients. Some materials can crack due to thermal stresses.
- It must handle thermal shocks caused by rapid heating-cooling cycles.

Most of the research on air-based solar absorbers has emphasized the absorbers applied for concentrating solar power (CSP) systems, more exactly solar towers. The main difference between a solar tower and the solar oven is the concentration ratio for the solar beams, resulting in different irradiance (W/m^2) and thus temperature in the focal point. Yet, an introduction on solar tower absorbers can be interesting since these can be an alternative for the solar oven. Therefore the most common types of absorbers will be presented and described briefly.

The concentration ratio, k , is defined as the reflector area divided by the absorber area.

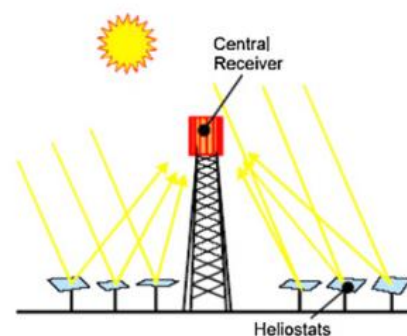


Figure 3 - Solar tower working principle [5].

3.1 Volumetric absorber

A common type of absorber for solar towers is a directly-irradiated absorber, also called open volumetric absorber [11]. The heat transfer from the incoming radiation takes place upon the surface where the working fluid is heated up directly in the absorber, as shown in Figure 4. The absorber is often located in a receiver as shown in Figure 4, exposed normal to the incident sunlight. In this case an air fan sucks cold, ambient air through the absorber.

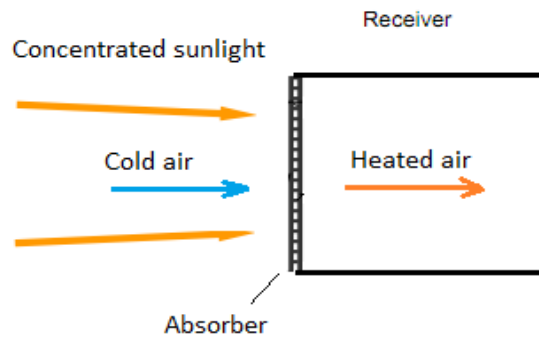


Figure 4 – Working principle of an open volumetric absorber.

There are several sorts of volumetric absorbers. For solar towers, the most typical absorber is a sort of a matrix absorber. Figure 5 shows four different kinds of matrix absorbers which are investigated and tested in different solar towers.

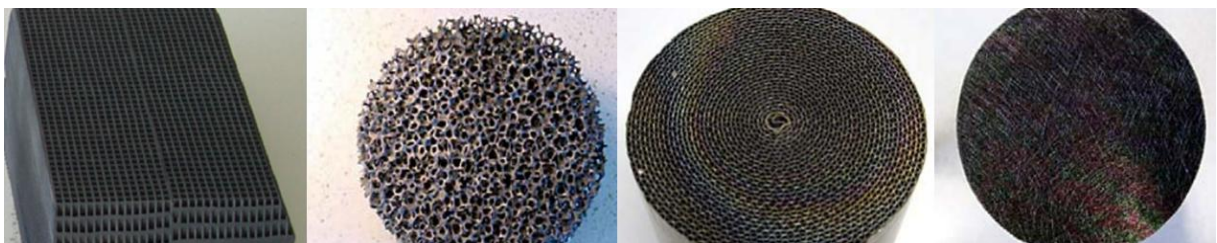


Figure 5 - Four different matrix absorbers applied to solar towers. From left to the right: Honeycomb [7], ceramic foam [6], wire mesh[6] and fiber mesh [6].

What differ the different matrix absorber from another is their ability to absorb radiation and transfer the energy in term of heat to the working fluid. Also, in some cases the absorbers are exposed to temperatures up to 1600°C [6] where they tend to expand and contract which can result in thermal stress and eventually cracking depending on the material. Another challenge regarding high temperature levels is the melting point of the absorbers. A clear advantage regarding the matrix absorbers however, especially for the wire mesh, is the simple design and the low production cost.

Matrix absorbers often operate with air as working fluid, which is sucked through the absorber from the surroundings at ambient pressure with a direction parallel to the incident light. However, if the working fluid is not air, or if it is pressurized, the absorber has to be encased in a transparent jar. For increased thermal efficiency, the jar can be made of a selective sort of glass, transmitting the rays with short wave-length and being opaque to rays with longer wavelength, as infrared radiation.

The absorbers tested so far at NTNU for the solar oven can be classified as volumetric absorbers. They are operating after the working principle shown in Figure 6, but different versions are constructed and tested. A hemispherical jar encases the fiber absorber made of coated steel wool. The cold inlet penetrates the hemispherical absorber inside the jar while it absorbs the heat through convection.

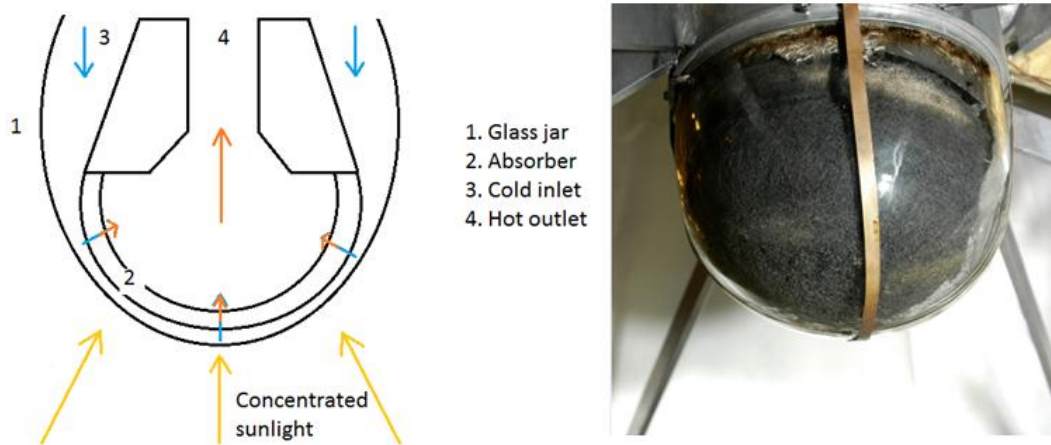


Figure 6 – Left: Schematic drawing of volumetric absorber tested for a solar oven at NTNU. Right: The absorber encapsulated in glass jar due to the circulation air.

The main difference between the different versions was adjustment of flow arrangements, resulting in different outlet temperatures. However, tests so far have resulted in outlet temperatures which have not met the requirements [12].

3.2 Finned absorber

Figure 7 shows the working principle of a finned absorber where the working fluid flows perpendicularly to the incident sun rays. A clear advantage regarding the finned absorbers versus matrix absorber is the possibility for the irradiation to penetrate into the depth of the absorber. This will provide for a better radiative exchange between the absorbing fins. Also, as the fins are located independently from each other, they are free to expand and contract due to temperature variation, avoiding the problem of thermal stress. Therefore, this type of absorber is very durable and has a long lifespan [11].

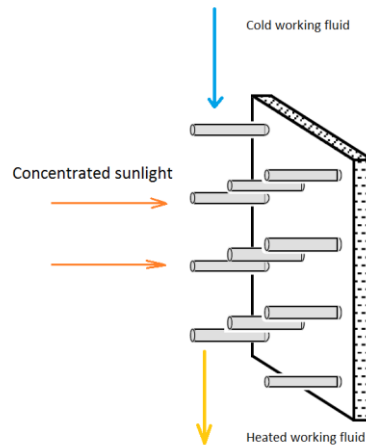


Figure 7 - Flow arrangement for a finned absorber.

Figure 8 shows an example of a finned absorber. The cold air working fluid is injected from the center of the absorber and spread radially towards the periphery. The fins are attached to a porous base plate, in which the heated working fluid flows through as an outlet. The absorber is encased in a jar because of the flow arrangement.

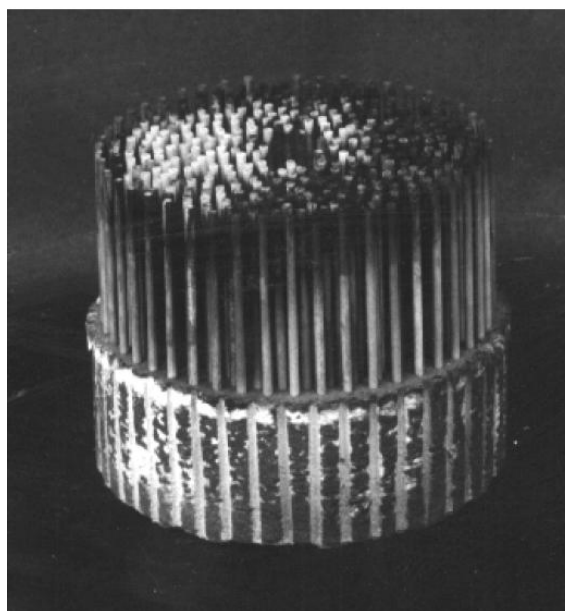


Figure 8 - Finned type of absorber [11].

3.3 Cavity receiver

For a cavity receiver the concentrated sunlight is reflected into a cavity with help from a concentrating parabolic compound, as shown in Figure 9. As the rays are more or less trapped in the cavity, the losses in terms of reflection and infrared emittance are significantly reduced.

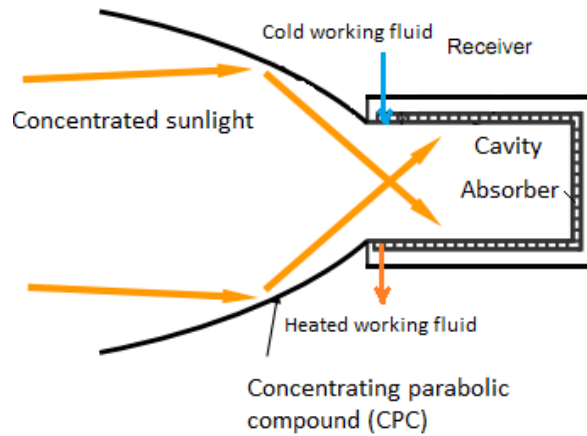


Figure 9 – Working principle for a cavity absorber.

The absorber used for a cavity receiver can be a tubular type of absorber which is coiled in such a way that it forms a cavity inside, as shown in Figure 10, Since the tube is closed from the surroundings, it can operate with various working fluids above atmospheric pressure. In contrast to the volumetric absorber where the heat transfer from radiation to the air takes place at the same surface, the heat has to be conducted through the tube wall at first. This principle can be classified as indirectly-irradiated absorber[11].

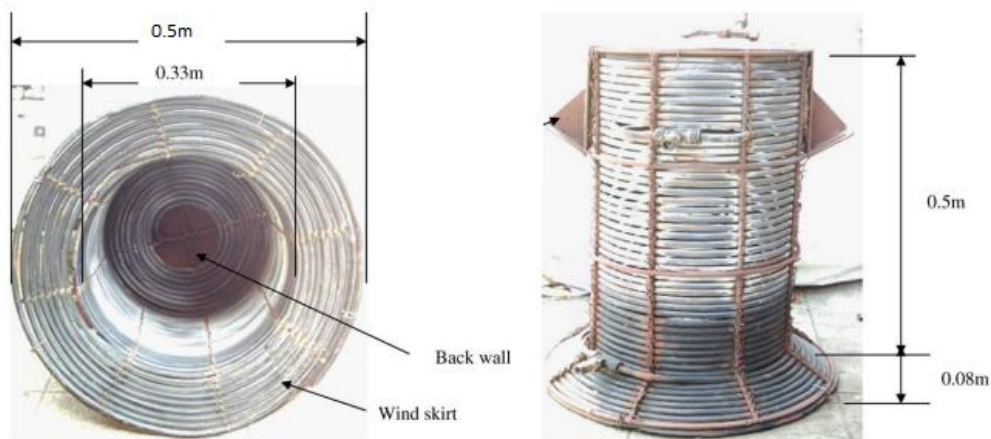


Figure 10 – Left: Cavity absorber seen from the front. Right: Cavity absorber seen from the side [13].

3.4 Small scale system demands

The main target group for the solar oven is African communities living in areas with high annual solar irradiation and in demand for fuel. Therefore the solar oven should be constructed as simple as possible in order to be robust, easy to repair and being as affordable as possible. This demand concerns every part of the solar oven, even the absorber.

Therefore not every absorber discussed in chapter 3 is suitable for the solar oven. The fiber mesh tested at NTNU earlier will still be put under investigation due to its low price and simplicity. An even simpler and therefore a cheaper system than that discussed in the end of chapter 1, is to suck cold air from the surroundings through the absorber and into the heat storage without circulating the air back to the absorber. This will be same working principle as discussed in 3.1, namely an open volumetric absorber. By employing this concept, several different absorbers may be tested, such as the fiber mesh absorber and the materials discussed in 3.1. The more complicated absorbers such as the finned absorber in chapter 3.2 and cavity receiver in chapter 3.3 are not relevant to the solar oven due of their complex construction.

4 Experimental work

4.1 Test objective

The objective of this experiment is to test different open volumetric absorbers in terms of size, shape and material to determine whether they are suitable for small scale concentrating systems. The absorber requirement is to heat air to at least 220°C to be applicable for the solar oven. In order to test and compare absorbers a test setup was needed to be constructed. Two test setups were constructed, since the first generation test setup (Test Setup 1. Abbreviation: TS1) was inaccurate. The second generation setup (Test Setup 2. Abbreviation: TS2) was an upgrade from TS1 and provided for more reliable data to be used as a basis for the evaluation of the different absorbers.

4.2 Test Setup 1

Originally, TS1 was constructed with regard to be employed for indoor testing, where 1 kW lamps were meant to simulate the radiation from the sun. This setup would not require any system for tracking and would allow for a simple system where no parts were meant to be moving during testing. Therefore, the system was constructed as simple as possible without any intention to be employed in outdoor testing.

4.2.1 Overview of Test Setup 1

Figure 11 shows TS1 schematically, where a 1.07 m² parabolic dish located directly under a high-intensity lamp reflects and concentrates the rays into the absorber housed in a receiver which is connected to a steel pipe. To make sure the entire absorber surface is illuminated, the receiver can be adjusted vertically above the center of the dish. At the other end of the pipe a controllable 220 V fan is connected to suck air through the absorber from the surroundings. Temperatures for the absorber surface and the through-flowing air were measured with thermocouples.

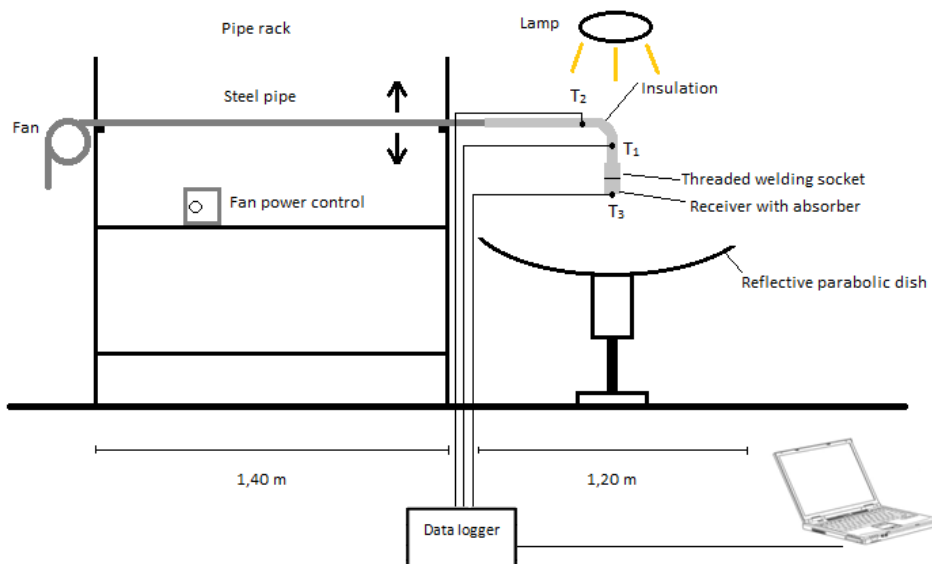


Figure 11 - Schematic drawing of Test Setup 1.



Figure 12 - Picture of Test Setup 1 during operation.

4.2.2 Test setup 1 components

4.2.2.1 Parabolic dish

The dish was made of a 2 mm thick aluminum plate pressed with a parabolic profile and covered with a 93 % solar reflective film manufactured by ReflecTech® [14]. The dish had been applied for solar related experiments before and no further modifications since then were done. The dish was supported by four rods in a center hole in the parabola with a diameter of 28 cm. The outer dish diameter D_{dish} measured 1.20 m, constituting a total aperture area of 1.07 m^2 . There was no support to stiffen up the parabola.

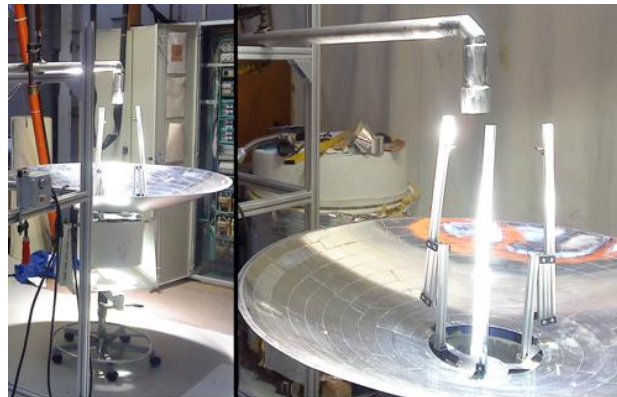


Figure 13 - Parabolic dish employed for TS1.

Figure 14 shows the dimensions for the dish which were used to calculate its focal point combined with the simplified equation for a parabolic line (1.1). As the dish height h was equal to $h=18.6 \text{ cm}$ and the dish diameter $D_{dish}=120 \text{ cm}$, the focal length p_f was calculated to be 48.4 cm above the dish center. However, due to a small dish deformation, far from all rays were collected in a small spot at the calculated focal point. This could be visualized by holding a sheet of

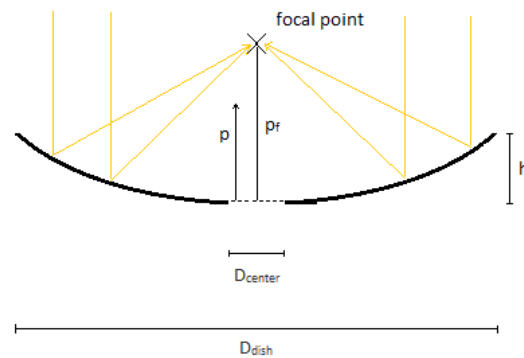


Figure 14 - Parabolic dish dimensions.

paper in the focal plane. Nevertheless, the dish was used during testing with TS1 without any further modifications.

$$P_f = \frac{x^2}{4y} = \frac{(D_{dish} / 2)^2}{4h} \quad (1.1)$$

4.2.3 Lamp

The lamps were originally applied to light up soccer stadiums about three decades ago with a power rating of 1 kW. However, the solar equivalent emission was some 250 W [15]. Since the full beam opening angle was 26 degrees the radiation was far from parallel directed and therefore only one lamp could be deployed at a time. By using more lamps the rays would not constitute the same focal point, but rather create multiple focal points.



Figure 15 - Lamp for simulating solar radiation.

4.2.4 Temperature measurement and logging

The air temperatures were measured using K-Type thermocouples located as shown in Figure 11. The thermocouples were connected to a data logger which recorded the temperatures about 3 times every 5 second. T_1 and T_2 were located right before and right after the 90° bend, respectively, while T_3 measured the surface temperature at the absorber. This thermocouple was not shielded against radiation entering the absorber. T_1 or T_2 were neither shielded. The data was recorded using National Instruments data logging system and National Instruments LabVIEW[®] was used for reading. During test with lamp as light source only thermocouple T_2 and T_3 were taken in use.

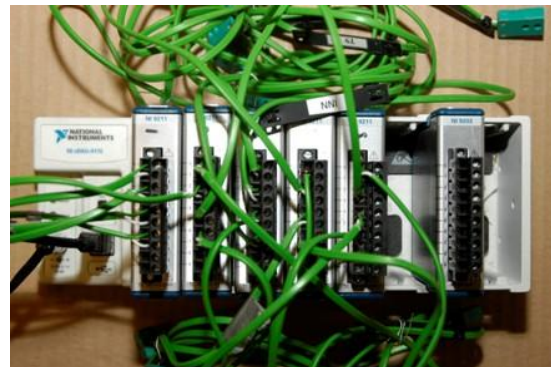


Figure 17 – Data logger with connected thermocouple cables.

4.2.5 Air fan

A 220 Volt radial air fan was connected to the outlet end of the steel pipe with high-temperature resistant glue. In order to regulate the air mass flow the fan was controlled by deployment of a controllable motor inverter.



Figure 16 – 220 V radial air fan for sucking ambient air through the absorber. The appurtenant controllable motor inverter is shown in the inlay picture.

4.2.6 Air velocity meter

Originally a flow meter was meant to be deployed for mass flow measuring, but because the pressure drop across the flow meter was higher than the pressure rise from the fan, it was not suitable for this application. Therefore a velocity meter consisting of a remote vane and an indicator was used during the tests despite its inaccuracy at rising temperatures. This is further discussed in chapter 5.5.



Figure 18 - Air velocity meter used at the fan outlet.

4.2.7 Steel pipe and pipe rack

The pipe rack was constructed with the purpose to maintain the stationary position of the receiver, since the test setup was intended to serve for indoor testing only. Because of uncertainty around the temperature that the fan could resist, the steel pipe was 2.0 m long in order to let the heated air be cooled down downstream. Therefore, a 1.40 meter long rack was needed to keep the steel pipe elevated in a steady position, according to Figure 12. AluFlex aluminum profiles were used to construct the pipe rack, making it easy to adjust the steel pipe and hence the receiver elevation, as indicated in Figure 11. A threaded welding socket was welded



Figure 19 - Threaded welding socket at the receiver end of the 5 cm steel pipe for easy attachment and removal of different receivers.

to the receiver end of the pipe in order to easily attach the receiver. This solution would also make the connection air tight. To maintain air temperatures past the thermocouples, the receiver end of the pipe was covered with 5 mm low conductive insulation from Aspen Aerogels® ($\lambda = 0.021 \text{ W/mK}$ [16]). The steel pipe had an external diameter equal to 5 cm.

4.3 Investigated absorbers Test Setup 1

A total number of five different absorbers in terms of material, geometry and size were tested in TS1, where one was tested indoors with lamp as light source. Chapter 4.3.1 will explain the materials tested and the construction of the absorber support, also called a receiver. Chapter 4.3.2 will deal with the general testing procedure carried out for the tested absorbers, while chapter 4.3.3 through 4.3.8 will explain each absorber in terms of assembly and testing procedure.

4.3.1 Test setup 1 receiver and absorber materials

4.3.1.1 Stainless steel fiber mesh

Most of the absorbers tested with TS1 were made of stainless steel fiber from the company STAX [3] whose data are listed in Table 1. Every absorber consisted of a certain number of layers to maximize heat transfer to the air. According to “Receiver for air based solar oven planned at EMU ©” written by professor Jørgen Løvseth the fiber mass pr. absorber area should have a value M between 1.25 kg/m^2 and 2.5 kg/m^2 for fibers aligned perpendicularly to the direction of entering solar radiation [17]. Therefore three layers of fiber were used to form an absorber, constituting an M equal to 1.5 kg/m^2 if not mentioned otherwise in chapter 4.3.3-4.3.8. In order to increase the fibers absorbance, each fiber mesh layer was sprayed with high-temperature black paint from Motip® [18].



Figure 20 – Sample of stainless steel fiber mesh used to form the fiber mesh absorber.

Table 1 - Stainless steel fiber mesh data [3].

Material	Stainless steel AISI 314
Material density	7900 kg/m^3
Material heat conductivity	14 W/mK
Melting point	1200 °C
Fiber geometry	Irregular shaped. Thickness about 0.1 mm .

4.3.1.2 Porous silicon carbide monolithic honeycomb

Recrystallized Silicon Carbide (ReSiC) is a high-temperature resistant material which has been extensively tested as open volumetric absorber for large scale concentrated solar radiation system, such as the solar towers SOLAIR-200 and SOLAIR 3000 on the solar platform in Almeria, Spain [7]. Advantages offered by the ceramic honeycomb include a large geometric surface, thin walls and low pressure drop. Further advantages include excellent shock resistance, high temperature tolerance and high thermal conductivity, according to Table 2. The honeycomb is manufactured by the Danish company Stobbe Tech Ceramics.

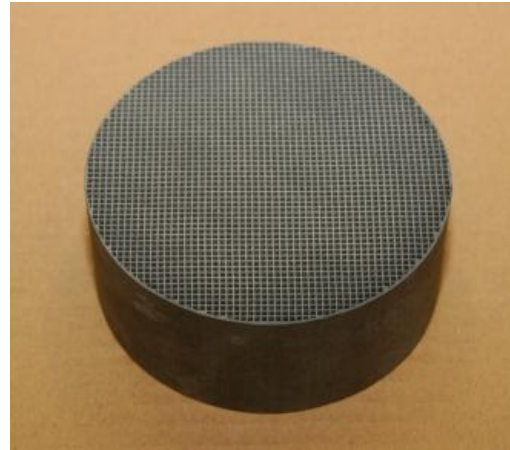


Figure 21 - ReSiC monolithic honeycomb as delivered to NTNU. The monolith was further shaped to serve as an absorber.

Table 2 - Silicon Carbide data [7], [8].

Material	Recrystallized Silicon Carbide (ReSiC)
Cell density	22.3 cells/cm ²
Measurements	Thickness wall: 0,5 mm Cell dimension. 1,6 mm
Material density Honeycomb density	1.8 kg/m ³ 730 kg/m ³
Heat conductivity	At 25 °C: 40 W/mK At 630 °C: 15 W/mK
Heat resistivity	Around 1000 °C for 5000 hours

4.3.1.3 Test Setup 1 Receiver

During testing each absorber was attached in a receiver with an internal diameter of 100 mm at the bottom side and a cone with a threaded welding socket at the top side to fit the steel pipe, as shown in Figure 22. When testing of a particular absorber was completed, it was removed before the next absorber was attached to the receiver.



Figure 22 – Receiver used to house and support the absorber during testing in Test Setup 1.

4.3.2 Testing procedure for absorbers - Test Setup 1

4.3.2.1 Positioning of absorber - indoors

Once the absorber was attached to the receiver it was connected to the steel pipe at the pipe rack before thermocouple T_3 was attached to the absorber surface. Subsequently the pipe rack was positioned such that the absorber was located above the center of the horizontally aligned reflector. To locate the optimal elevation p above the center bottom of the dish, the receiver was adjusted to the point where most possible of the absorber was illuminated by the reflected rays. Since the dish was not adequately stiffened up, its deformation caused the reflected rays to form a non-circular shaped profile (projected from above) as may be seen to the left in Figure 23.

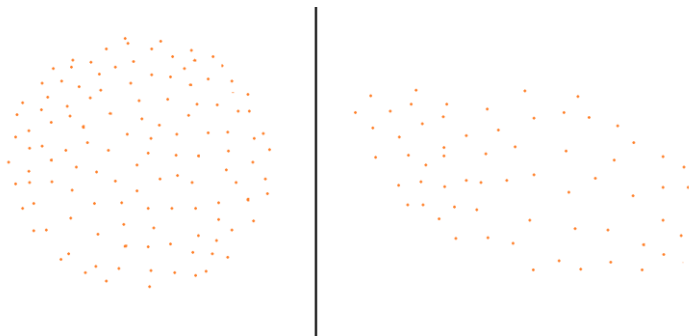


Figure 23 – Left: Reflected rays forming a circular shaped profile. This is ideal since the reflector is circular when seen from above. Right: A non-circular shaped profile, which demonstrates the case of using the reflector without any support. The figure to the left is not based on any experiments, but shows the phenomena qualitatively.

This caused either many of the rays to pass by the absorber, or would cause non-illuminated regions (cold spots) on the absorber depending on the receiver elevation p . In the first case most of the absorber would be illuminated with a concentration ratio relatively lower than that in the second case. By reading of the air temperatures T_1 and T_2 from the computer while adjusting the receiver elevation, the case of having larger concentration ratio seemed to yield highest air temperatures despite of the cold spots. Also, in this case most of the reflected rays entered the absorber.



Figure 24 - Test setup 1 indoors with lamp as light source

4.3.2.2 Positioning of absorber – outdoors

More or less the same technique as discussed in 4.3.2.1 was performed for directing the concentrated solar rays into the absorber. Because of the continuously moving sun, the dish and the pipe rack had to be tracked manually, making it challenging to keep a constant radiation flux entering the absorber. Also in this case the dish was not stiffened up, creating the same issue as mentioned in 4.3.2.1 regarding the shape of the reflecting radiation entering the absorber.

4.3.2.3 Testing procedure

Each absorber in TS1 was tested at three different flow rates corresponding to 1 m/s, 1.5 m/s and 2 m/s measured at the hot air outlet from the fan. Due to a very sensitive control button at the motor inverter, maintaining a constant air velocity at low flow rates could be difficult.

When the optimum position of the receiver relatively to the dish was established, temperature logging was initiated. The tests were ran for a necessary time lapse such that the air temperatures reached a steady state for at least 15 minutes, which could take up to 2 hours to achieve due to e.g. challenging regulation of the air fan and correct positioning of receiver. About every second minute the air velocity meter was used to make sure the air flow was kept at a constant level. During the tests, the dish needed to be manually tracked due to the movement of the sun. To reflect the rays to the stationary receiver, the parabola was moved since it was easier to move than the pipe rack. About every hour the pipe rack also had to be re-positioned. Equipment adjacent to the heated air acting as cooling surfaces also had to be heated up, causing a time lapse of about 10 minutes to heat up the system until it stabilized.

4.3.3 Flat fiber mesh absorber

The flat fiber absorber was the only one to be tested indoors with the lamp as light source. The fiber mesh was cut out with a diameter of 100 mm to fit the receiver opening, where the three fiber layers were sandwiched and fixed together with steel wires. To make the receiver airtight a steel foil was attached to the periphery, changing the absorber opening to $d_{\text{abs}}=70\text{mm}$. Since the parabolic dish had a diameter of $D_{\text{dish}}=1.20\text{ m}$ the concentration factor k was calculated to around $k=300$. The steel foil was attached to the absorber by using a high temperature sealing compound (temperature resistant up to 1100°C [19]), allowing air through the absorber opening only. The steel foil was folded around the receiver outer edge and fastened by steel wire. Finally the receiver and the external side of the steel foil were covered with insulation from Aspen Aerogels @ [16]. Figure 25 shows the order of assembly of the absorber into the receiver. This receiver was the first one to be constructed for TS1.

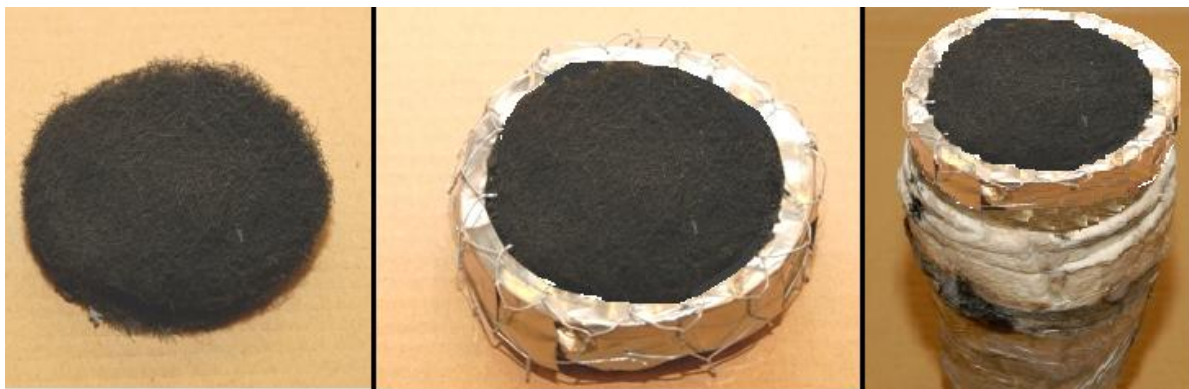


Figure 25 - Assembly of flat fiber absorber. Left: 3-layer black painted fiber mesh. Middle: Steel foil attached to absorber. Right: Absorber fixed to receiver (without insulation around the steel foil)

4.3.4 Testing of flat fiber mesh absorber

Due to technical issues the pictures taken of the absorber when testing indoors were lost. However, Figure 26 shows the absorber in the position which gave the greatest air temperatures (the picture is slightly underexposed, making the dark areas appear completely un-illuminated, although they were illuminated to a small degree). The wire which touches the most illuminated area is thermocouple T_3 . The distance between the absorber surface and the dish was not measured since the angle between the receiver and the dish varied due to manually tracking, hence the optimum distance varied.



Figure 26 - Flat fiber absorber illuminated by reflected solar rays. More or less the same radiation profile at the absorber was observed when tested indoors.

When tested indoors, the absorber was tested with air velocity equal to 1.0 m/s measured at the air fan outlet. Due to safety reasons the lamp rig was removed and further testing needed to be carried

out outdoors. The radiation profile at the absorber when tested indoors appeared more or less as in Figure 26, but not with such a distinct outer edge due to a large beam opening angle from the lamp.

4.3.5 Concave fiber mesh absorber

The concave fiber mesh absorber was built in the same manner as the flat absorber, also with aperture diameter of $d_{abs}=70$ mm and 3 layers of fiber mesh. In addition, to maintain the concave shape the fiber mesh was covered with a skeleton of thin wire netting. The idea behind this shape was to make the absorber less exposed to wind passing by it, which causes losses due to forced convection. The concave absorber was attached to the receiver after the flat fiber mesh absorber was removed.

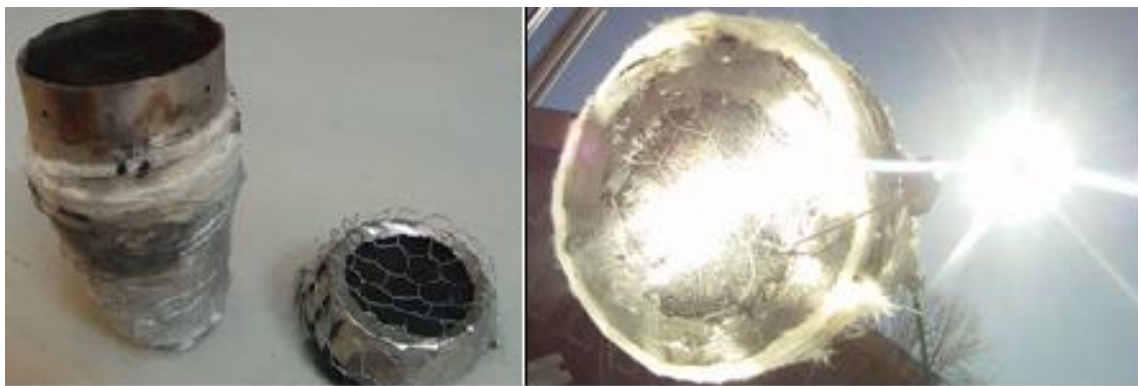


Figure 27 – Left: Assembly of 70 mm concave fiber mesh absorber. Right: Concave absorber illuminated.

In addition to the testing at the three discussed air velocities, the concave absorber was tested with different number of layers, ranging from two to five layers. The objective behind this was to reveal any correlation between number of fiber layers and change in air temperature.

4.3.6 3D fiber mesh absorber – large

Two nearly hemispherical shaped absorbers were tested, each with different size. The larger had a diameter of 80 mm and a height of 50 mm. The 3D absorber has been investigated and tested in a larger size in relation to the NUFU project in the past, corresponding to a concentration factor of about 30. With a well shaped parabolic dish the rays are intended to strike the absorber somewhat perpendicularly to the absorber surface. As with the flat shaped absorber, it was built up of 3 layers of black painted fiber mesh. To maintain the shape, it was stiffened up by steel netting on both the inside and the outside.



Figure 28 – 80 mm 3D absorber illuminated.

4.3.7 3D fiber mesh absorber – small

The smaller 3D absorber was constructed with the idea to increase the solar flux entering the absorber surface, compared to that for the absorber discussed in 4.3.6. Apart from the size the other characteristics were the same. This absorber had an outer diameter of 50 mm and height of 30 mm.



Figure 29 - Small 3D absorber illuminated.

4.3.8 Flat honeycomb absorber

The honeycomb absorber was the last one to be tested at Test Setup 1, and the only absorber made of another material than fiber mesh. The honeycomb was cut down to diameter of 90 mm, wrapped in insulation and put in the receiver where it had a very tight fit, letting air through the absorber only. To reduce convection, the honeycomb was pushed 1,5 cm inwards the receiver. To make sure the honeycomb would not fall out of the receiver, it was fixed with a set screw. The absorber was not painted black due to lack of spray paint.



Figure 30 - Assembly of honeycomb receiver

The parabolic dish was after extensively use getting further deformed. In addition, a tracking system had been developed at NTNU, at which the dish had been attached and removed several times for testing purposes, leading to further deformations. A negative consequence having the dish mounted on the tracking system included the necessity of always moving the pipe rack corresponding to the sun`s movement, which position was very hard to fine-tune.



Figure 31 - Left: Parabolic dish on a solar tracking system. Right: Large un-illuminated areas on absorber.

4.4 Test Setup 2

Test Setup 2 was constructed based on the experiences that were obtained from TS1. The objective of constructing a new test setup was to both determine if the temperature target of 220°C was achievable at all, and that a well-operating test setup would yield reliable results to create a basis for comparing absorbers. In Table 3 the main problems regarding TS1 that were desired to be eliminated are listed with their respective cause and solution.

Table 3 – Problems occurring at TS1

Problem	Cause	Solution
Partial reflection of rays	Reflective film wear and tear	Change reflective film
Non-uniform flux entering absorber	Deformed dish	Dish support
	Manual tracking	Automatic tracking
	Receiver and parabolic dish two independent systems	Receiver on a fixed position above center of dish
Unsteady air flow	Problematic air fan	Change fan and controller

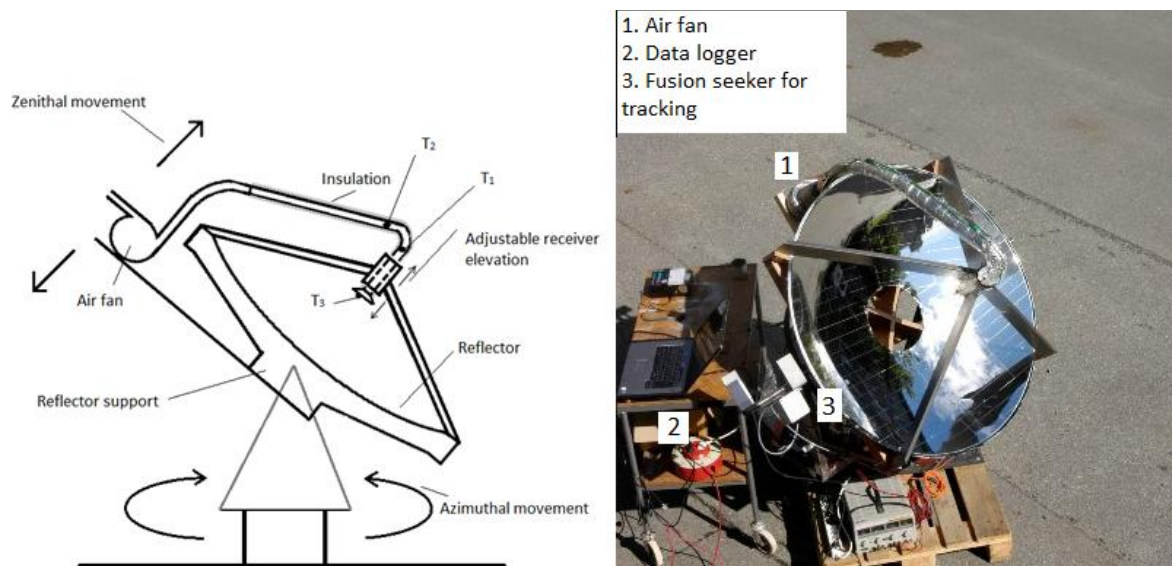


Figure 32 – Left: Schematic drawing of Test Setup 2. Right: Picture of Test Setup 2 during use.

To satisfy the desired changes from TS1, TS2 was constructed as shown in Figure 32.

According to Figure 32, the parabola is stiffened up by a wooden support. The hot air steel pipe is kept centered above the center of the parabola, where the receiver end of the steel pipe can be adjusted vertically to keep the receiver correctly positioned. The steel pipe is connected to a flexible steel pipe which is further connected to the air fan, blowing the hot air to the surroundings. The parabola will stay directed towards the sun thanks to zenithal and azimuthal tracking movements. Chapter 4.4.1 through 4.4.5 will explain step by step the construction of TS2.

4.4.1 Replacement of reflective film

The reflective film used for Test Setup 1 was removed using white spirit and steel fiber mesh. A stronger solvent is recommended for removing the adhesive from the dish, e.g. acetone, since white spirit did not dissolve the adhesive. The previous film was attached with small circular-shaped film strips cut out of a larger patch. In this case 5 cm x 40 cm rectangular pieces were cut and attached to the dish all in the same direction across the dish as seen in Figure 33. The same film as in TS1 was used for TS2.



Figure 33- Replacement of reflective film to increase the dish's reflectance.

4.4.2 Constructing dish support

The wooden dish support was constructed to create an opportunity for fixing the parabola to the automatic tracking system and keeping the shape of the dish. A support located above the dish to keep the receiver above the center and at correct elevation above the parabola was intended to be fastened to the dish support.

An exact parabolic line was drawn on a 20 mm thick plywood plate with respect to the calculated focal length of $p_f=48,5$ cm. The technique of drawing the line has earlier been used for constructing parabolic dishes for traditional solar cookers using a T-shaped tool. A non-elastic string was fixed to a slim nail located at the focal point on the plywood plate. The string was placed around the tip of a pencil and fixed on the top of the T-tool as it was kept stretched. The tool was moved sideward as the pencil was forced upwards, creating a parabolic line (see Figure 34). Two profiles were cut out from the plate using compass saw and they were eventually fitted perpendicularly in a cogging joint, which was reinforced using angle hinge. Finally redundant weight was removed.

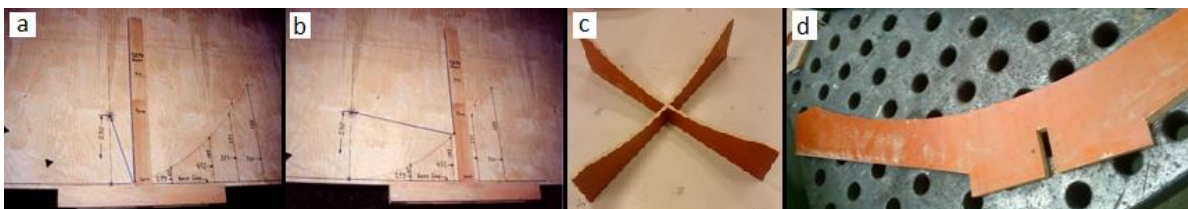


Figure 34 – (a), (b) Drawing of parabolic line by use of a T-shaped tool [2], (c) two parabolic profiles combined together with a cogging joint, (d) Redundant weight removed

4.4.3 Tracking system

The dish was placed and fitted into the wooden structure before it was attached temporarily with clamps to the solar tracking system which had been constructed by a group of students from Høyskolen i Sør-Trøndelag (HiST). The system was able to track the sun in respect to zenith and azimuth axes with the help from two independent motors controlled by a fusion seeker (diodes) [20]. The fusion seeker consists of a small box with one diode on each of the four sides fixed to the reflector structure. A DC power supply provided for the electrical power supply. The tracking error peaked at 0.2° .

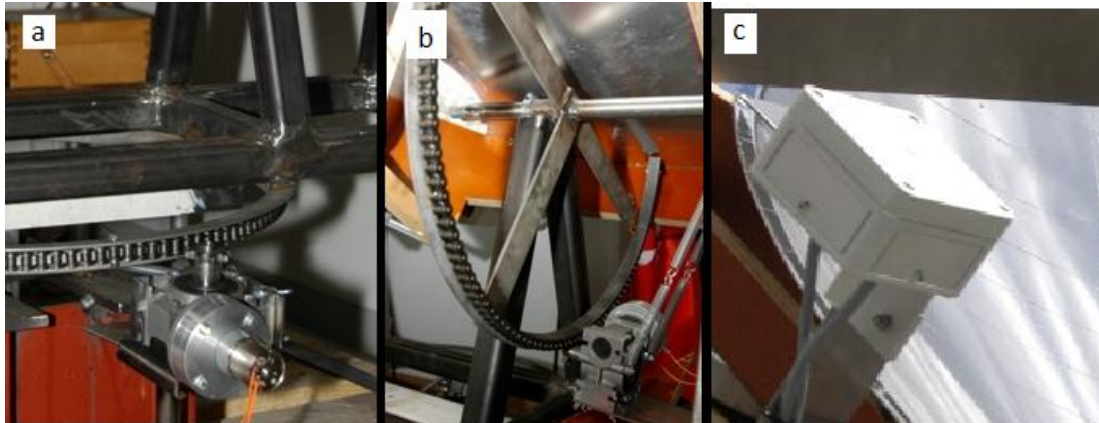


Figure 35 – Pictures of the two axis tracking system employed for TS2; (a) the azimuthal tracking axis, (b) zenithal tracking axis, (c) Fusion seeker with diodes.

4.4.4 Receiver rack

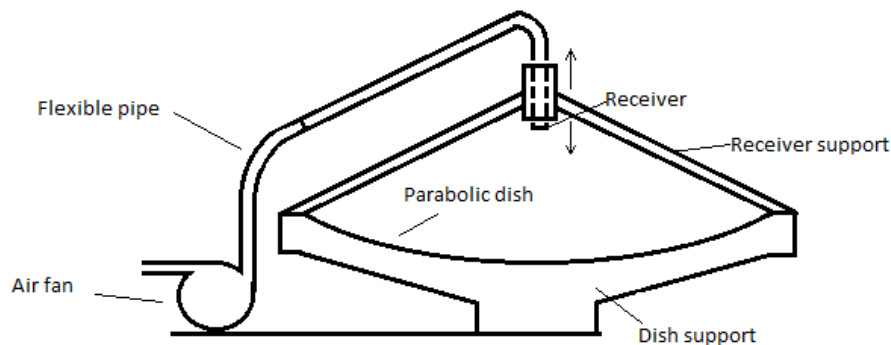


Figure 36 - Schematic of receiver support, where the receiver may be adjusted vertically.

A receiver support was necessary to keep the receiver positioned above the center of the parabolic dish. As employed in TS1, a threaded welding socket was welded to the receiver end of a steel pipe, making it possible to switch receivers with ease. Since absorbers with different dimensions were intended to be tested, the steel pipe was allowed to be adjusted vertically inside a short pipe with a larger diameter. When the receiver had been adjusted to the correct elevation above the center of the reflector, it was fixed with 6 set-screws screwed through the short steel pipe. At the other end of the pipe a flexible steel pipe was attached to an air fan, making it possible to let the air fan stay stationary during vertically adjustment of the receiver.

4.4.5 Other

A 12 Volt air fan similar to that depicted in Figure 16 replaced the air fan used in Test Setup 1, and was used in combination with a controllable DC power supply.

Regarding location of thermocouples this can be seen in Figure 32. T_1 is located before the 120° pipe bend and T_2 right after. Having some distance between the thermocouples would more easily reveal any temperature differences in the hot air flow.

The same type of data logger as in TS1 was used for TS2.



Figure 37 - DC power supply used for the tracking system and the air fan.

4.5 Investigated absorbers Test Setup 2

Several absorbers with different opening diameter and material were tested in TS2. Since TS1 was a source of several errors, the same materials were tested over again to produce more conclusive and reliable results. Generally, a more thorough effort was put into TS2 which resulted in less sources of error during testing.

4.5.1 Test Setup 2 receivers and absorber materials

Most of the absorbers tested in Test Setup 2 were made of the same materials as the absorbers discussed in chapter 4.3.1. In addition a silicon carbide foam sample was tested, as described in 4.5.1.1.

4.5.1.1 SiC foam absorber

The foam was given to EPT as a sample from the manufacturer Institut für Keramische Technologien und Sinterwerkstoffe in Dresden, Germany. The characteristics of relevance are listed in Table 4.

Table 4 – SiC foam characteristics [6]

Material	Silicon carbide (SiC)
Pore size	0,4 mm
Cell density	45 ppi (pores per inch)
Absorber density	340 kg/m ³
Heat conductivity	2,7 W/mK (overall absorber heat transfer coefficient, see [6] for details.
Sample size	40x40x24 (mm)

4.5.1.2 Test Setup 2 receivers

Three different receivers were made to house the absorbers of three different dimensions.



Figure 38 - Three receivers in increasing order.

Figure 38 shows the three different receivers which housed absorbers with three different dimensions in term of absorber diameter. For the two largest receivers, a 0.5 mm thick steel plate was bent to form a circle, which was welded to threaded welding sockets for easy attachment to the steel pipe. For the smallest receiver, the welding socket itself performed as a receiver.

The receivers were constructed to house absorbers with diameter of 40 mm, 50 mm and 70 mm, which corresponds to concentration ratios of respectively 900, 600 and 300 which were the desired concentration ratios to work with. $k=300$ is equivalent to the concentration ratio at TS1, and testing with the same ratio would be worthwhile to perform at TS2 for comparison purposes between TS1 and TS2. $k=600$ and $k=900$ would be interesting to test in order to see any correlation between concentration ratio and outlet air temperature.

4.5.2 Testing procedure

The absorbers were tested at three different air velocities; 1 m/s, 2 m/s and 4 m/s measured at the air fan outlet. As with Test Setup 1, the experiments were ran until the temperatures stayed more or less constant for at least 15 minutes. Due to time constraint during testing, longer test duration was not preferable. The time constraint was mainly caused by the unstable weather, and it was preferred to run as many tests as possible when the weather allowed it.

4.5.2.1 Absorber positioning

Correct positioning of the receiver regarding correct distance p between absorber surface and the dish was according to experiences from TS1 crucial to achieve high temperatures. Before designing the receivers, the reflector's ability to collect the reflected rays around the focal point was mapped by the use of a vertically self-aligning, moveable laser whose laser beams were reflected in the leveled dish. At different elevations p around the calculated focal plane the beams were marked on a paper resting on a transparent plate, according to Figure 39.

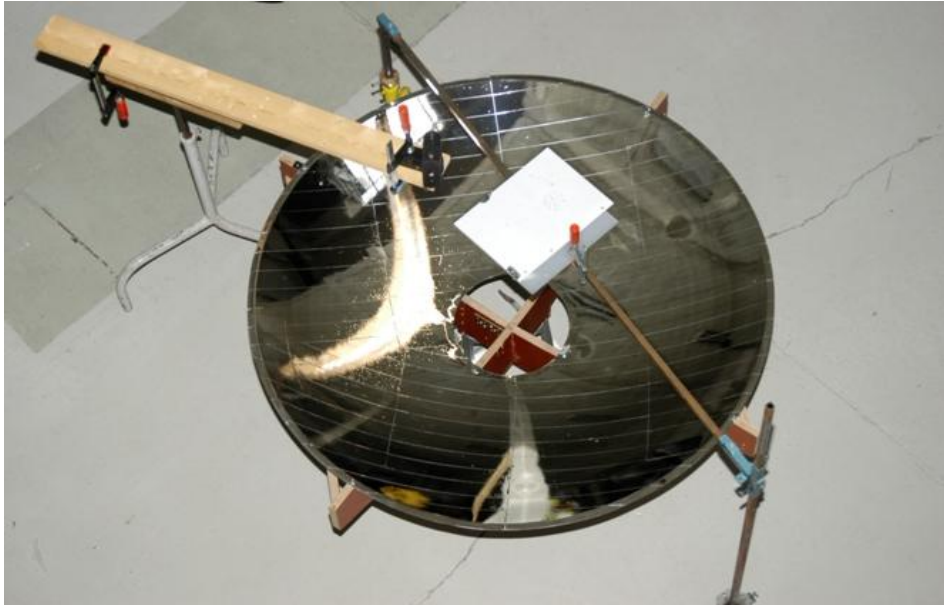


Figure 39 - Calibration of reflector.

Due to the small indentations in the dish, some of the beams were reflected off the densest areas. Positioning of the absorbers was based upon the prints in Figure 41, avoiding any reflected beams to strike outside the absorber but at the same time making sure that the whole absorber was illuminated. Once the receiver was positioned correctly with respect to p , the fusion seeker was adjusted both in azimuthal and zenithal direction to make the direction of reflection relative to the absorber correct (see Figure 40). During positioning of receiver the air fan was turned on to avoid any local overheating of the receiver.



Figure 40 - Adjustment of fusion seeker to provide for an even distribution of reflected rays entering an absorber.

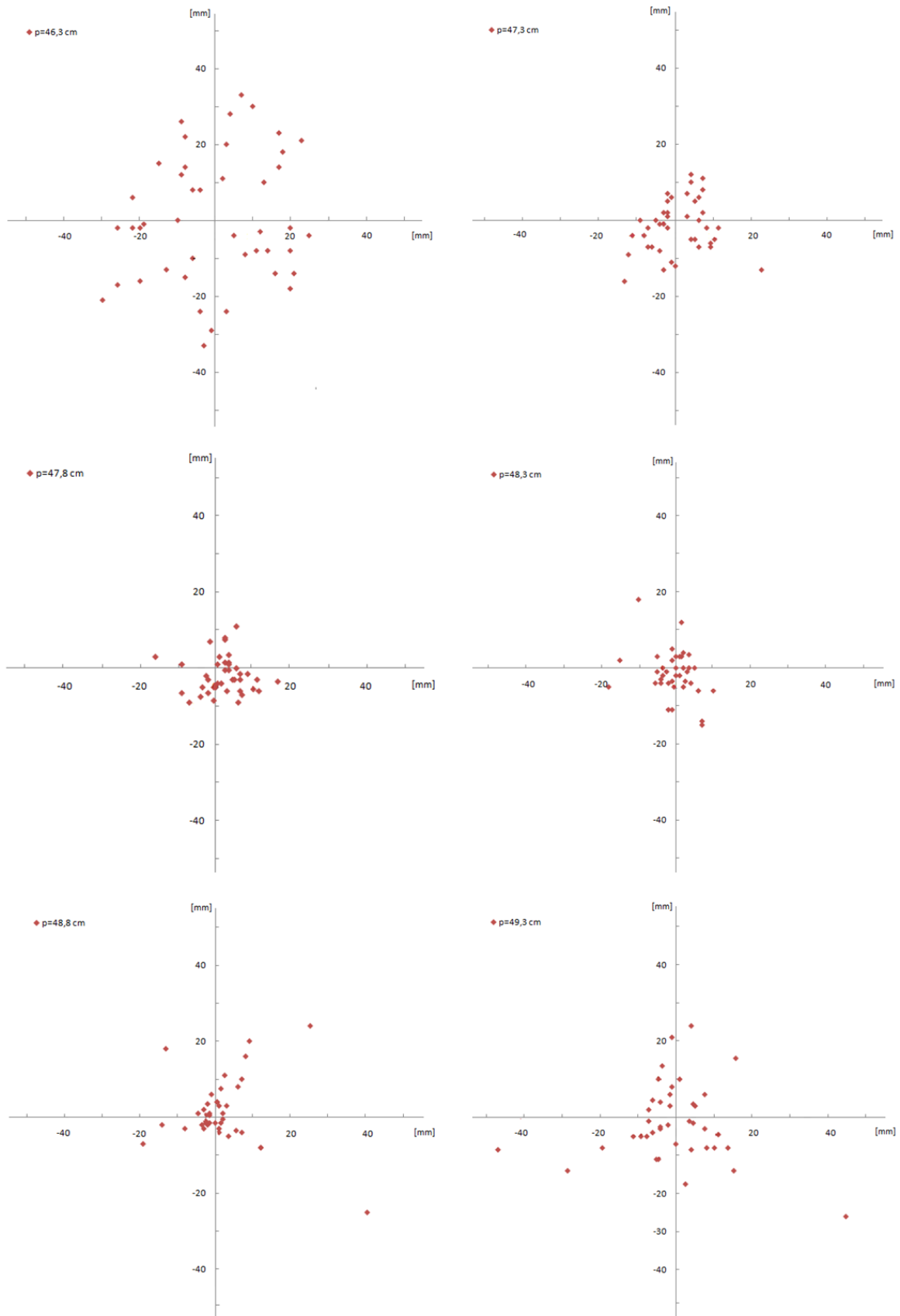


Figure 41 - Mapping of reflected laser beams at different elevations around the focal plane

4.5.3 70 mm SiC honeycomb absorber

This was the first absorber to be tested in Test Setup 2, where the absorber was positioned 46.3 cm above the reflector center. The same piece of monolith as used in Test Setup 1 was fitted tightly in the receiver with a strip of insulation wrapped around it making it both air tight and keeping the absorber in the right position. The thickness of the monolith was cut down to 40 mm, which was the honeycomb thickness for every test in TS2. To avoid the insulation to catch fire, its front part facing the reflector was covered with a high-temperature sealing compound. The compound has a curing time of 12 hours, but this recommendation was never taken into consideration. The compound also forced the air to flow through the absorber only. A set-screw was used to avoid the possibility of the absorber falling out of the receiver, which would have caused further damage to the reflector.

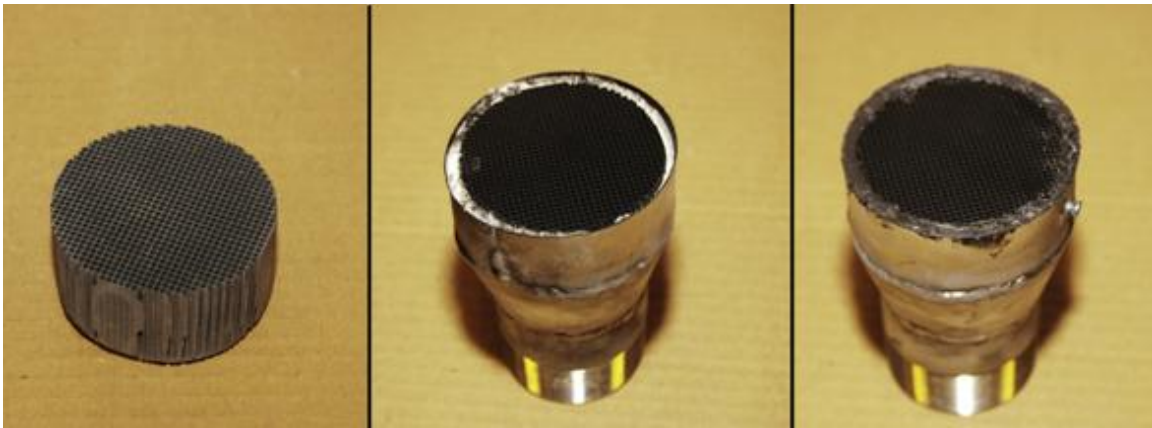


Figure 42 - Making of 70 mm SiC honeycomb receiver. Insulation was wrapped around the receiver at last.

Figure 43 shows the absorber exposed and a far more even distribution of the reflected rays may be observed. The few cold spots which may be seen are caused by minor deformations of the dish. The wire which touches the absorber is thermocouple T_3 . An underexposed photo of the absorber may be seen in Figure 40.



Figure 43 - 70 mm absorber illuminated.

4.5.4 70 mm fiber absorber

The suggestion regarding absorber thickness discussed in 4.3.1.1 was followed, but the M-value was adjusted upwards to about $M=2,0$, yielding an absorber weight of 7,5 gram constituting of four fiber mesh layers. The procedure of receiver construction was similar to that described in 4.3.4, where the same receiver as used for the 70 mm SiC honeycomb was taken in used to house the fiber. Due to the same opening diameter as the honeycomb absorber, the same position regarding distance p was used, which was 46,3 cm.



Figure 44 – Left: 70 mm fiber absorber positioned and ready for testing. Right: Underexposed picture of the absorber while illuminated.

4.5.5 50 mm SiC honeycomb absorber

The 50 mm honeycomb absorber was made in the same manner as the one explained in 4.5.3, but with the receiver depicted in the middle of Figure 38. With an absorber diameter of 50 mm the corresponding distance p was according to Figure 41 about $p=46,8$ cm, in which it was positioned. The picture to the right in Figure 45 shows the absorber illuminated, where the densest illumination is to be observed in the middle of the absorber.



Figure 45 - Left: 50 mm SiC honeycomb absorber before testing. Right: Underexposed picture of absorber during testing.

4.5.6 40 mm SiC honeycomb absorber

The 40 mm SiC honeycomb receiver was made exactly the same way as the foam receiver, which is shown in Figure 47. As the picture to left in Figure 46 shows, much of the reflected radiation entered the periphery of the absorber. The right picture shows, however, that the majority of the highest flux radiation entered the absorber.



Figure 46 - Left: 40 mm SiC honeycomb absorber during testing. Right: Picture showing areas with highest flux.

4.5.7 40 mm SiC foam absorber.

For the 40 mm absorbers simply a threaded welding socket was used to house the absorber. Just like any other receiver tested in Test Setup 2, one layer of insulation around the absorber was used in addition to one layer of insulation around the receiver.

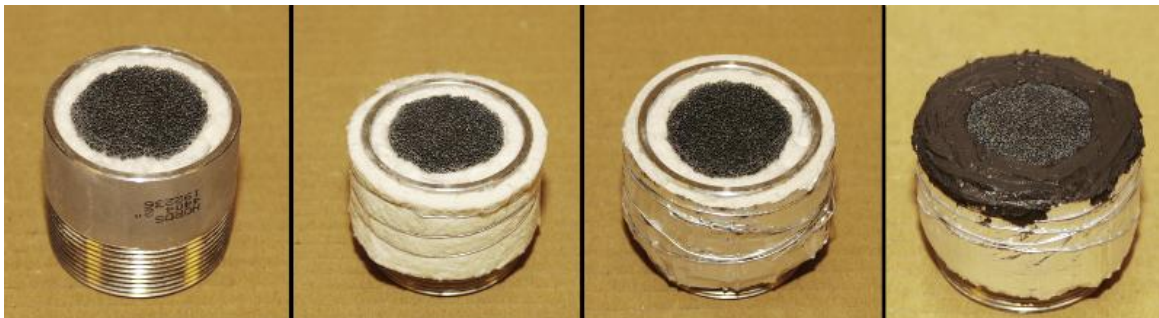


Figure 47 - Making of SiC foam absorber.

As the absorber diameter measured 40 mm a concentration factor of about $k=900$ was achieved. Due to a mistake during absorber positioning, it was located approximately 48 cm above the dish center, causing a far too small collection of rays at the absorber (see Figure 48). To the right in the figure the receiver position has been lowered to about 47.3 cm, where most of the absorber surface was illuminated.

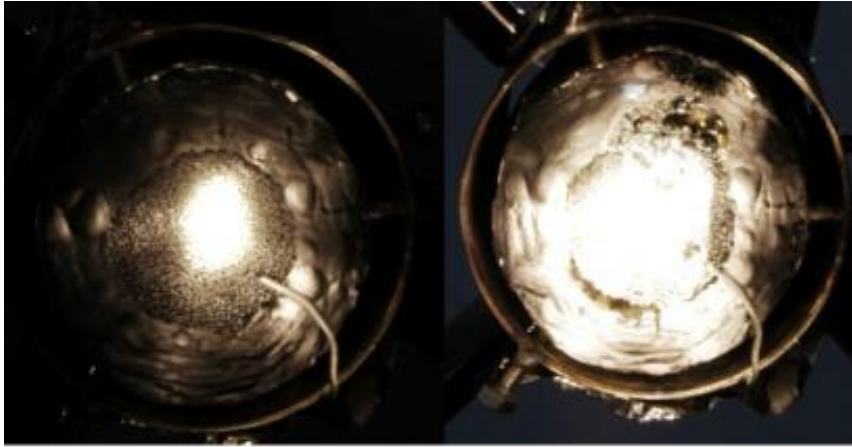


Figure 48 - Left: 40 mm foam absorber misplaced. Right: After repositioning.

Due to relatively high pressure fall through the air fan it was not able to suck ambient air through the absorber. Even though the air fan was adjusted to a power way higher than that used for any other absorber, it was not able to suck air through the foam at all. Combined with the initially wrong positioning parts of the absorber surface was exposed to relatively high solar flux.

5 Results and discussion

Two different small scale concentrating solar systems were deployed to test and compare absorbers in terms of shape, size and material. The purpose of the solar concentrating system is to heat air at temperatures above 220°C, which depends strongly on the absorbers ability to transfer heat to the adjacent air flowing through it.

The tests were performed in two different experimental setups; Test Setup 1 which was constructed to serve indoor testing purposes, and Test Setup 2 which was based on the flaws experienced with Test Setup 1. Each absorber was tested at different air velocities, and in each case the hot air temperatures were measured using two thermocouples (T_1 and T_2). A thermocouple was also located at the absorber surface (T_3). It is important to note that this thermocouple only represents a very local temperature and not the absorber surface temperature as a whole. Therefore T_3 is represented only to indicate an approximate surface temperature. For TS1 the absorbers were intended to be tested at 1 m/s, 1.5 m/s and 2 m/s. The temperature recording for the tests are given in Appendix A.

5.1 Example Test Setup 1 – 70 mm fiber absorber at 1.5 m/s

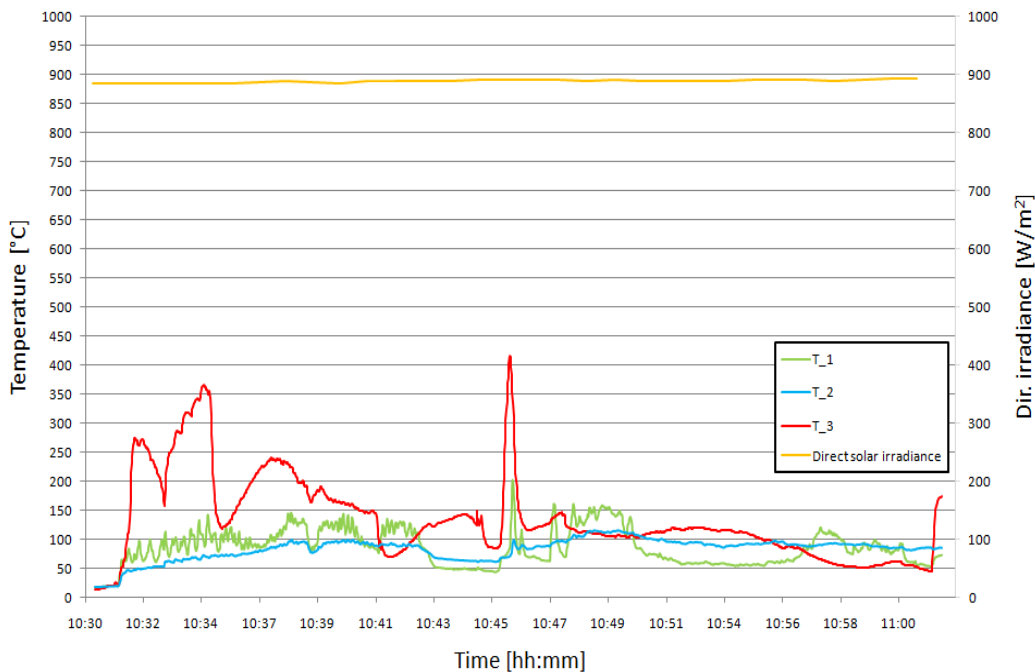


Figure 49 - 70 mm absorber employed in Test Setup 1 at 1.5 m/s air velocity.

As an example, test results for the 70 mm flat fiber absorber at an air velocity of 1.5 m/s is shown in Figure 49. As expected, the temperature profiles seem to vary significantly over time which is representing for the majority of the absorbers tested in TS1. Neither T_1 nor T_2 achieved the target temperature of 220°C, which also is the case for the other absorbers tested in TS1. The change in air viscosity and density resulted in air velocity change, and the fan needed to be adjusted accordingly which caused fluctuating air temperatures. This was the main source of error together with the uneven flux distribution at the absorber during tests in TS1. However, not every test carried out in TS1 resulted in uneven temperature profiles. T_3 varied significantly since it at certain times was occasionally illuminated by the concentrated reflected rays. The yellow line represents the direct solar irradiance, which was measured at Department of Physics, NTNU. The direct irradiance was measured by a pyrheliometer directed against the sun throughout the day.

In Figure 50, the temperature profiles for the 90 mm 3D absorber is shown, and the air temperatures are apparently kept at a more constant level than what is shown in Figure 49 for the flat fiber absorber. In this case the manual tracking has accidentally been carried out successfully, and the air fan was operating at a constant level. The air temperatures were kept constant at around 150°C and resulted in the most successful test which was carried out with TS1 (based on the average temperature between T_1 and T_2 during a time lapse of 30 minutes).

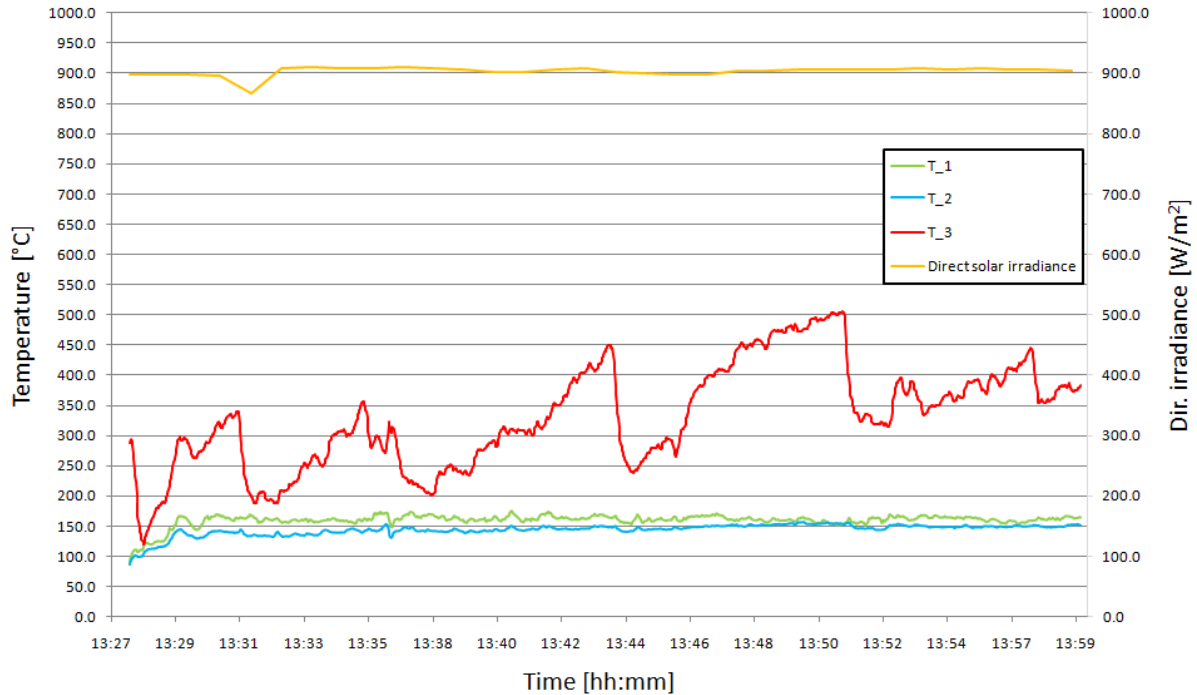


Figure 50 - 90 mm 3D absorber in TS 1 with 1 m/s air velocity.

5.2 Comparing absorber shapes – Test Setup 1

Opposite of what was expected based on Figure 50, the 90 mm 3D absorber shows surprisingly the poorest air temperature compared to the corresponding temperatures for the other absorbers tested in TS1 at 1.5 m/s (see Figure 51).

This underlines that the results from Test Setup 1 are not reliable and should therefore not be considered as conclusive. However, due to the low difference between the temperature profiles, the shape of the absorber does not seem to be of significance relatively to the flux density and the flux distribution striking the absorber.

As mentioned in chapter 4.3.5 the concave fiber absorber was tested with different number of fiber layers. The results will not be discussed due to great fluctuations of air velocity due to the air fan, but can be found in Appendix A.

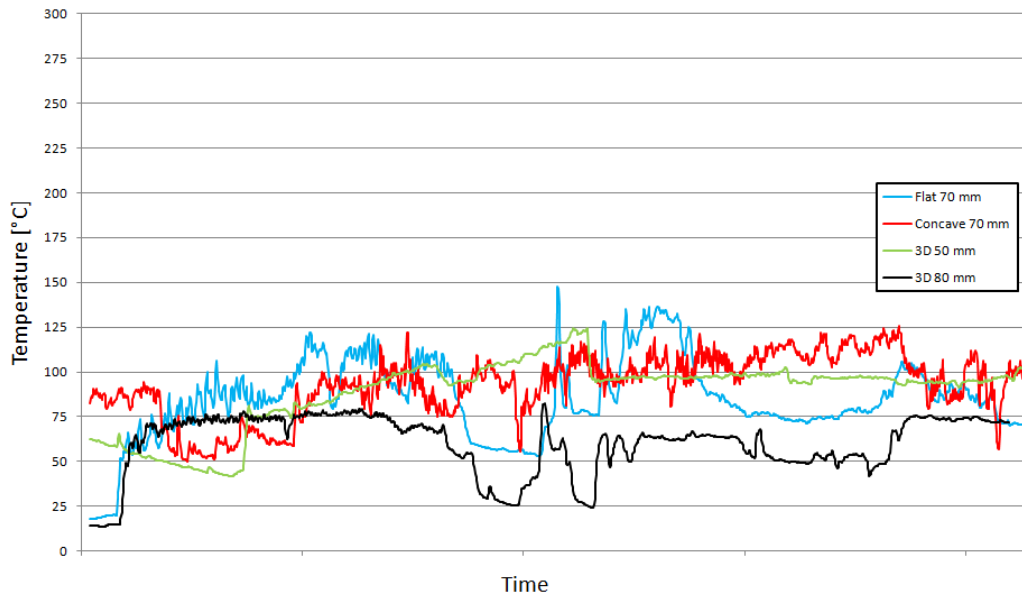


Figure 51 - Comparison of differently shaped fiber absorbers at 1.5 m/s in TS1. The curves represent the average temperature between T_1 and T_2 for each absorber.

The temperature fluctuations while running the experiment with Test Setup 1 outdoors are quite clear, according to Figure 49 and Figure 51. The fact that the system was divided into two parts, the reflector and the receiver rack being two independent systems, resulted in continually misplaced position of the absorber compared to the optimal position. By accident, T_3 equal to a surface value beyond 1050°C was logged occasionally with the 70 mm concave absorber in Test Setup 1, as shown in Figure 52.

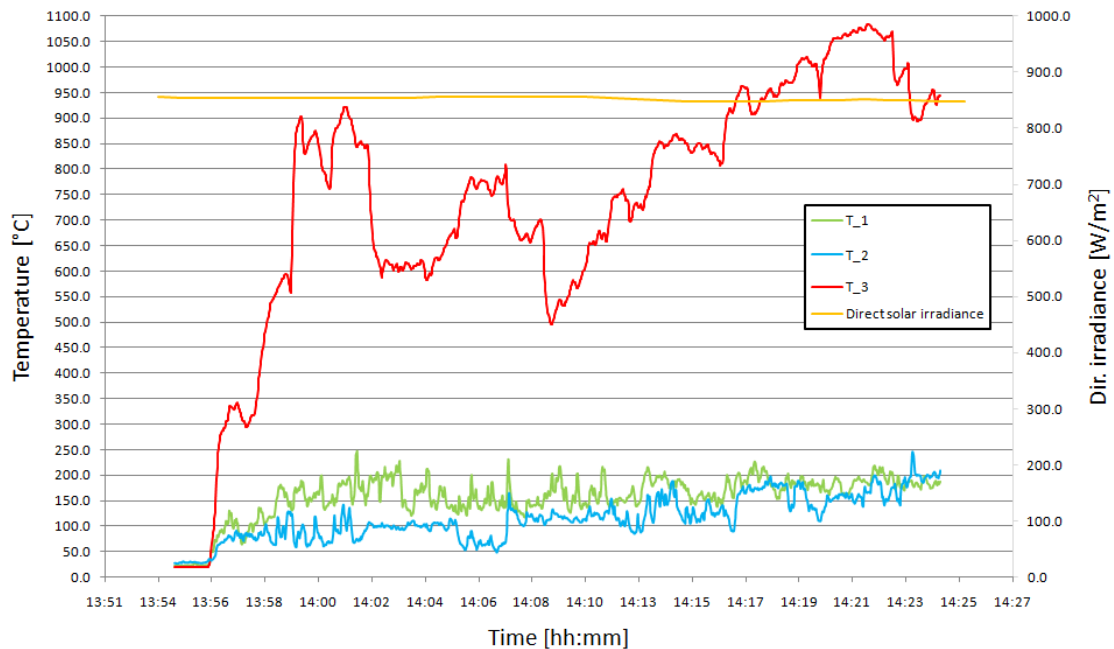


Figure 52 - 70 mm concave fiber absorber employed in TS1 with accidentally high temperature at the surface.

It is difficult to make quantitative use of the test results with TS1. For comparison, however, the results are given in Appendix A.

5.3 Comparison between indoor and outdoor testing

One test was carried out indoors with the flat 70 mm fiber absorber in Test Setup 1. Figure 53 combines the temperature profiles from indoor and outdoor testing at 1 m/s, where T_1 and T_3 are represented by black dashed and unbroken lines, respectively.

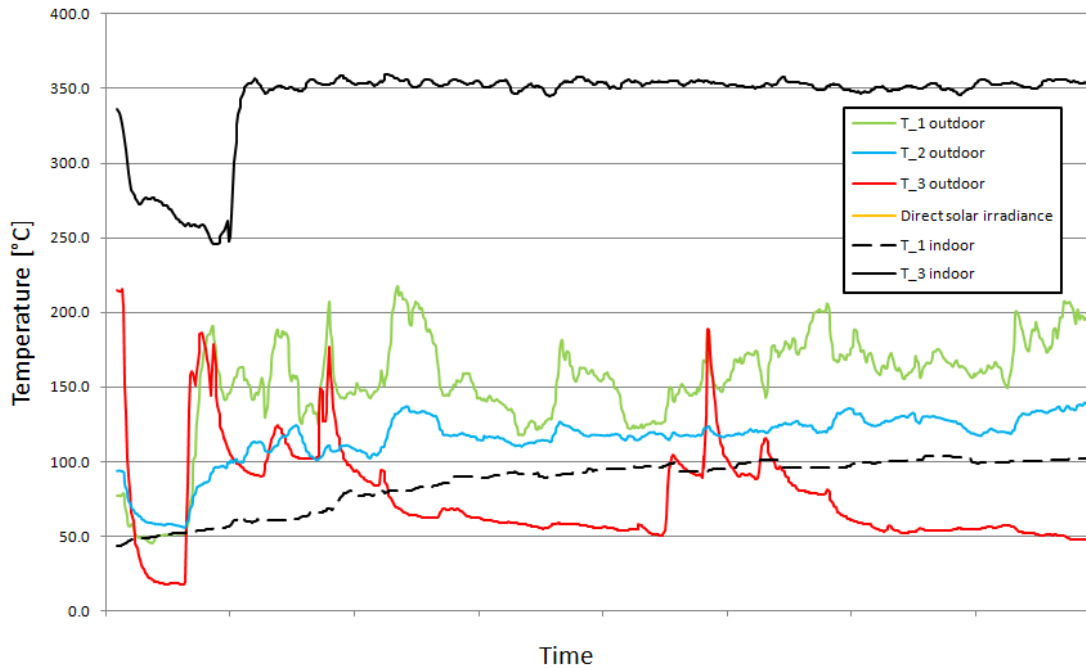


Figure 53 - Testing of 70 mm absorber at 1 m/s outdoors and indoors (black lines).

Due to technical difficulties during the indoor experiment, the logging only lasted for some 20 minutes. The tendency of the dashed line shows a flattening-out of T_1 at an estimated value of 110°C. “ T_3 indoor” reached a constant temperature relatively quickly after correct positioning of the thermocouple which can be seen on the graph. Due to the very thin fibers and fiber material, the low heat conduction within the absorber results in quick temperature rise. Even though the fiber also possesses the ability to cool down quickly, T_3 was kept at a very stable level. The stable temperature profiles representing the indoor testing may be caused by:

- Stationary located reflector and receiver, which provides for a constant heat flux entering the absorber over time.
- Constant radiation emitting from the lamp, which causes the phenomena discussed in the point above.
- Low air movement in front of absorber, which maintains the convection loss at a minimum over time.
- Due to stable temperatures the changes in viscosity and density are kept at a minimum over time, which keeps the course for the air fan on a stable level.

Due to more air movement outdoor than under the lamps the absorber was more exposed to convection loss. More exactly, the wind gusts passing by the absorber caused a varying loss which also is indicated by the fluctuating temperature profiles in Figure 53.

Using lamps turned out to not be a good replacement for the sun for testing purposes since they did neither emit parallel directed beams nor correspond to the solar heat flux density, which was discussed in 4.2.3. Due to the large opening angle the non-parallel directed rays reflected into a focal point above the focal point calculated in the case of parallel directed rays.

Using multiple lamps was also tested, but due to the direction of the rays multiple focal points were observed, instead of merged focal points as desired.

Since the testing conditions were kept constant indoor, testing for comparison purposes between different absorbers could have been carried out. However, testing outdoor generates more realistic results to determine whether a specific absorber can work for the solar oven, and provide air temperatures above 220°C.

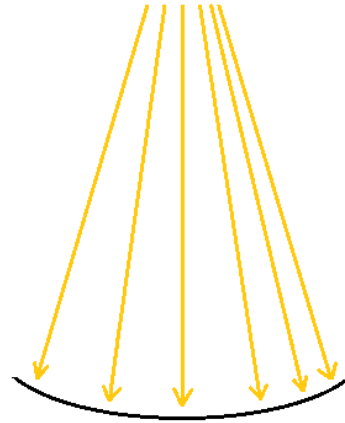


Figure 54 – Non-parallel directed lamp radiation striking the reflector.

5.4 Example Test Setup 2 – 50 mm honeycomb at 2 m/s

Figure 55 illustrates the temperature profiles for the 50 mm honeycomb absorber tested with TS2. T_3 is quite fluctuating despite of the solar tracking system, while T_1 and T_2 are kept at a constant level after initiating the test. In this case the air temperature entered a constant level at about 240°C after some 10 minutes. Reaching a temperature of 240°C, the target temperature of 220°C has been achieved and even exceeded.

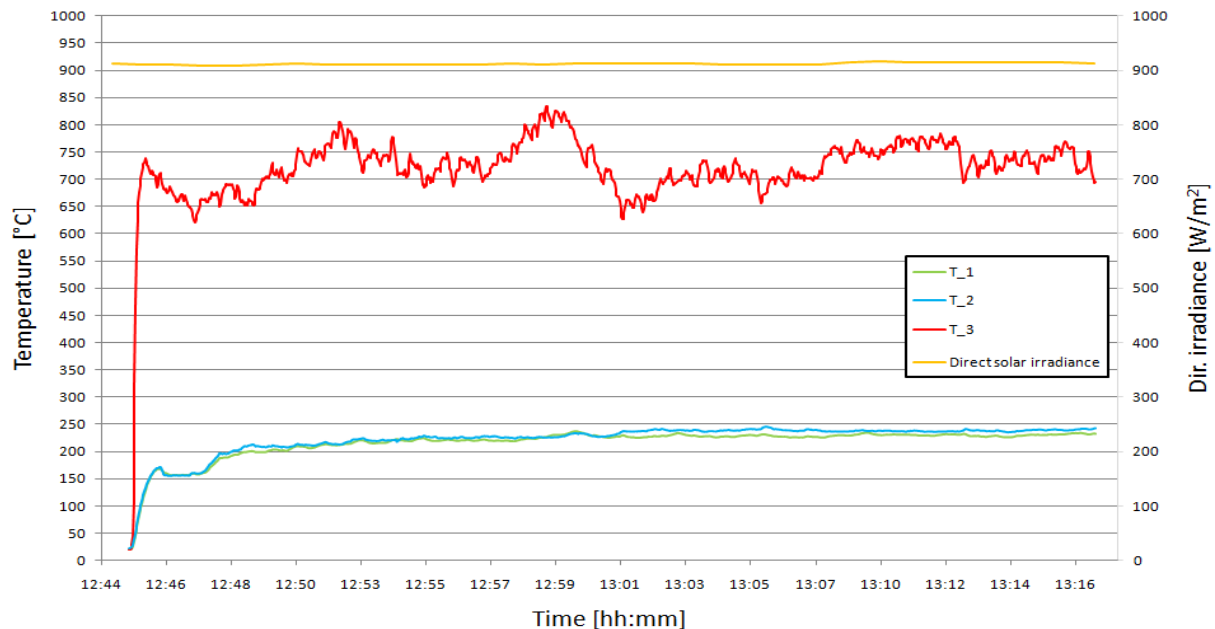


Figure 55 - 50 mm honeycomb absorber tested at 2,0 m/s air velocity.

5.5 Comparison of different air velocities – Test Setup 2

Most of the absorbers employed in TS2 were tested at 1 m/s, 2 m/s and 4 m/s. The absorbers were tested for different air velocities for two reasons:

1. See the correlation between air temperature and air velocity
2. Discover which air velocity that resulted in the highest energy output

Figure 56 shows the air temperatures at 1 m/s, 2 m/s and 4 m/s for the 50 mm honeycomb absorber with the corresponding absorber surface temperatures. Since the three tests were not carried out simultaneously, the time values along the x-axis are removed. The time lapse shown is about 30 minutes. The solar irradiance did not differ significantly during the three tests and had a value around 900 W/m². The actual time and the data for the direct solar irradiance may be found for each test which is represented in appendix A. The tests were employed with TS2.

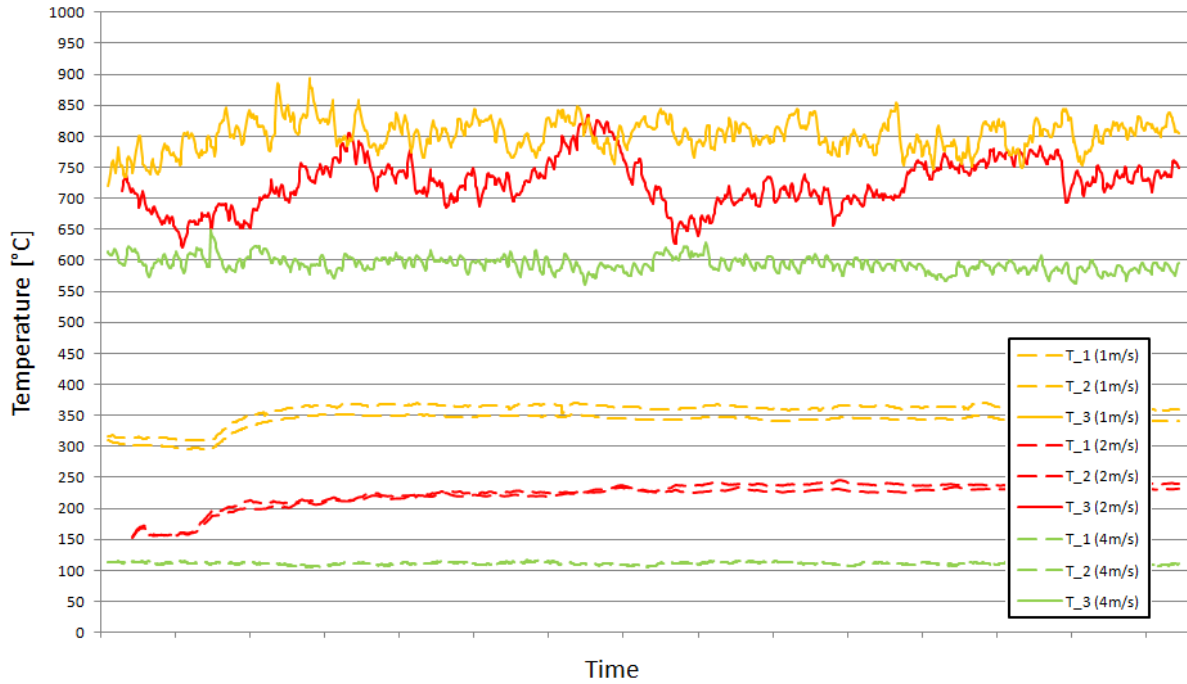


Figure 56 - Surface and air temperatures at 1 m/s, 2m/s and 4 m/s for 50 mm honeycomb absorber, Test Setup 2. Dashed lines represent the air temperatures, and the unbroken lines with the corresponding color indicate the absorber surface temperatures.

As expected, a decrease in air temperature (dashed lines) occurred as the air velocity increased since the absorber gets cooled down with more ambient air flowing through it. The reason for the very fluctuating T_3 recorded at 2 m/s was the location of the thermocouple, as it was located just on a boundary between high- and relatively low-flux areas. Therefore a small movement from the tracking system caused the thermocouple to switch between the hot and the relatively colder areas. However, due to a small change in location for T_3 at 4 m/s, a less fluctuating temperature may be observed.

The increase of energy content for the air during heating can be based on (1.2), where Q denotes the change in heat content (W) for the air flowing through the absorber and \dot{m} represents the air mass flow (kg/s) measured at the fan outlet.

$$Q = \dot{m} \cdot c_p \cdot \Delta T \quad (1.2)$$

ΔT represents the temperature difference between the average of T_1 and T_2 (during a time lapse of 15 minutes) and the surrounding temperature T_{surr} (assumed to be 20°C during each test). Air heat capacity c_p and air density ρ are found in tables with properties of air at 1 atm pressure as a function of the air mean temperature, according to (1.3).

$$\rho, c_p = f\left(\frac{T_{surr} + (T_1 + T_2)/2}{2}\right) \quad (1.3)$$

An extended version of (1.2) which was employed for calculation of Q is shown in (1.4), where V_{pipe} denotes the air velocity measured at the air fan outlet.

$$Q = \rho_{mean} \cdot A_{pipe} \cdot V_{pipe} \cdot c_{p,mean} \cdot [(T_1 + T_2) / 2 - T_{surr}] \quad (1.4)$$

In the case of the 50 mm honeycomb absorber, the heat output Q was calculated based on the numbers represented in Table 5. The calculated energy output Q and the efficiency η are shown at the bottom of the table and the appurtenant formulas are to be found in appendix B.

Table 5 – Calculation of energy output and efficiency.

Air velocity, V_{pipe} [m/s]	1	2	4
Pipe area, A_{pipe} [m ²]	19.6*10 ⁻⁴	19.6*10 ⁻⁴	19.6*10 ⁻⁴
Avg (T_1, T_2) [°C]	353	234	111
T_{surr} [°C]	20	20	20
ΔT [K]	333	214	91
(Avg (T_1, T_2)+ T_{surr})/2 [°C]	187	127	66
c_p [J/kgK]	1056	1011	1007
ρ [kg/m ³]	0.78	0.90	1.06
Dish area, A_{dish} [m ²]	1.07	1.07	1.07
Irradiance, I [W/ m ²]	908	912	893
Flowrate [kg/s]	1.5*10⁻³	3.5*10⁻³	8.3*10⁻³
Q [W]	536	761	760
η [-]	55 %	78 %	79 %

The efficiency η indicates the ratio between the calculated Q and the direct solar irradiance I striking the reflector, according to (1.5). In this case η is based on the average solar irradiance during the same time lapse as for the averaged temperatures, which must be multiplied with the aperture area of the parabolic dish of 1,07 m².

$$\eta = \frac{Q}{I \cdot A_{dish}} \quad (1.5)$$

The efficiency for the 50 mm honeycomb absorber seems to be lowest at 1 m/s, which may be explained by higher radiation and convection loss from the absorber due to a higher surface temperature T_3 . Table 5 shows also that the tests were carried out under the same conditions and the same settings except for the air velocity. However, the air velocity was measured at the fan outlet, which means after the air is heated up. Due to the manner of operation of the air velocity meter discussed in 4.2.6, it is not sensible for important property changes such as density drop due to temperature rise. Therefore the mass flow is based upon crude approximations regarding air velocity, since the error increases with the air temperature. A mass flow meter would be a better and more reliable instrument to use than the air velocity meter.

At 4 m/s, the efficiency is high but the air temperatures are not suitable to serve cooking purposes due to the low values. Yet the efficiency at 2 m/s still is 78 %, the air temperature of around 230°C is sufficient for cooking purposes.

5.6 Comparison of different concentration factors – Test Setup 2

Figure 57 represents the air temperatures for the honeycomb absorber tested at 2 m/s and opening diameters of 7 cm, 5 cm and 4 cm, respectively $k=300$, $k=600$ and $k=900$. The temperatures are averaged between T_1 and T_2 in each case, and the direct irradiance was about 900 W/m^2 , except in the case for the smallest absorber where the irradiance was around 800 W/m^2 . The time lapse along the x-axis is about 30 minutes.

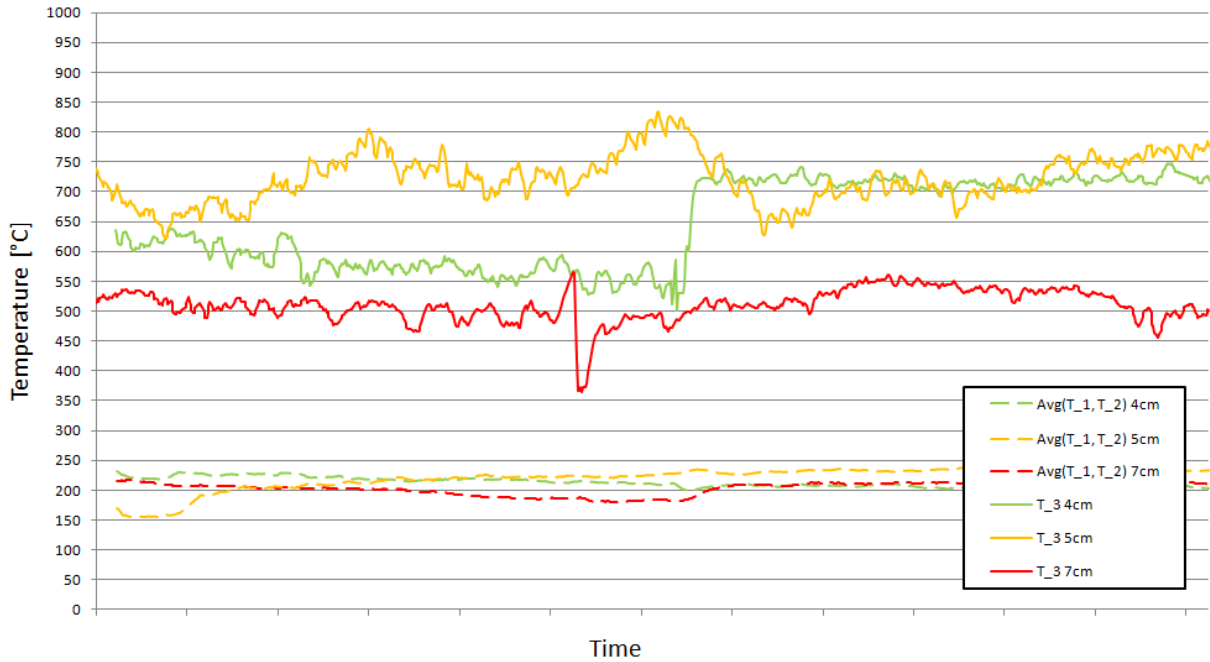


Figure 57 - Comparison of honeycomb absorbers with diameter of 4 cm, 5 cm and 7 cm at 2 m/s in TS2.

Keeping in mind that the air velocities are measured at the exit of the air fan, the inflowing air velocity to the absorber must increase as the cross sectional absorber area decreases with increasing k . As discussed in 5.5, the correlation between air velocity through the absorber and the output temperature was clear, and is the reason for that the temperature profiles in Figure 57 do not show a greater difference. Due to this issue, the comparison of their respective energy increase Q and efficiency η does not necessarily lead to any conclusive results regarding change in the concentration factor.

Table 6 - Energy rise and efficiency at different concentration factors and air velocity of 2 m/s.

Concentration ratio	300	600	900
Q [W]	667	741	681
η [-]	0.7	0.76	0.79

Another source of error is also the way of mass flow measurement which is discussed in the previous chapter. However, according to Figure 57 the absorber at $k=600$ yielded the highest air temperature, despite of a higher inflowing velocity of air than for the $k=300$.

The reason for the surprisingly low temperature for the smallest absorber, in addition to the high local mass flow through the absorber and irradiance of 800 W/m^2 , may be the difficulties of illuminating the absorber correctly and the high radiation loss which occurred at high T_3 .

As expected, T_3 for the 70 mm absorber showed a lower value than that for the 50 mm and 40 mm absorbers. On the other hand, T_3 for the 50 mm has a greater value than that for the 40 mm. This also may have been caused by the increasing air velocity with decreasing absorber area. The same occurred at 1 m/s and 4 m/s with the discussed absorbers, which can be seen in Appendix A.

Another absorber with 40 mm diameter was the foam absorber, which had a pressure drop too large for the air fan to suck air through it. The air temperature reached about 250°C , but due to the pressure drop the air flow out of the air fan could not be measured no matter which power the fan was adjusted to.

5.7 Fiber versus honeycomb

Figure 58 shows the averaged air temperatures (between T_1 and T_2) with air velocity at 1 m/s for honeycomb and fiber at 70 mm, meaning a concentration factor of about $k=300$. The relatively slower increase for the fiber absorber is caused by regulation of the air fan at the start of the experiment. The air temperatures in this case were exceeded only by the air temperature achieved with the 50 mm honeycomb absorber at 1 m/s.

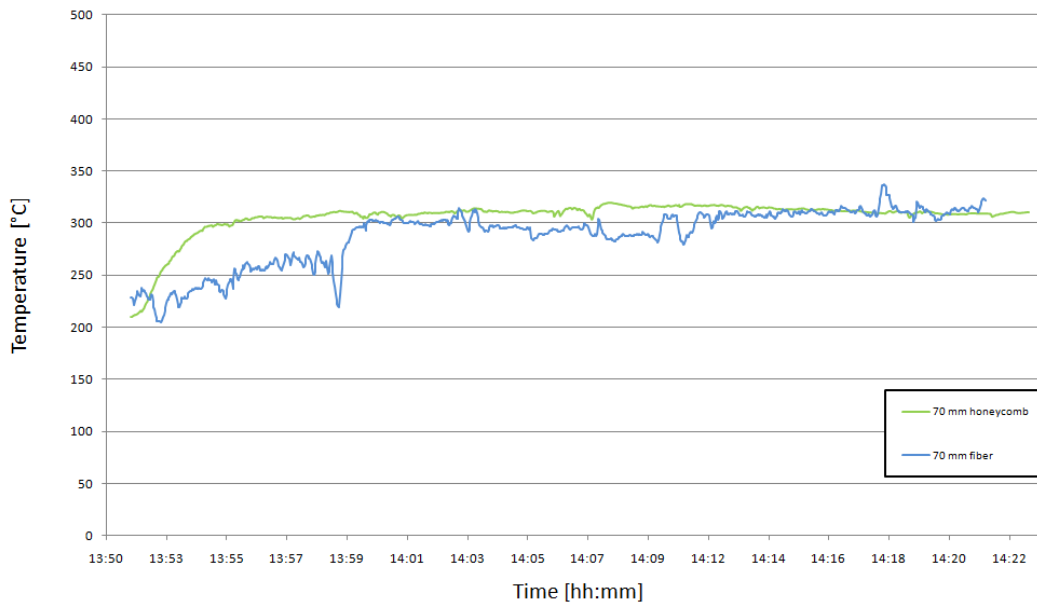


Figure 58 - Averaged air temperatures for 70 mm honeycomb and 70 mm fiber mesh.

With temperature profiles exceeding 300°C, both of the absorbers seem to be applicable for cooking purposes. However, material durability and ability to resist heat must also be taken in consideration. Even though the temperatures that were achieved may be described as successful, the energy output and efficiency are lower than seen in sections 5.5 and 5.6.

Table 7 - Air heat increase and heat transfer efficiency for 70 mm honeycomb and fiber absorber.

Absorber	70 mm honeycomb	70 mm fiber
Flow rate [kg/s]	$1.6 \cdot 10^{-3}$	$1.6 \cdot 10^{-3}$
Q [W]	474	458
η [-]	0.5	0.48

5.8 Absorber wear



Figure 59 - Left: 70 mm flat absorber tested at TS2. Right: 80 mm 3D absorber tested at TS1.

Although the absorbers were tested for only a maximum of about 5 hours, wear of the absorbers was already observable especially for those tested in TS1. As shown to the right in Figure 59, the uneven flux distribution caused damage to the absorber; more specifically burned holes in the fiber and melted the steel netting. Every absorber exposed in Test Setup 1 was damaged after testing, except from the honeycomb absorber.

Absorbers with $k=300$ tested in TS2 did not experience the same local heat fluxes as in TS1. Therefore the only change after exposure was some signs of faded paint, which can be seen to the left in Figure 59 (grey areas). This may be either caused by the heat the absorber was exposed for, or the high radiation flux.



Figure 60 - Left: 40 mm foam absorber after testing. Right: 40 mm honeycomb after testing.

Due to the pressure-drop through the foam absorber the surface was not cooled down and holes were burned. This was also due to the initially misplacement of the absorber. In the case of the 40 mm honeycomb absorber, the wear seen on the surface to the right in Figure 60 is due to the paint which did not seem to resist the test conditions. Also, the sealing compound turned crispy and eventually fell off. This is might due to the neglected curing time. The honeycomb absorber itself did

not seem to be affected by the heat generated at a concentration ratio of $k=900$. Extended testing in terms of material durability of the SiC honeycomb absorber was not carried out, since it has been tested through a period of more than 182 hours, providing air temperatures above 700 in previous tests [7].

In order to determine the fibers ability to withstand the high temperatures, it should be tested for a longer period of time. Although the fiber mesh did not suffer from any damage after testing in Test Setup 2, its durability can yet not be determined.

5.9 Heat losses during testing

The intention of locating the thermocouples T_1 and T_2 by the pipe bend (both for TS1 and TS2) was to minimize the risk of the air to be cooled significantly after leaving the absorber. At the same time some mixing of the air after leaving the absorber was also desired before measuring the temperature.

Figure 61 indicates the heat losses for Test Setup 2. The red arrow indicates the conductive heat transfer, where heat is transferred inside the steel pipe wall from the receiver end of the pipe towards the fan end of the pipe. Since the steel pipe was not insulated the last 70 cm before the fan, heat loss in terms of convection and radiation occurred especially in this area. This is shown by the bold yellow arrows. The pipe losses in especially TS1 could have been reduced by shortening the steel pipe.

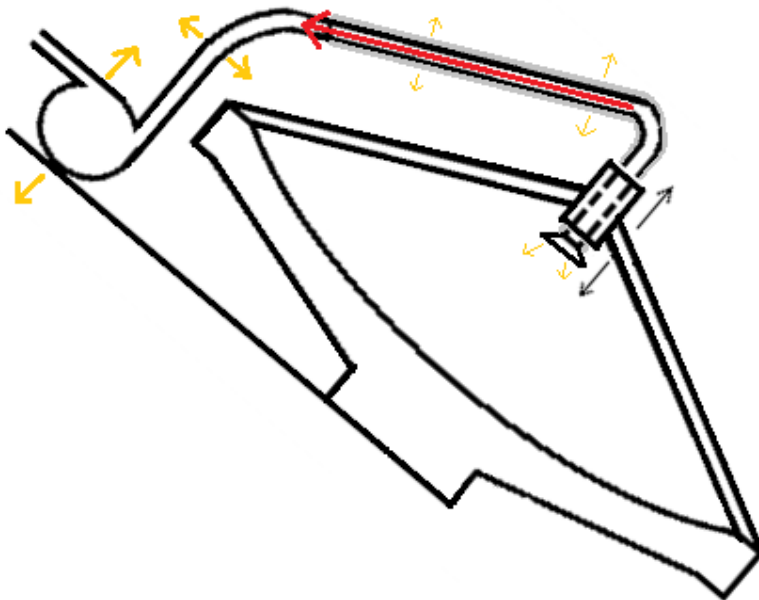


Figure 61 - Heat losses for Test Setup 2.

Some heat penetrated through the insulation also, from where it was transferred to the surroundings through convection and radiation. This is shown by the small yellow arrows by the pipe. If the test setup were to be connected to any heat storage, the pipe must be insulated all the way, preferable with two layers of insulation to prevent unnecessary heat loss.

As discussed in chapter 5.1 through 5.7, heat loss finds place on absorber also due to the high temperatures achieved at the absorbers surface.

Other losses which affects the TS1 and TS2 efficiency:

- The reflector was not perfectly shaped. Therefore a non-perfect distributed radiation flux stroke the absorber, creating local cold and hot spots. This was improved significantly when constructing Test Setup 2.
- The film attached to the parabolic dish had a solar reflectance of 93 %, creating 7 percentage-points optical loss. In addition the film was not perfectly attached to the dish, both in terms of covering the whole dish and small unevenness due to air bubbles.

6 Conclusion

The target air temperature of 220°C has been exceeded for air passing through heat absorbers positioned in the focal point of a parabolic solar collector. With a reflector aperture area of 1.07 m² and a concentration ratio of 300 and higher, stable air temperatures exceeding 300°C were achieved with 3 different absorbers at sufficiently low air flow rate through the absorber, showing that the target temperature of 220°C can be achieved with a good margin as long as the test rig is constructed with adequate accuracy.

The heat absorbers were tested in two laboratory setups. An indoor setup using a lamp as light source provided too low power. Outdoor tests were improved in a second setup, including an automatic solar tracking system. The factors that seem to be crucial for achieving high air temperatures are mainly an even distribution of the reflected radiation striking the absorber and a sufficiently high concentration ratio. As expected, the air temperature increased as the flow rate was adjusted down.

A stainless steel fiber mesh absorber worked just as well as a silicon carbide honeycomb monolith absorber at a concentration factor of 300, yet the material costs are quite lower than that for the honeycomb. However, the fiber mesh suffered occasionally damage in terms of melting at local spots during testing in Test Setup 1, but no sign of damage occurred as it was employed in Test Setup 2. The honeycomb has been tested extensively as absorber in solar towers without any sign of damage due to high temperatures and may with assurance be applied as absorber for small scale concentrating thermal solar systems.

The tests has shown that it is feasible to arrive at high temperatures (250°C -300°C) in a small scale concentrators with air as heat transfer medium .

1. *Background NUFU Solar*. 2006 [cited 2006; Available from: <http://www.ntnu.no/ept/nufusolar/background>.
2. Initiative, A.M.S. *Parabola Design Wood Model*.
3. GmbH, D.M., *Material data sheet: STAX Stainless Steel Fibres 1.4841*, M.d.s.S.S.S.F. 1.4841, Editor. 2003.
4. Armines, M.P. *Yearly mean irradiance in the world*. 2006; Available from: http://www.soda-is.com/img/carte_Ed_13_world.pdf.
5. Alexopoulos, S. and B. Hoffschmidt, *Solar tower power plant in Germany and future perspectives of the development of the technology in Greece and Cyprus*. *Renewable Energy*, 2010. 35(7): p. 1352-1356.
6. Fend, T., et al., *Porous materials as open volumetric solar receivers: experimental determination of thermophysical and heat transfer properties*. *Energy*, 2004. 29(5-6): p. 823-833.
7. Agrafiotis, C., et al., *Evaluation of porous silicon carbide monolithic honeycombs as volumetric receivers/collectors of concentrated solar radiation*. *Solar Energy Materials and Solar Cells*, 2007. 91(6): p. 474-488.
8. Stobbe, P. *Stobbe Tech Ceramics A/S material data sheet*. 2000; Available from: http://stobbe.com/research/solar/spec/mds_mono.asp.
9. Schwarzer, K. and M. da Silva, *Characterisation and design methods of solar cookers*. *Solar Energy*, 2008. 82(2): p. 157-163.
10. Telkes, M., *Solar cooking ovens*. *Solar Energy*, 1959. 3(1): p. 1-11.
11. Karni, J., et al., *The "Porcupine": A Novel High-Flux Absorber for Volumetric Solar Receivers*. *TRANSACTIONS-AMERICAN SOCIETY OF MECHANICAL ENGINEERS JOURNAL OF SOLAR ENERGY ENGINEERING*, 1998. 120: p. 85-95.
12. M. Karlsen, S.S., S.O. Edvardsen, *Konsentrerende solfanger med varmelager*. 2010, HiST. p. 65.
13. Prakash, M., S. Kedare, and J. Nayak, *Investigations on heat losses from a solar cavity receiver*. *Solar Energy*, 2009. 83(2): p. 157-170.
14. ReflecTech®. *ReflecTech® Mirror Film*. 2011; Available from: <http://www.reflectechsolar.com/technical.html>.
15. Drangsholt, F., *Sintef report STF15 "Solsimulator"*. 1985, Sintef.
16. Aerogels®, A. *Aspen Aerogels® Datasheet*. 2010; Available from: http://www.aerogel.com/products/pdf/Pyrogel_XT_DS.pdf.
17. Løvseth, J., *Receiver for air based solar oven planned at EMU*. 2011.
18. Dupli, M. *Technical Information Heat-resistant Spray*. 2011; Available from: http://www.motipdupli.de/index.php?id=tm_1369&L=2.
19. Tolmer. *HMS Datablad Ovnskitt-HTSC1100*. 2007; Available from: http://www.tolmer.no/pdf_filer/hms/ovnskitt.pdf.
20. Ellen Stølen, K.B., Liv Marit Hustad, Mads Aas, Vgard Storm, *Two-axis solar concentrator*. 2011, Høgskolen i Sør-Trøndelag: Trondheim.

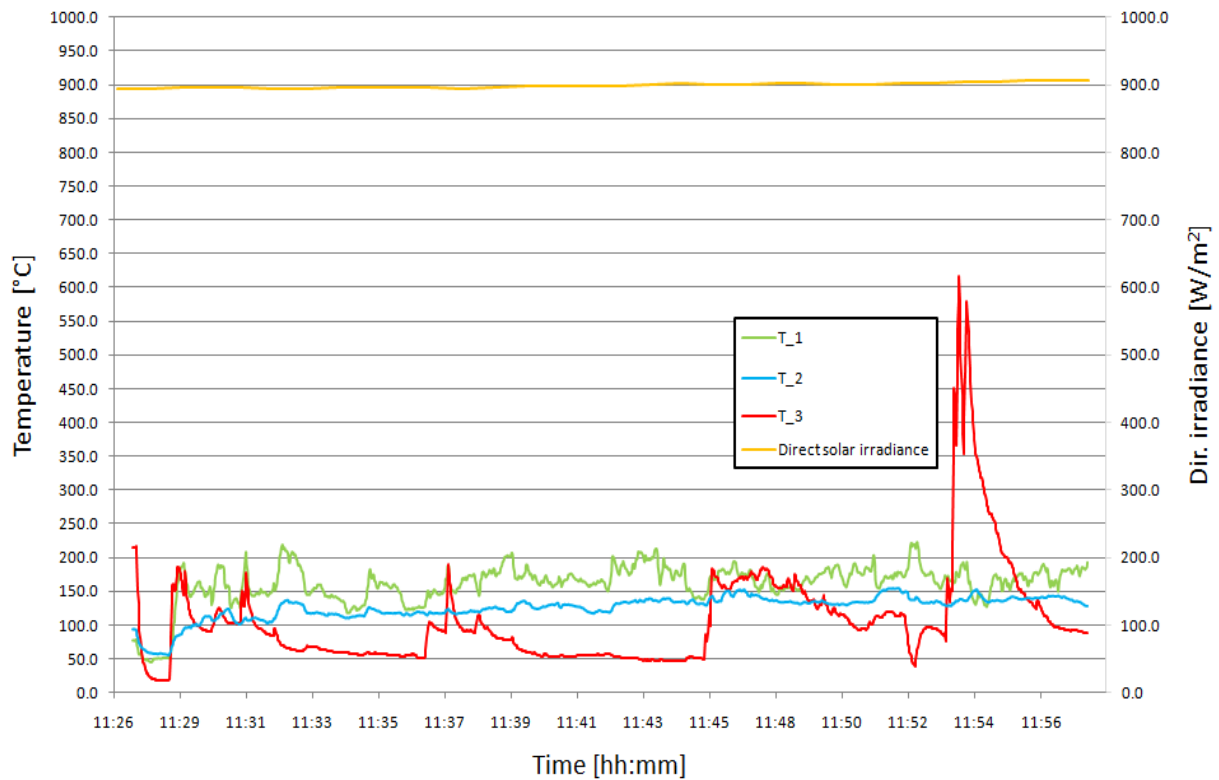
7 Appendix A

In this appendix graphs for each absorber at each air velocity are shown. Each graph depicts the direct solar irradiance (W/m^2), temperature adjacent to the absorber surface (T_3), and the air temperatures after heated up by the absorber (T_2, T_3). 7.1 and 0 contain respectively the temperature graphs for Test Setup 1 and Test Setup 2.

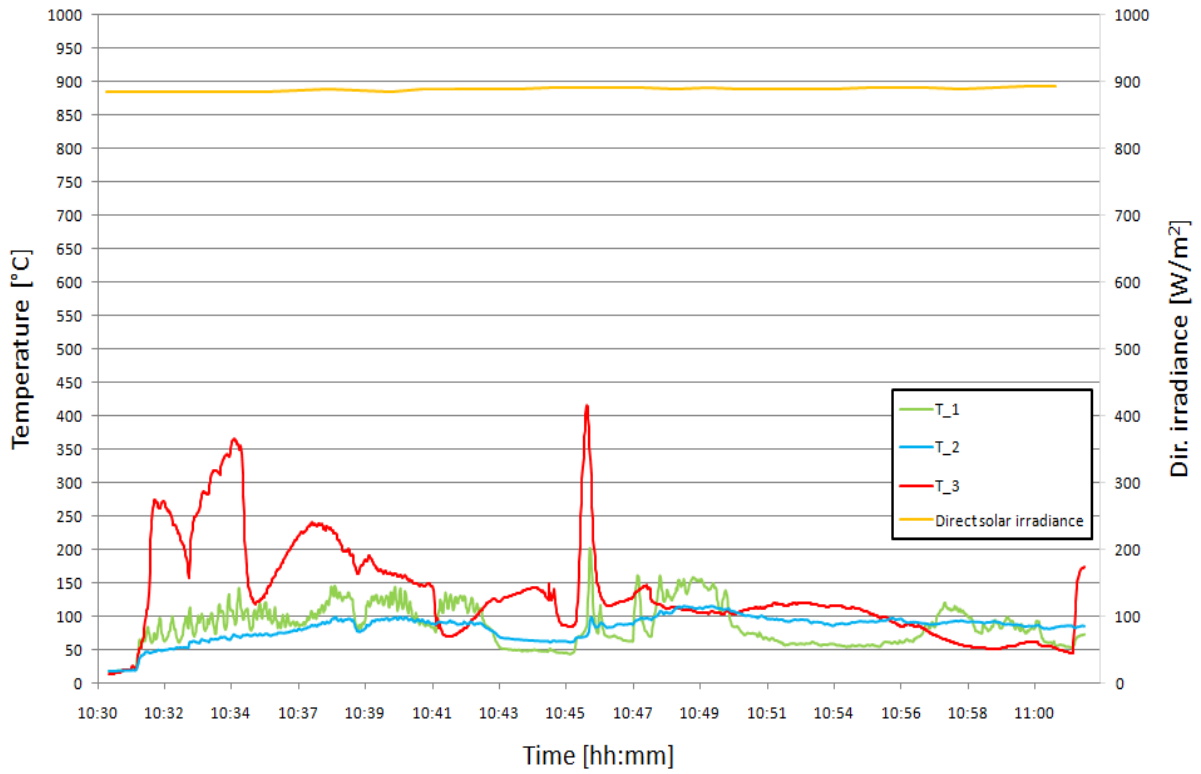
7.1 Test Setup 1

7.1.1 Flat 70 mm fiber absorber

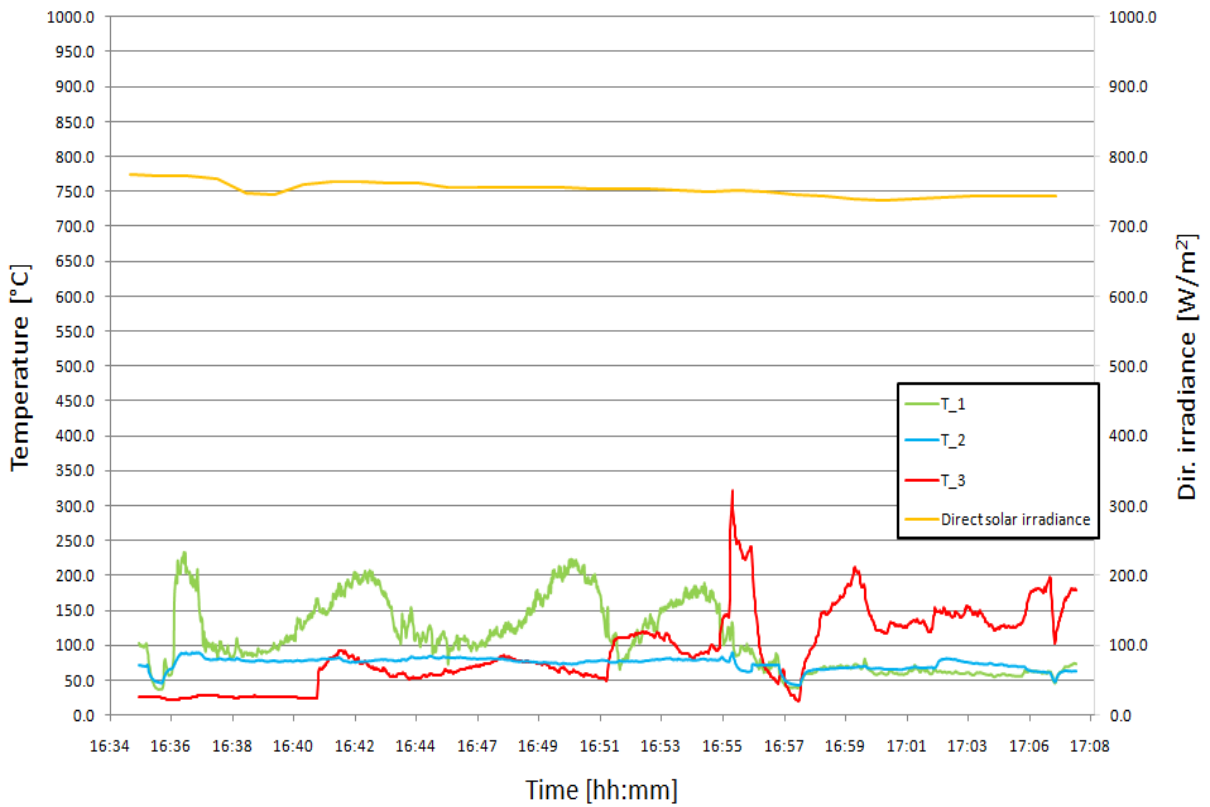
7.1.1.1 1,0 m/s



7.1.1.2 1,5 m/s

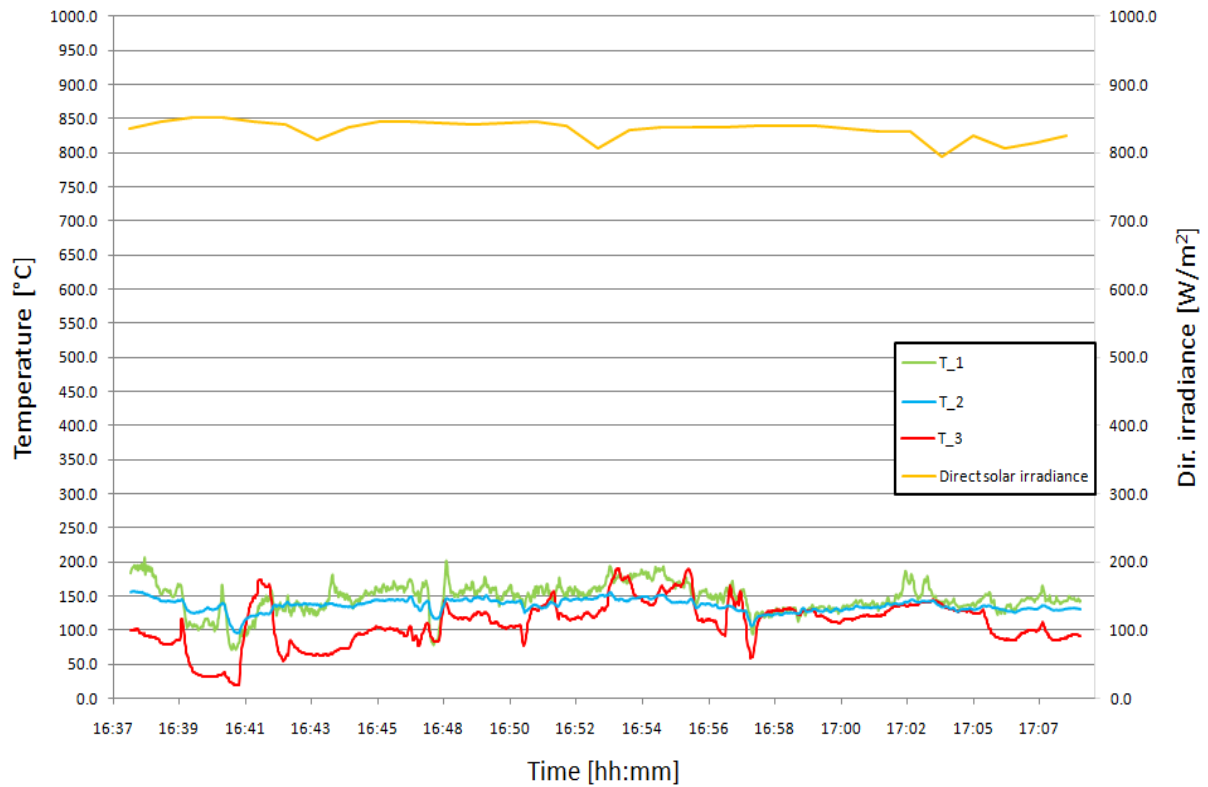


7.1.1.3 2,0 m/s

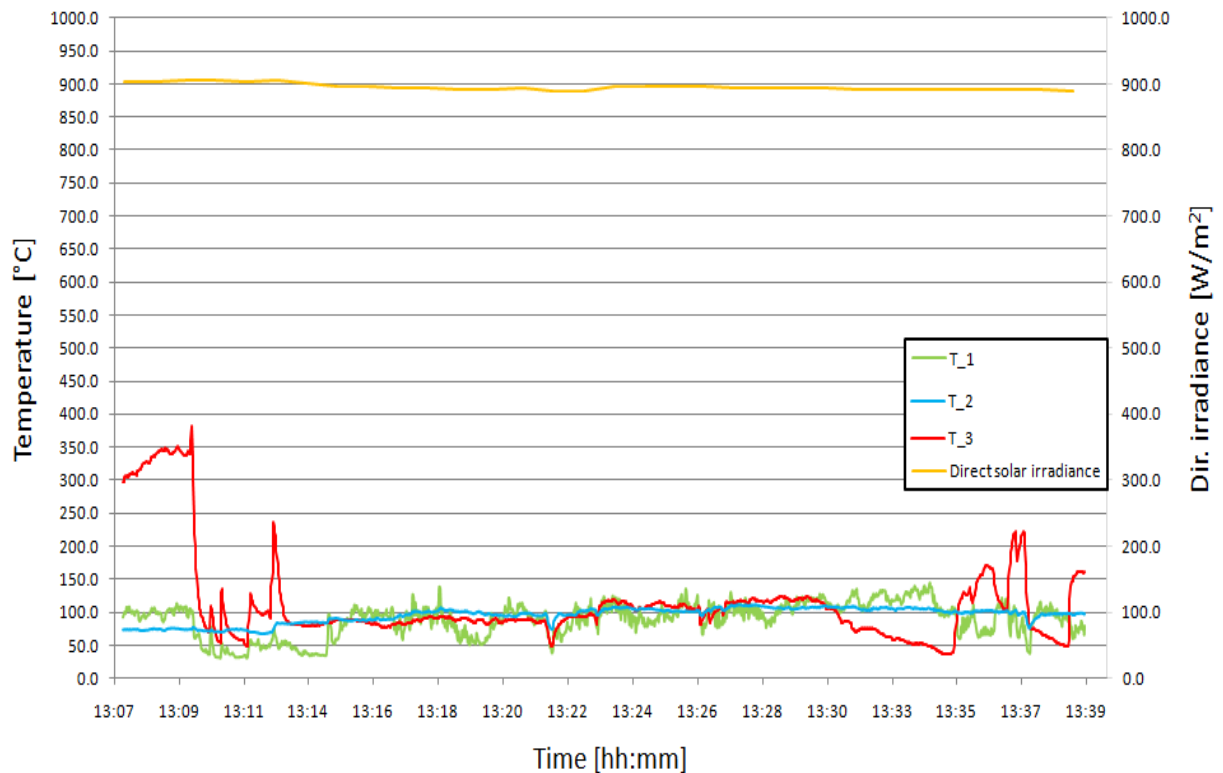


7.1.2 Concave 70 mm fiber absorber

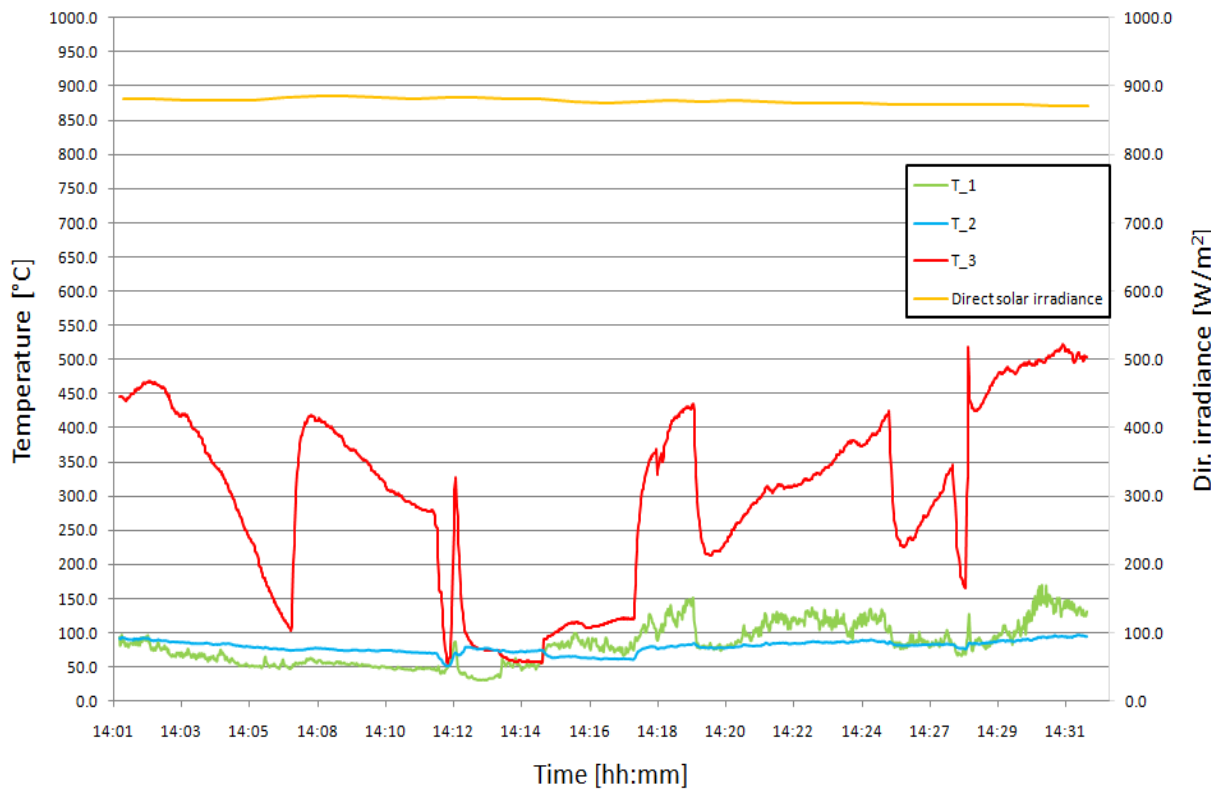
7.1.2.1 1,0 m/s



7.1.2.2 1,5 m/s

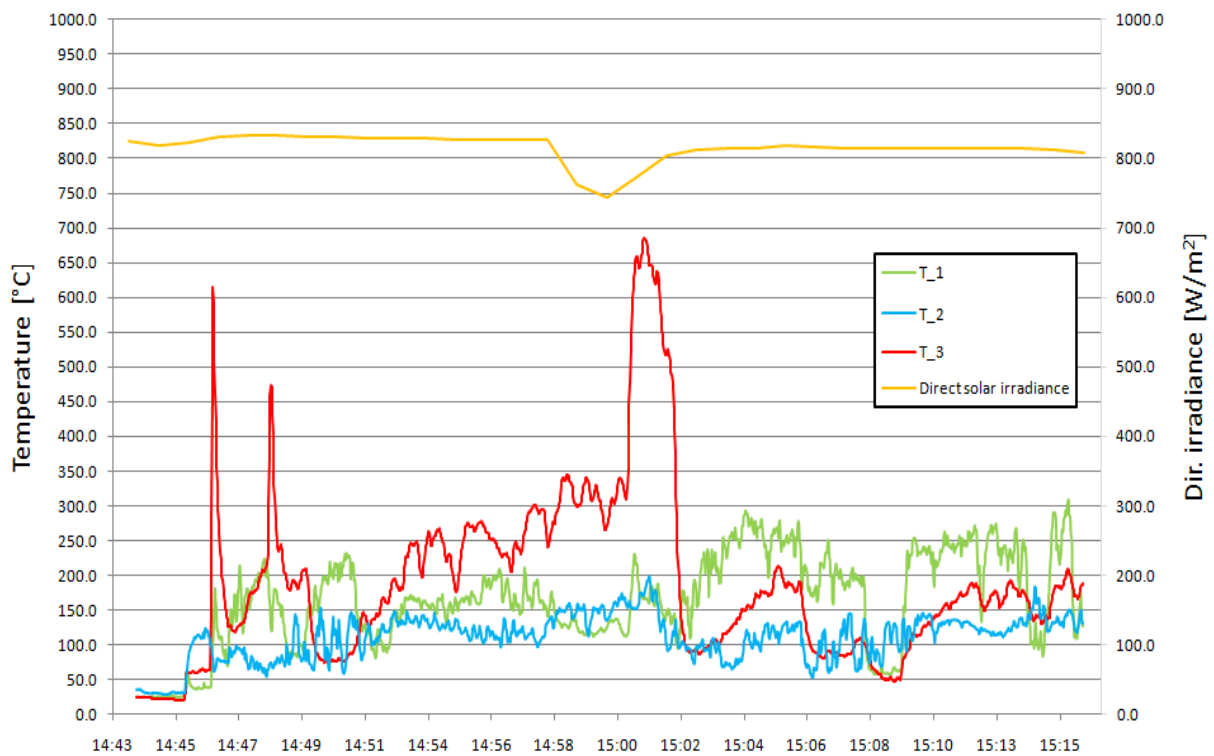


7.1.2.3 2,0 m/s

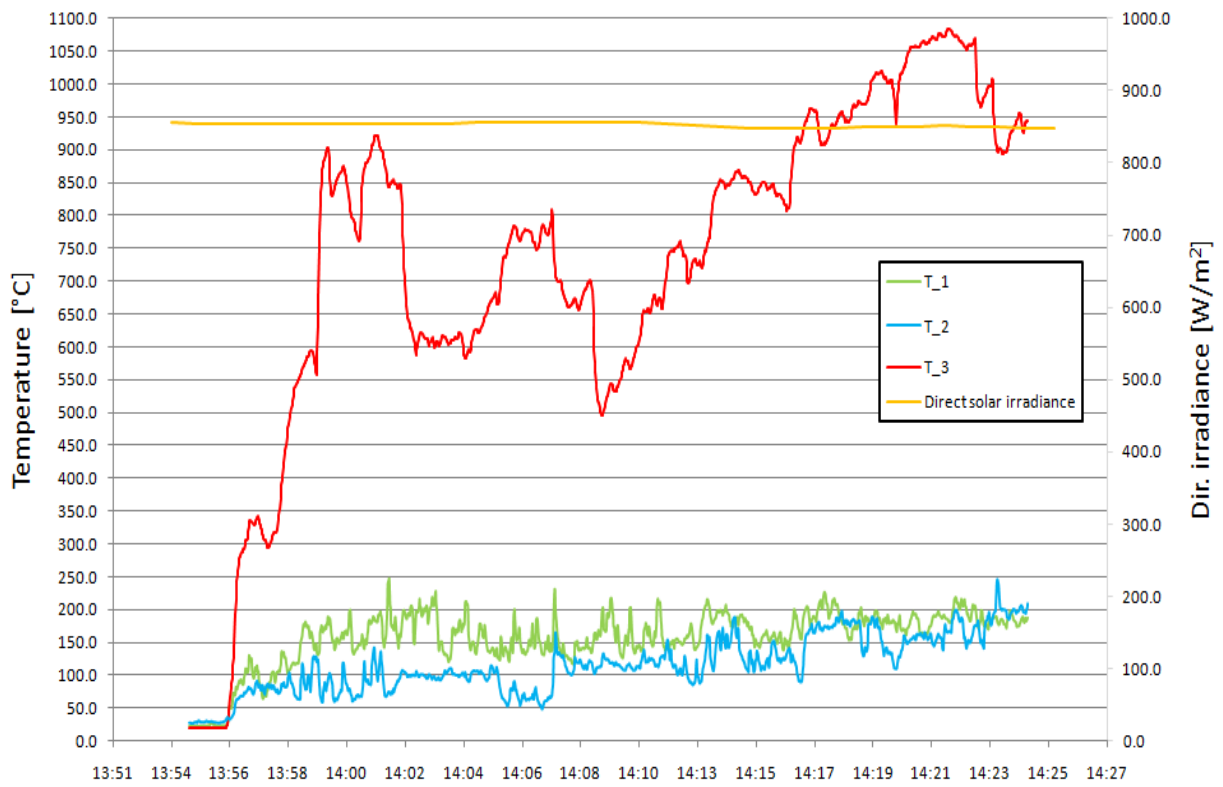


7.1.3 Concave 70 mm fiber absorber with different thickness - 1,0 m/s

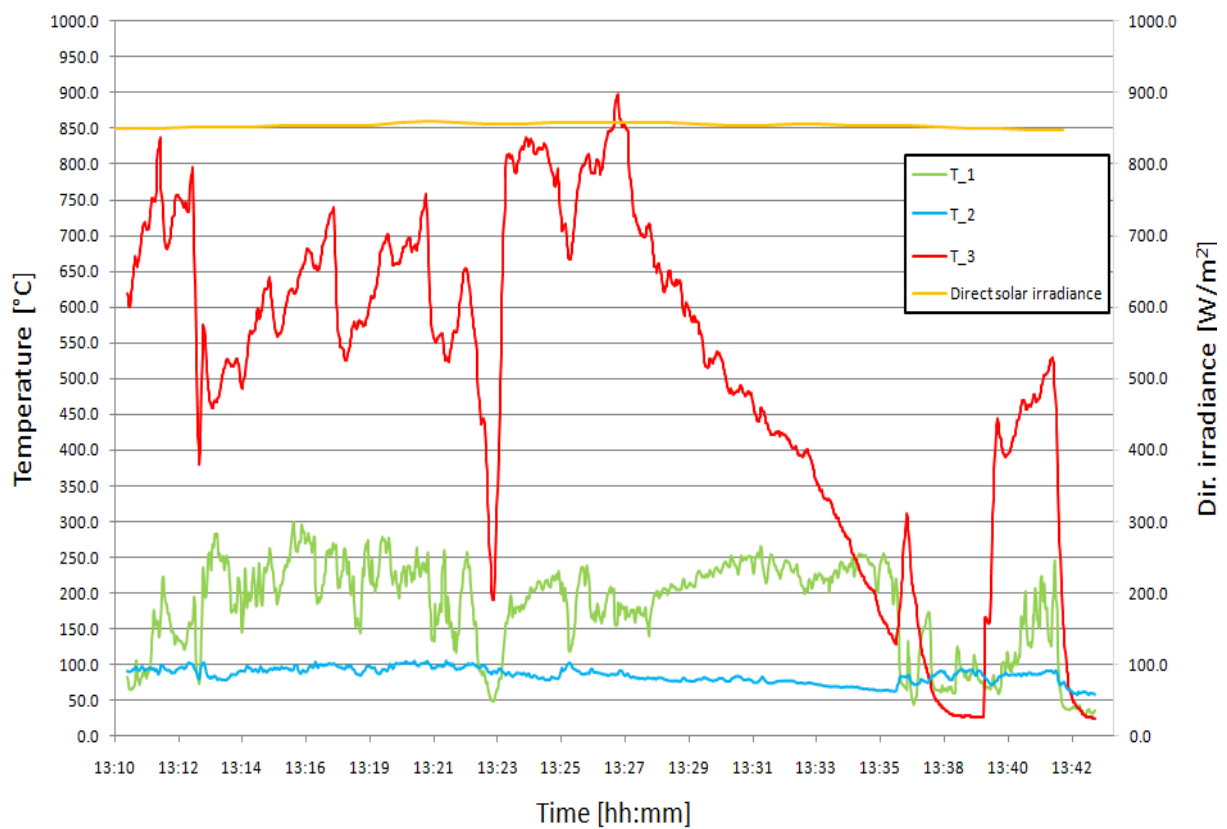
7.1.3.1 Two layers



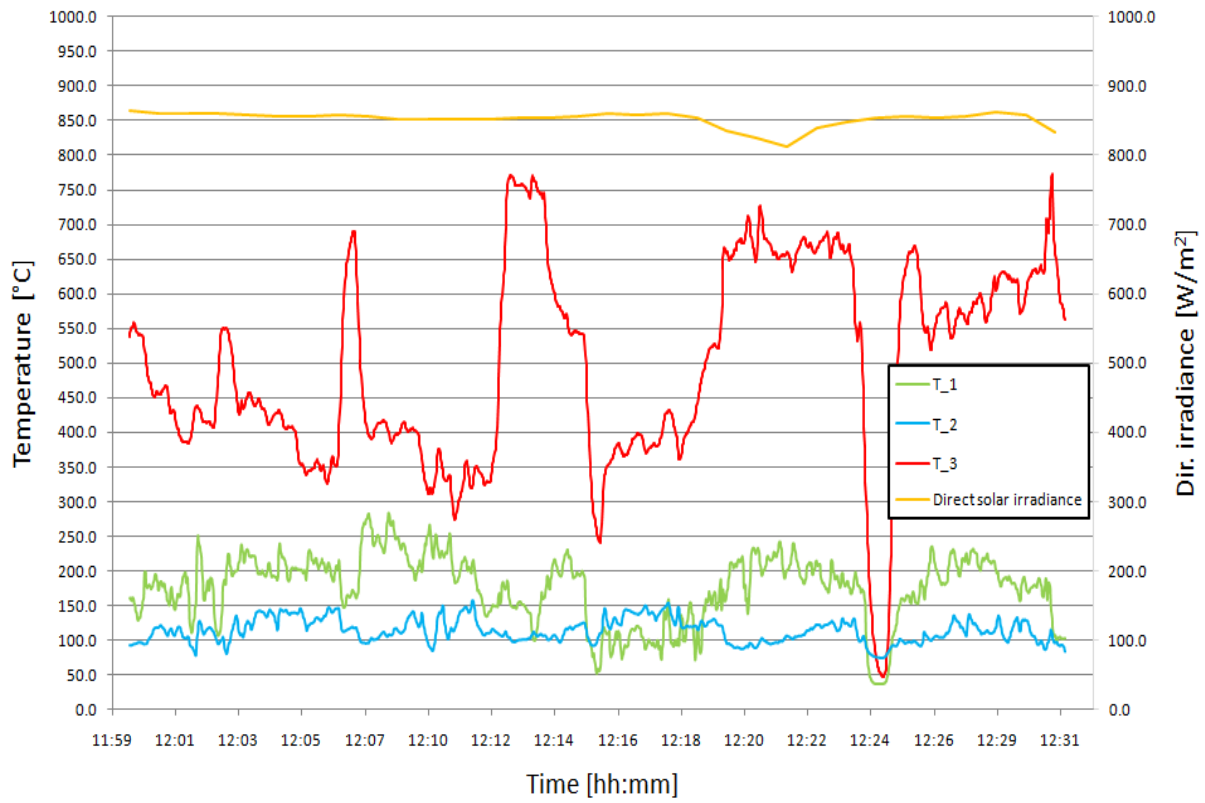
7.1.3.2 Three layers



7.1.3.3 Four layers

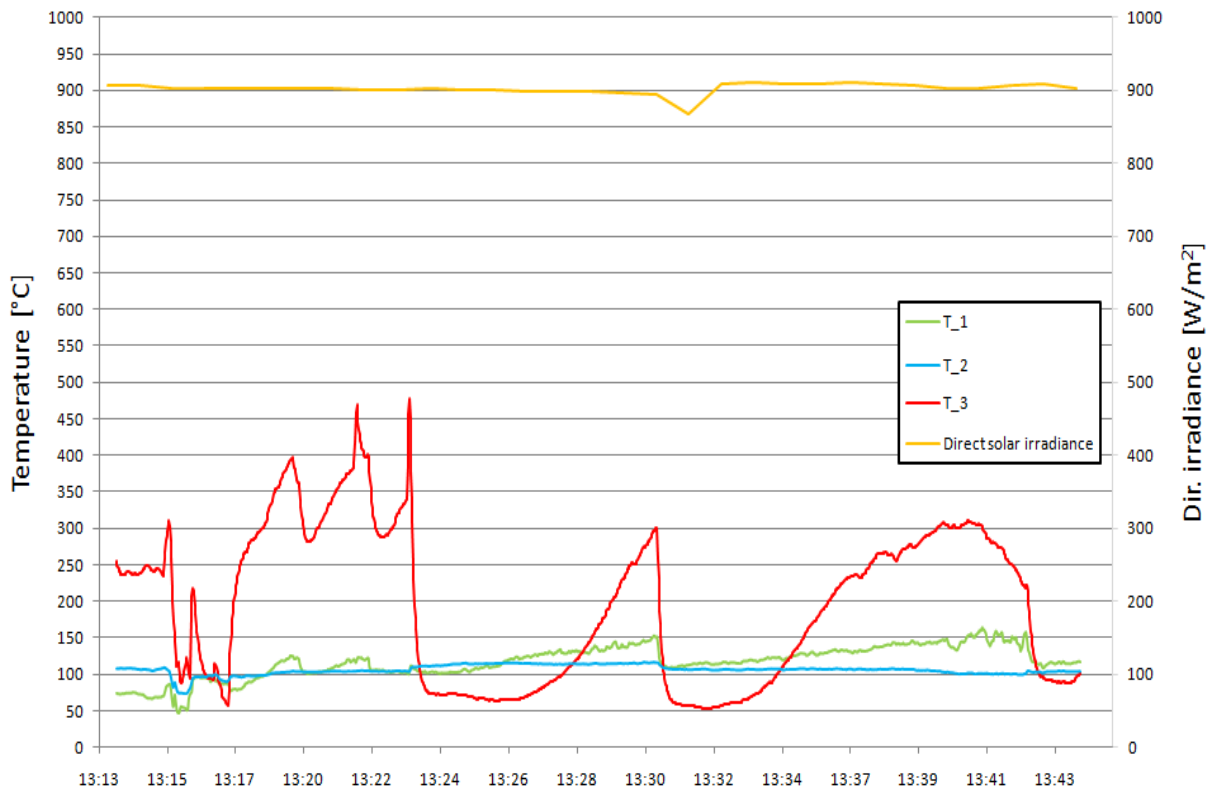


7.1.3.4 Five layers

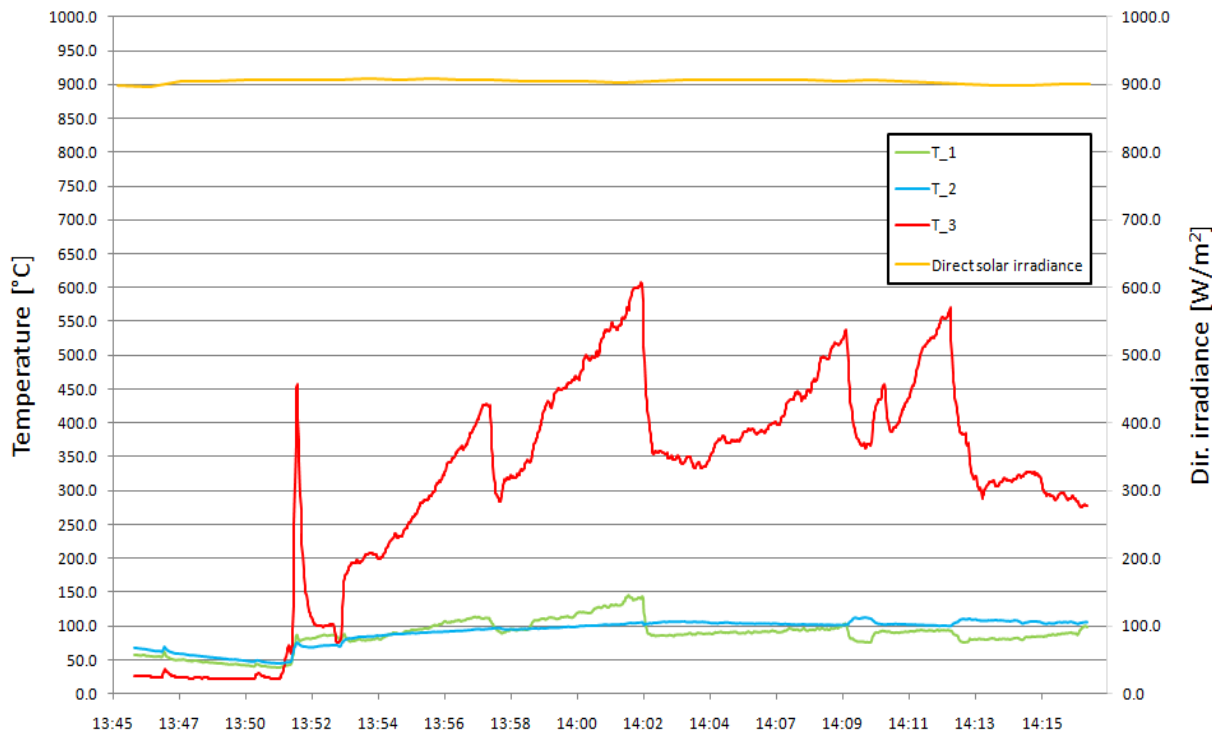


7.1.4 50 mm 3D fiber absorber

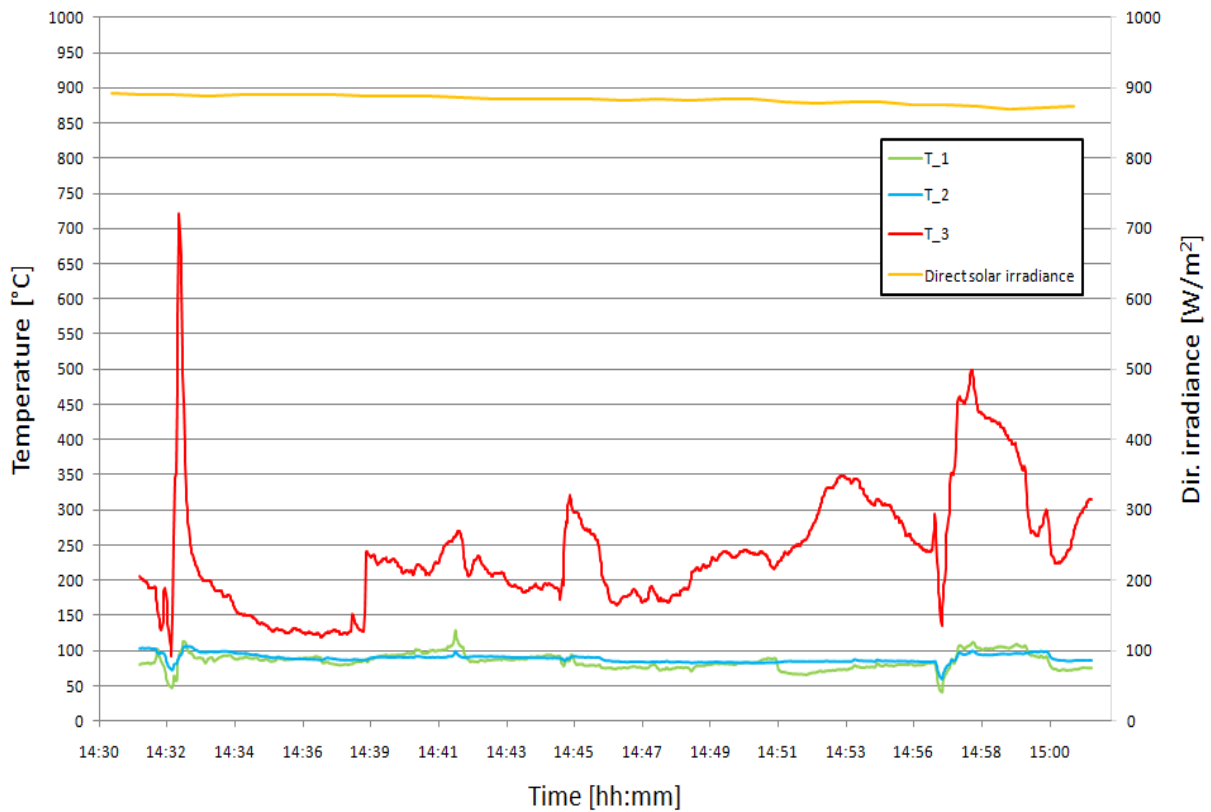
7.1.4.1 1,0 m/s



7.1.4.2 1,5 m/s

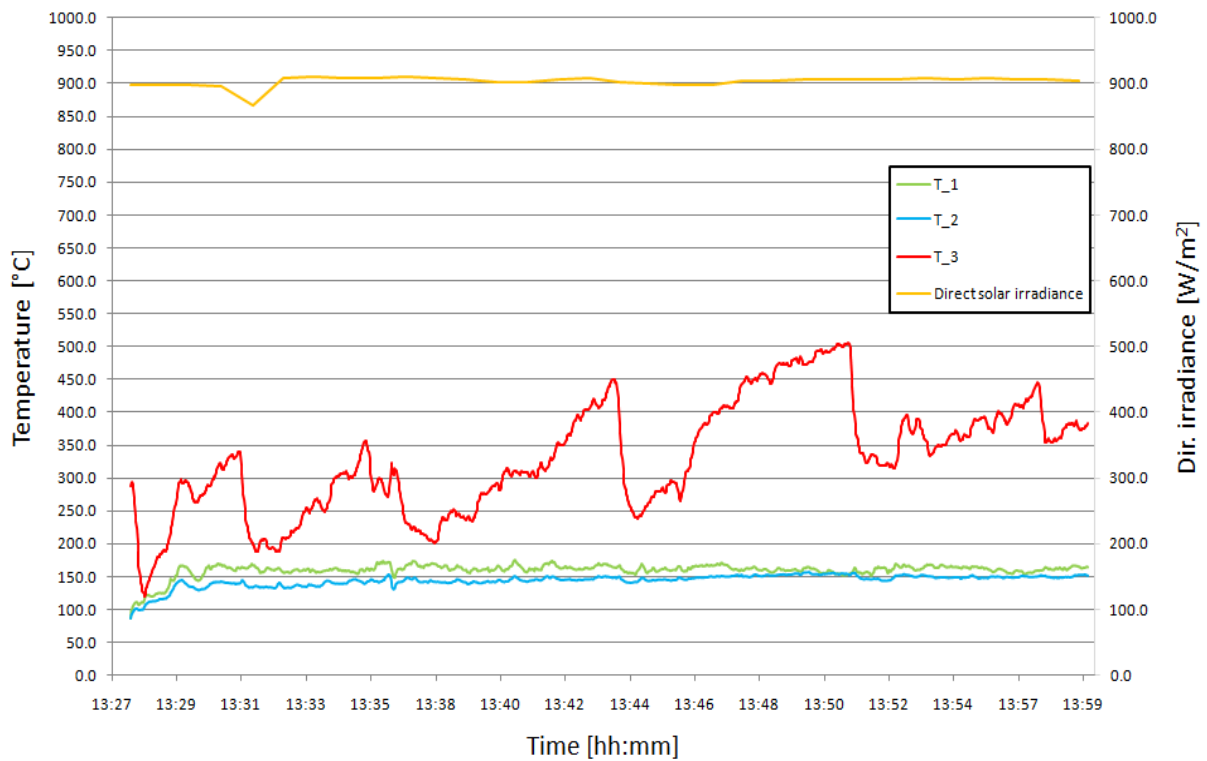


7.1.4.3 2,0 m/s

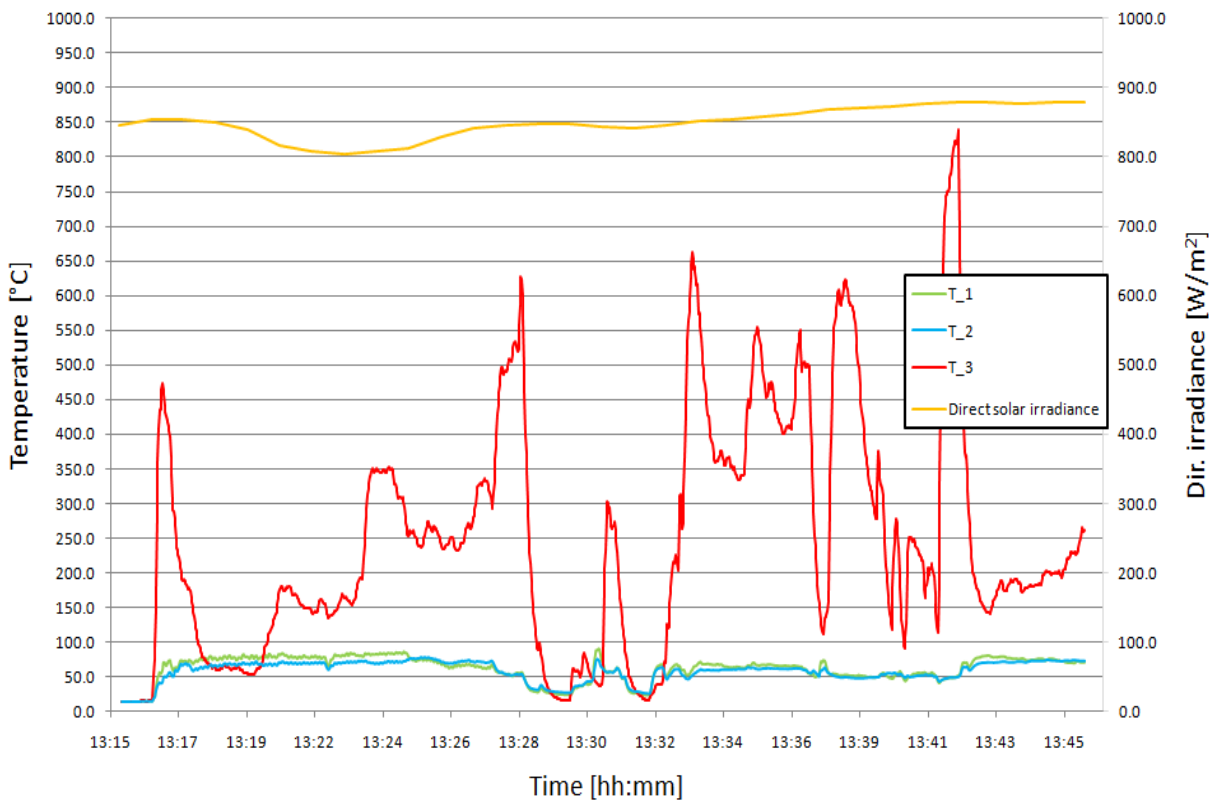


7.1.5 80 mm 3D fiber absorber

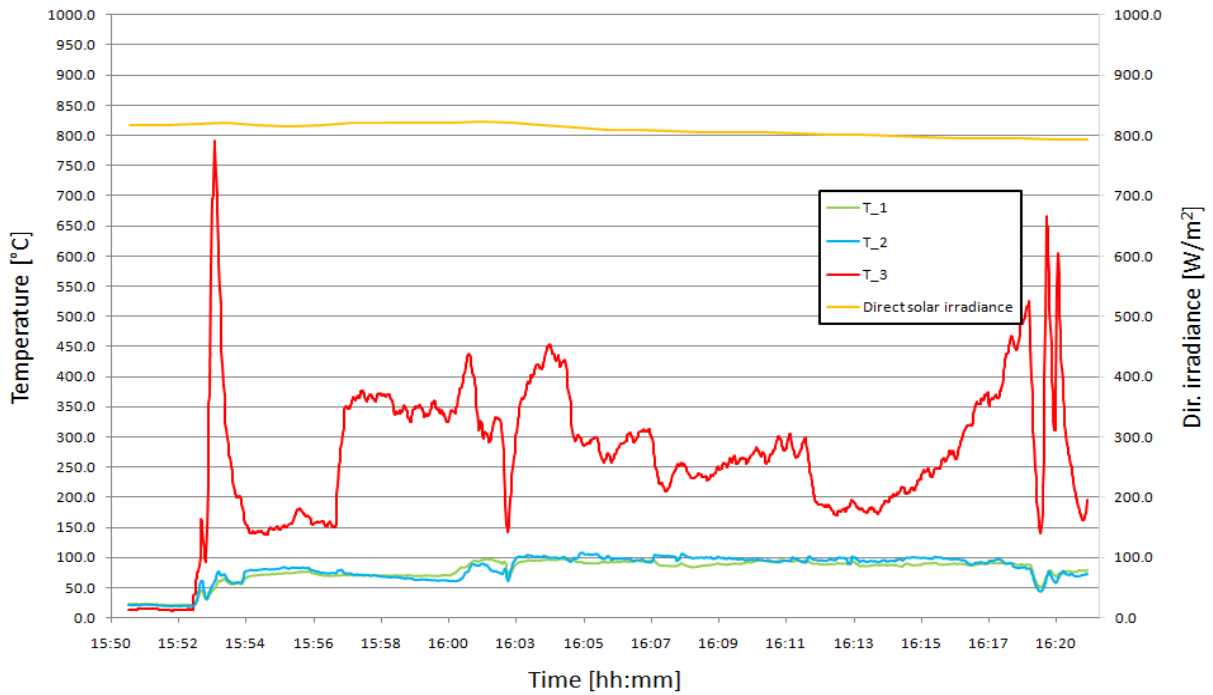
7.1.5.1 1,0 m/s



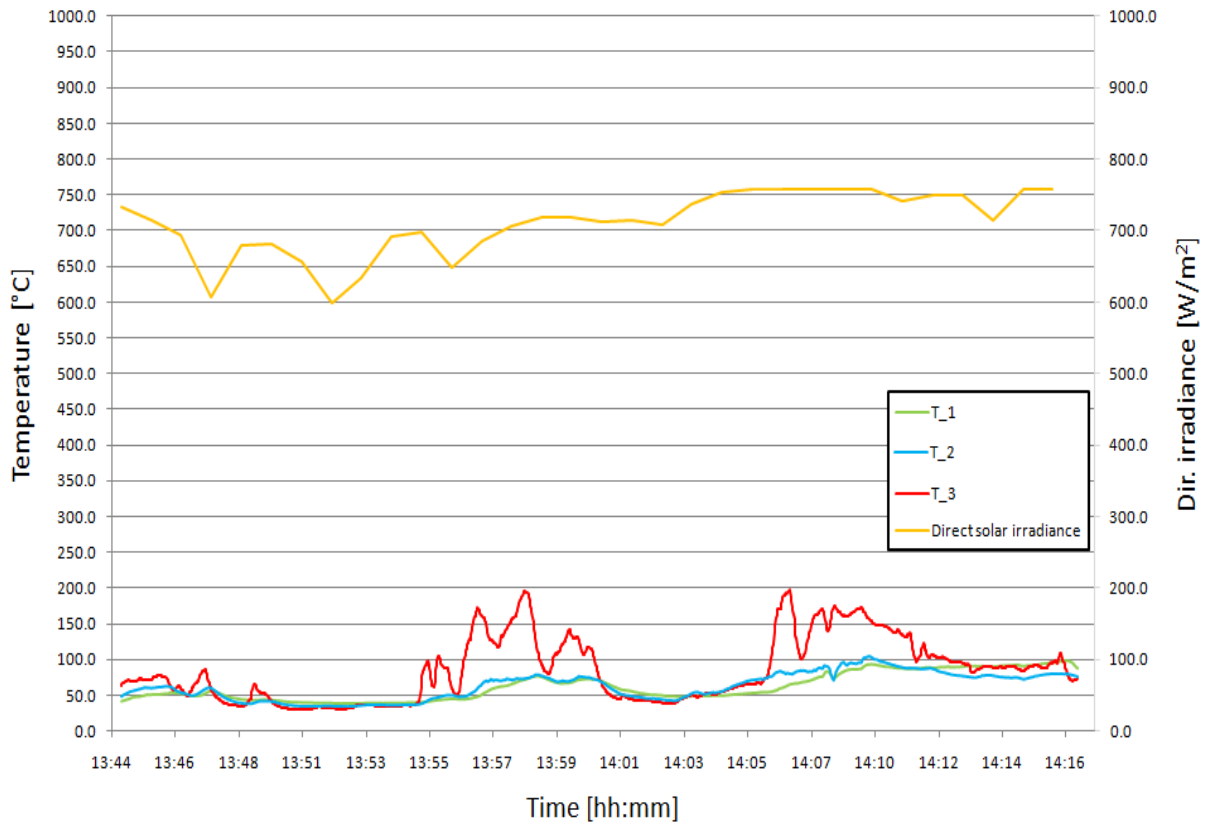
7.1.5.2 1,5 m/s



7.1.5.3 2,0 m/s

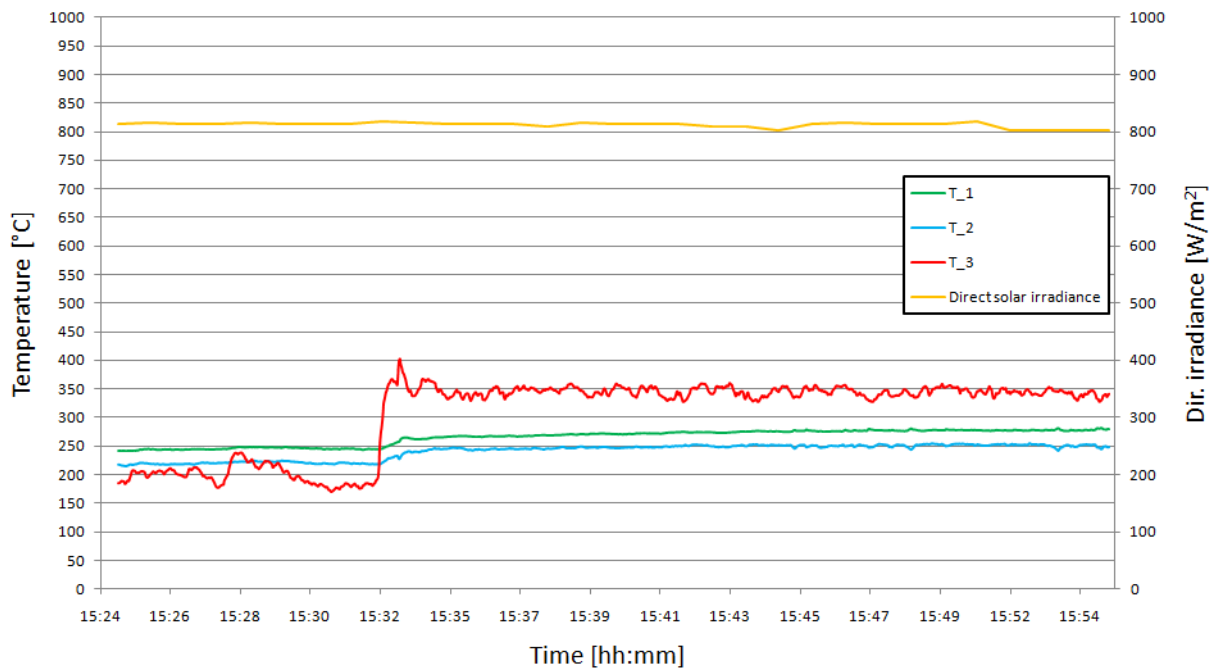


7.1.6 70 mm honeycomb absorber



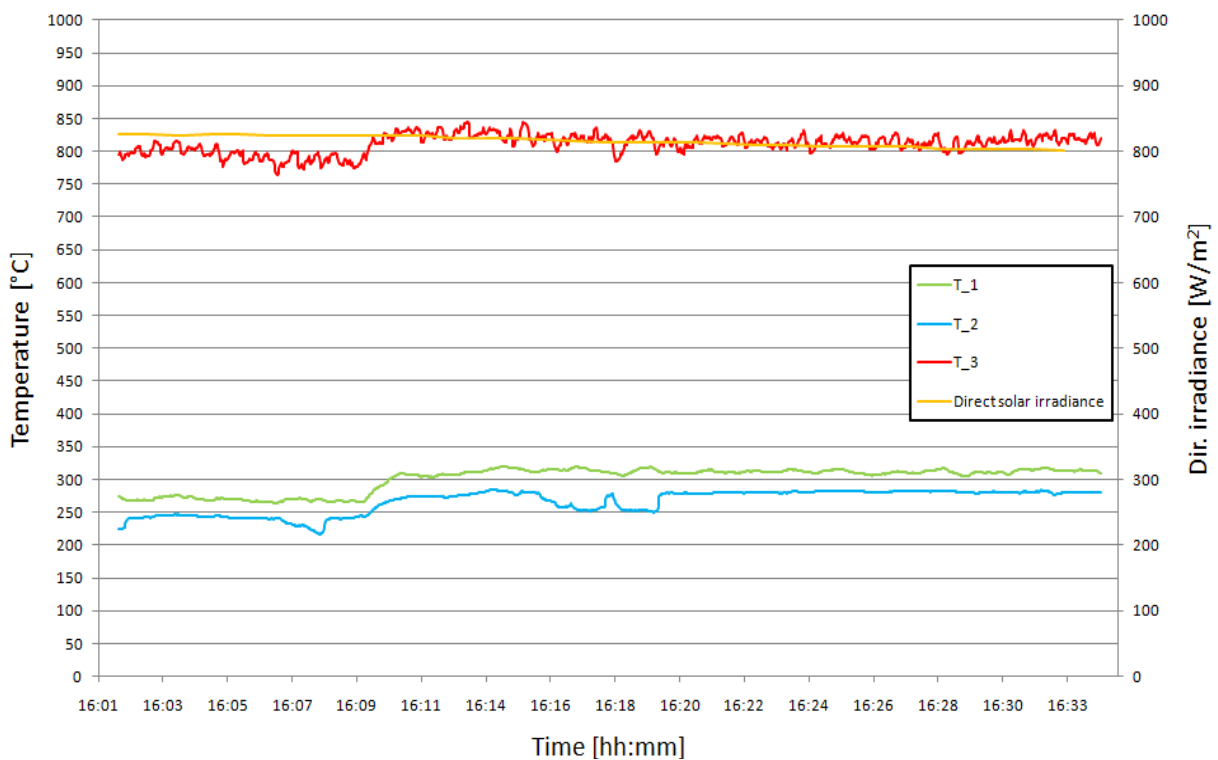
7.2 Test Setup 2

7.2.1 40 mm foam absorber

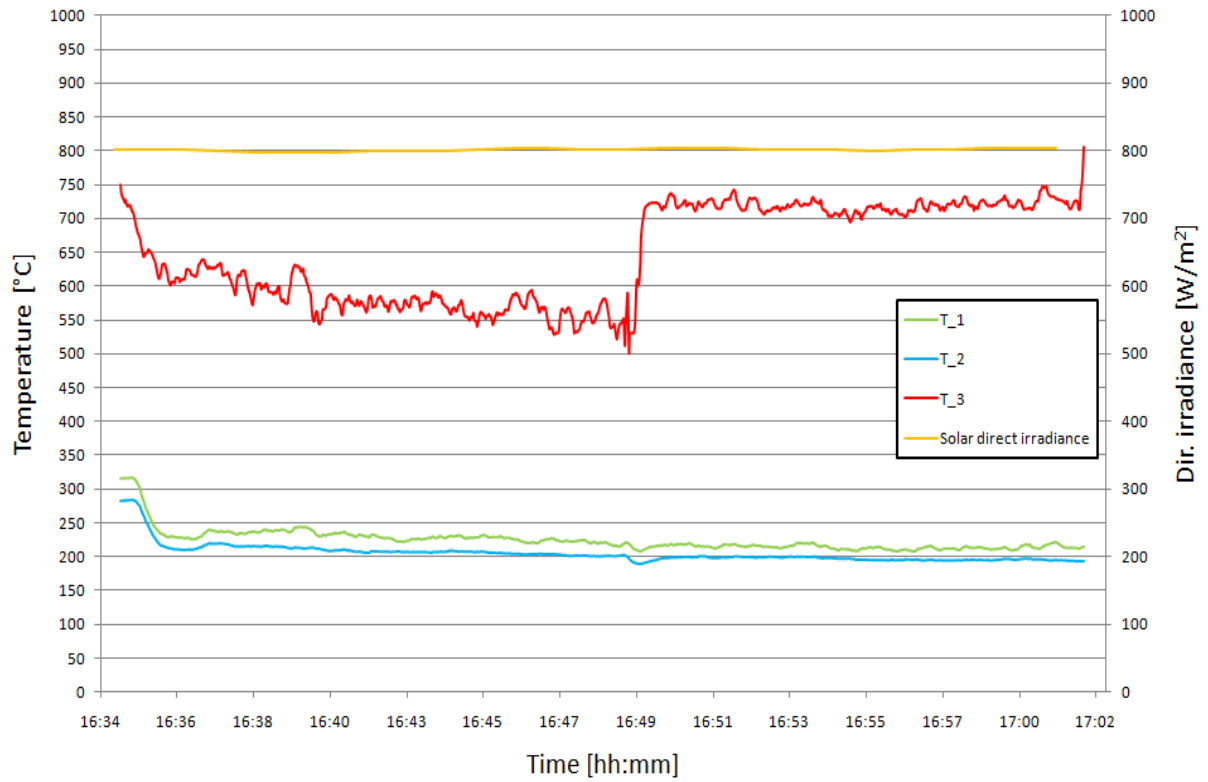


7.2.2 40 mm honeycomb absorber

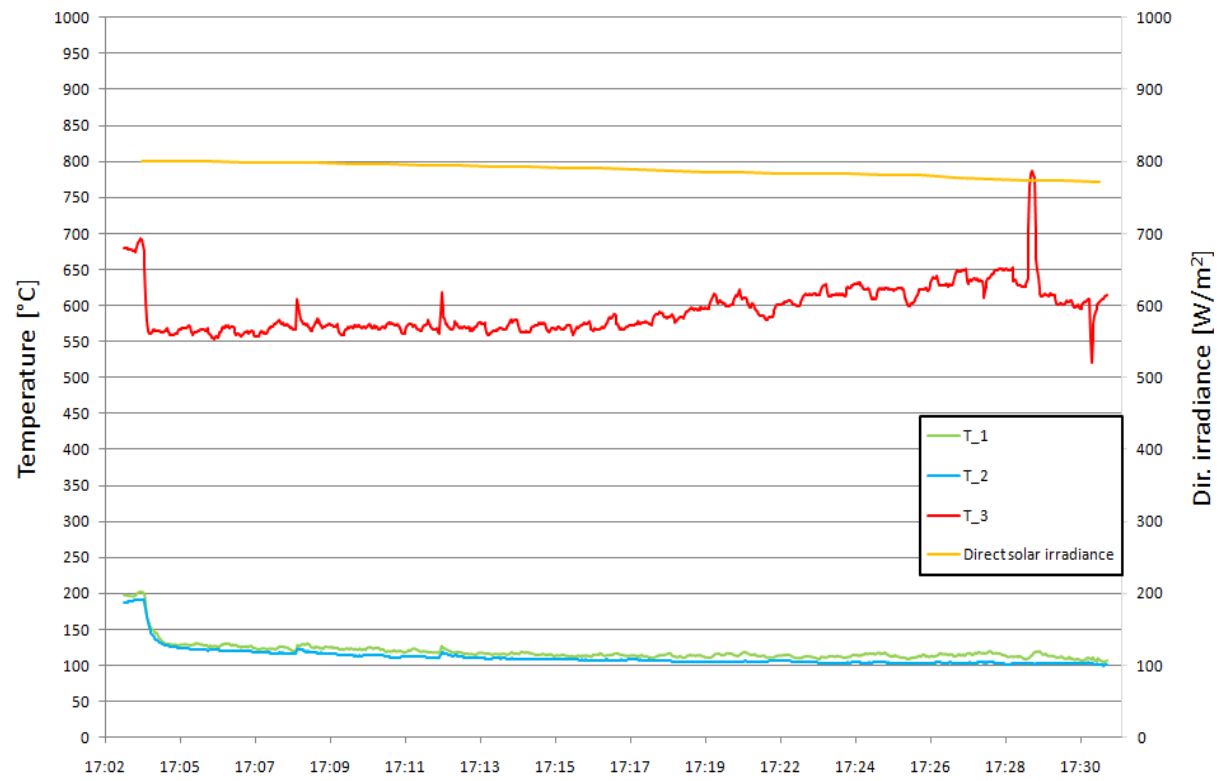
7.2.2.1 1,0 m/s



7.2.2.2 2,0 m/s

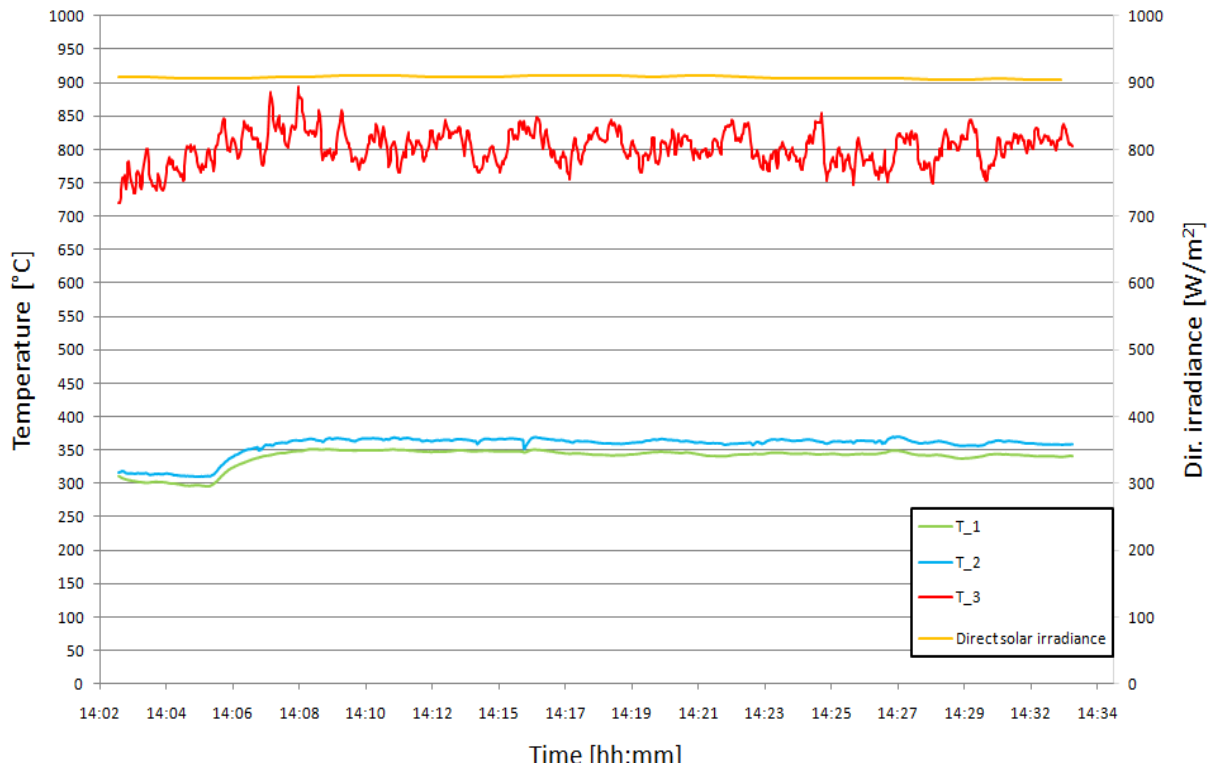


7.2.2.3 4,0 m/s

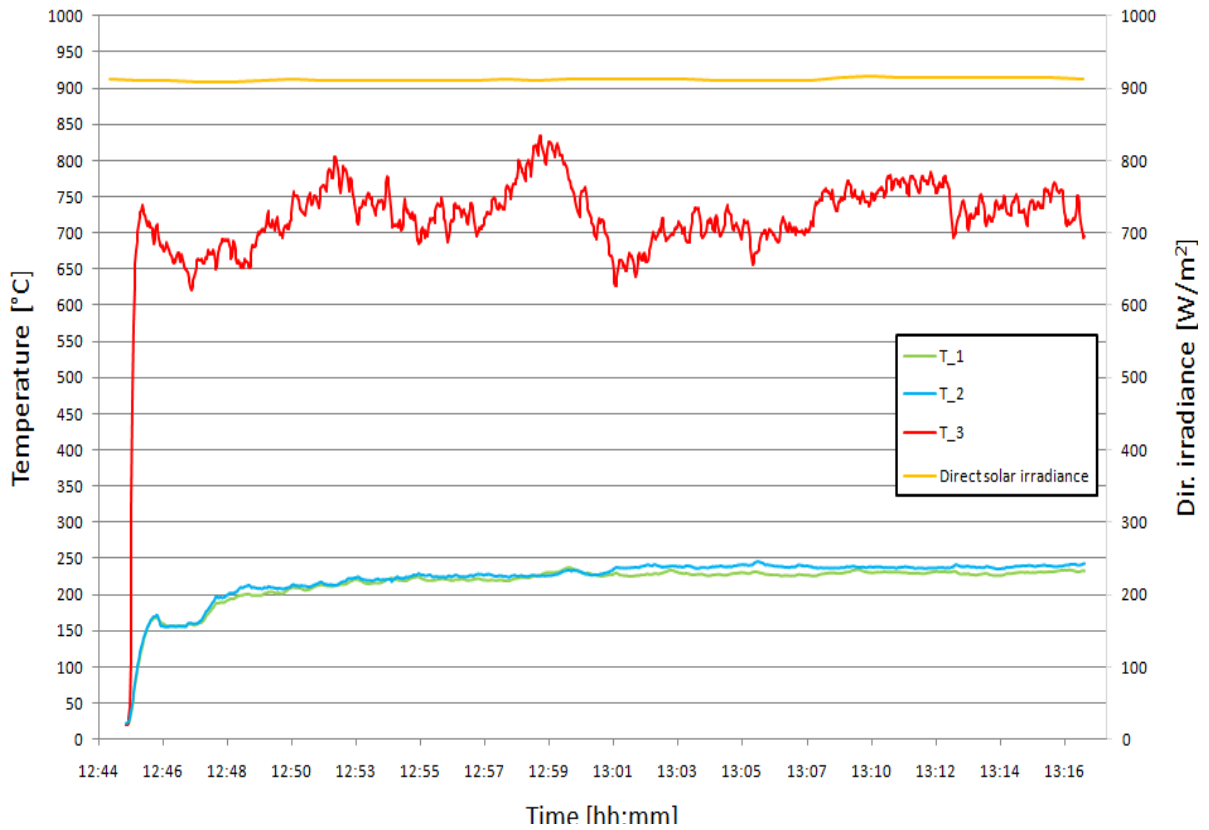


7.2.3 50 mm flat honeycomb absorber

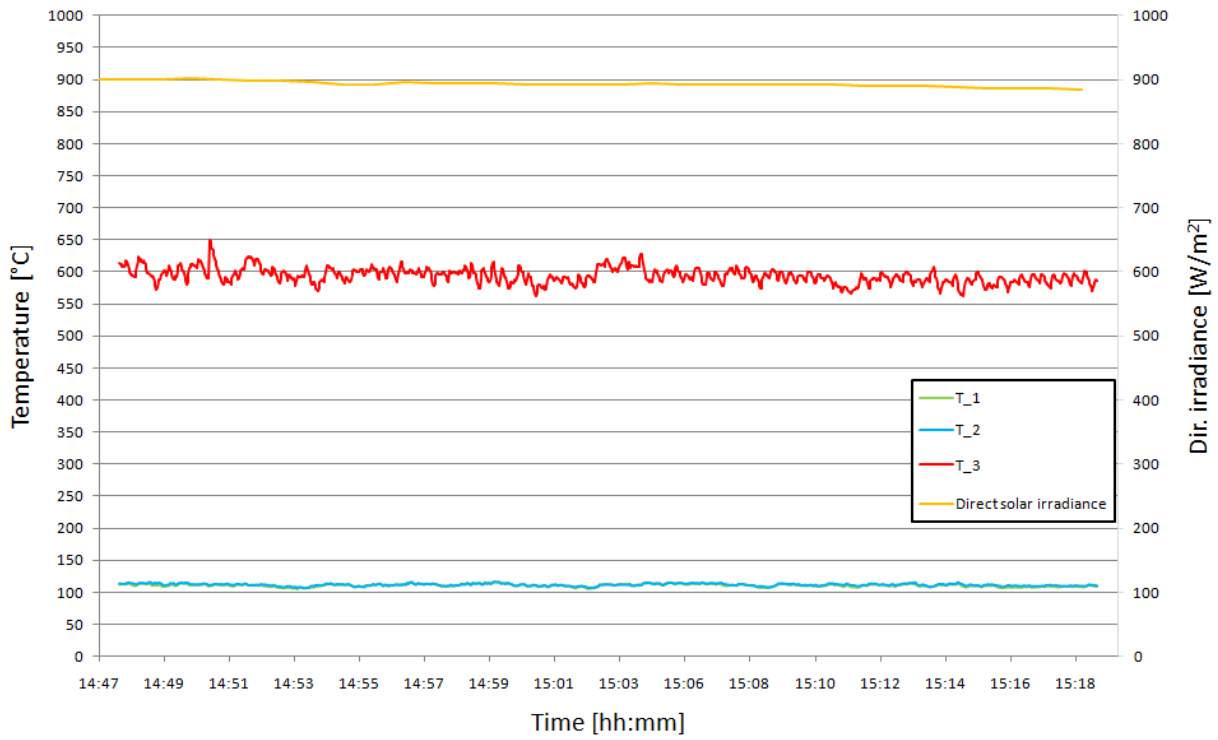
7.2.3.1 1,0 m/s



7.2.3.2 2,0 m/s

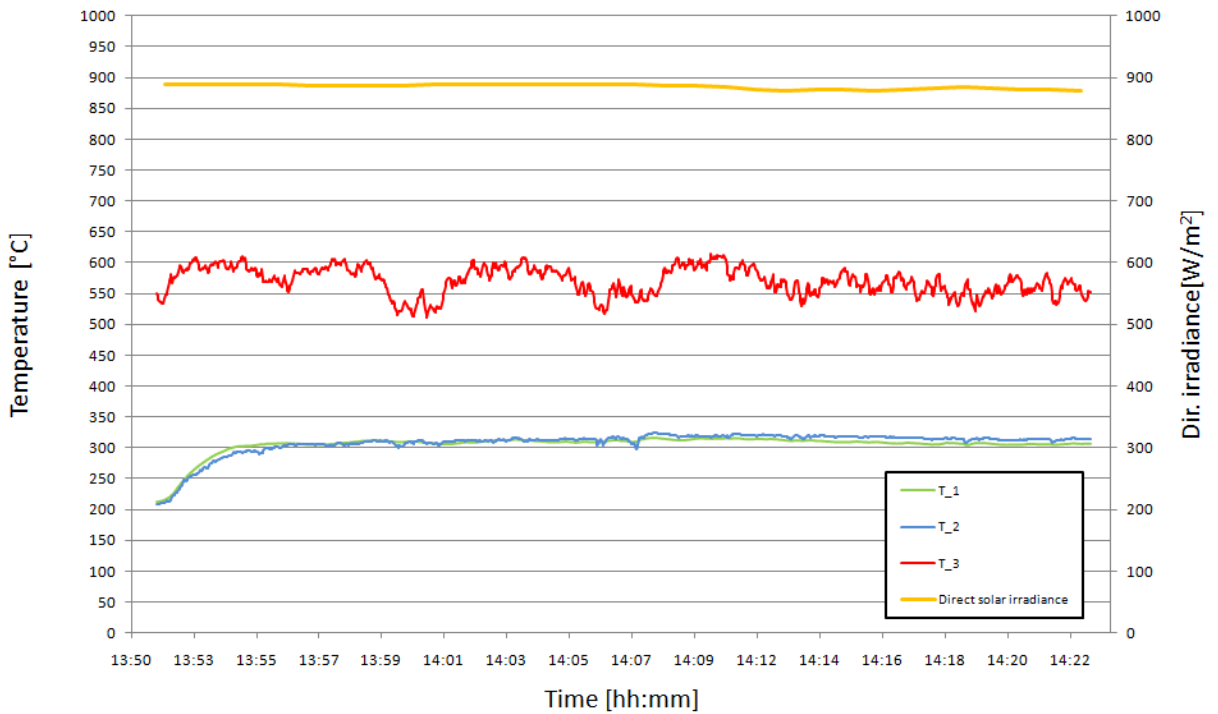


7.2.3.3 4,0 m/s

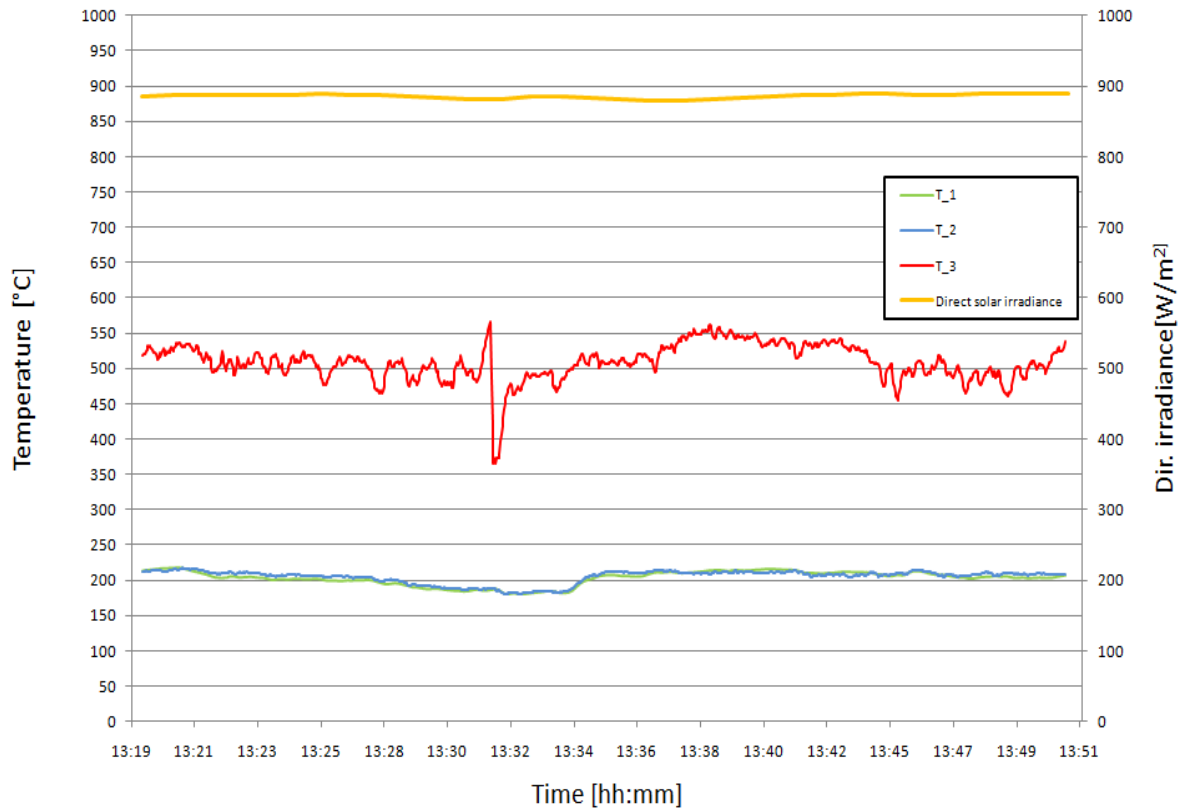


7.2.4 70 mm flat honeycomb absorber

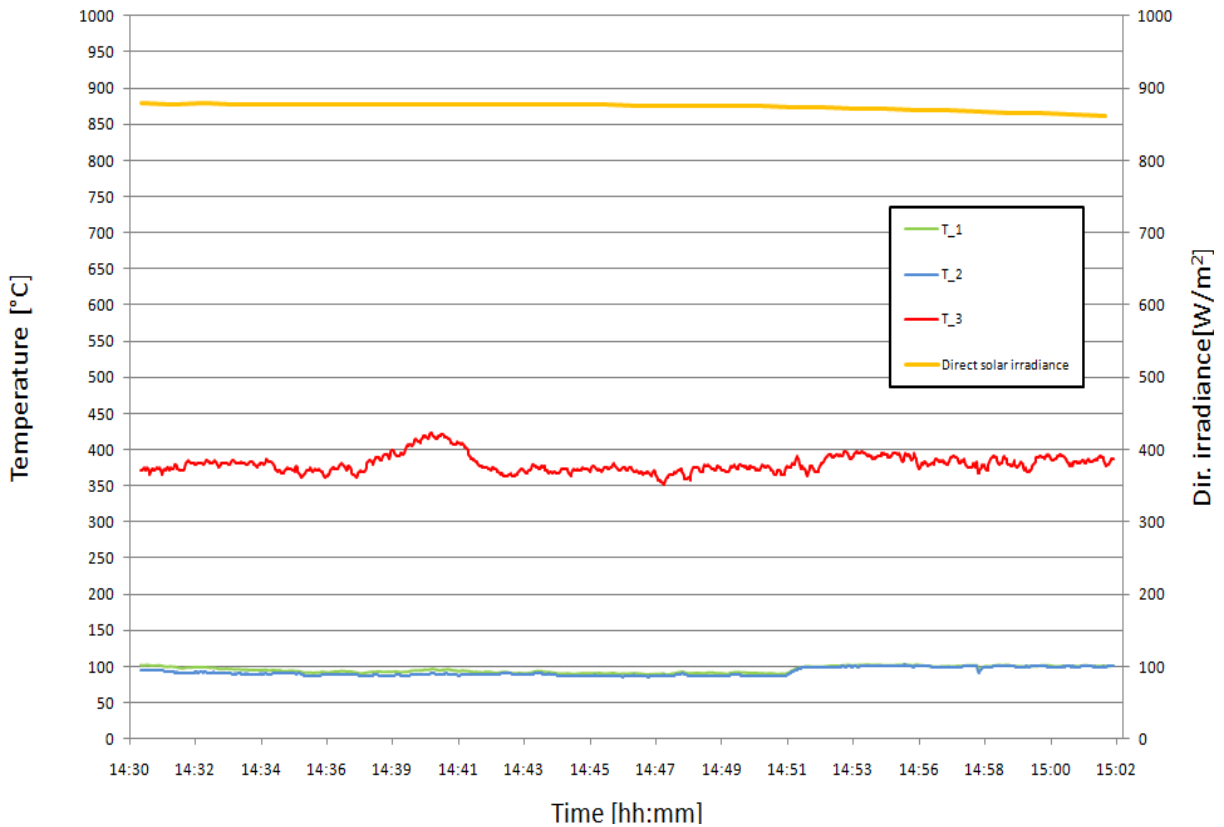
7.2.4.1 1,0 m/s



7.2.4.2 2,0 m/s

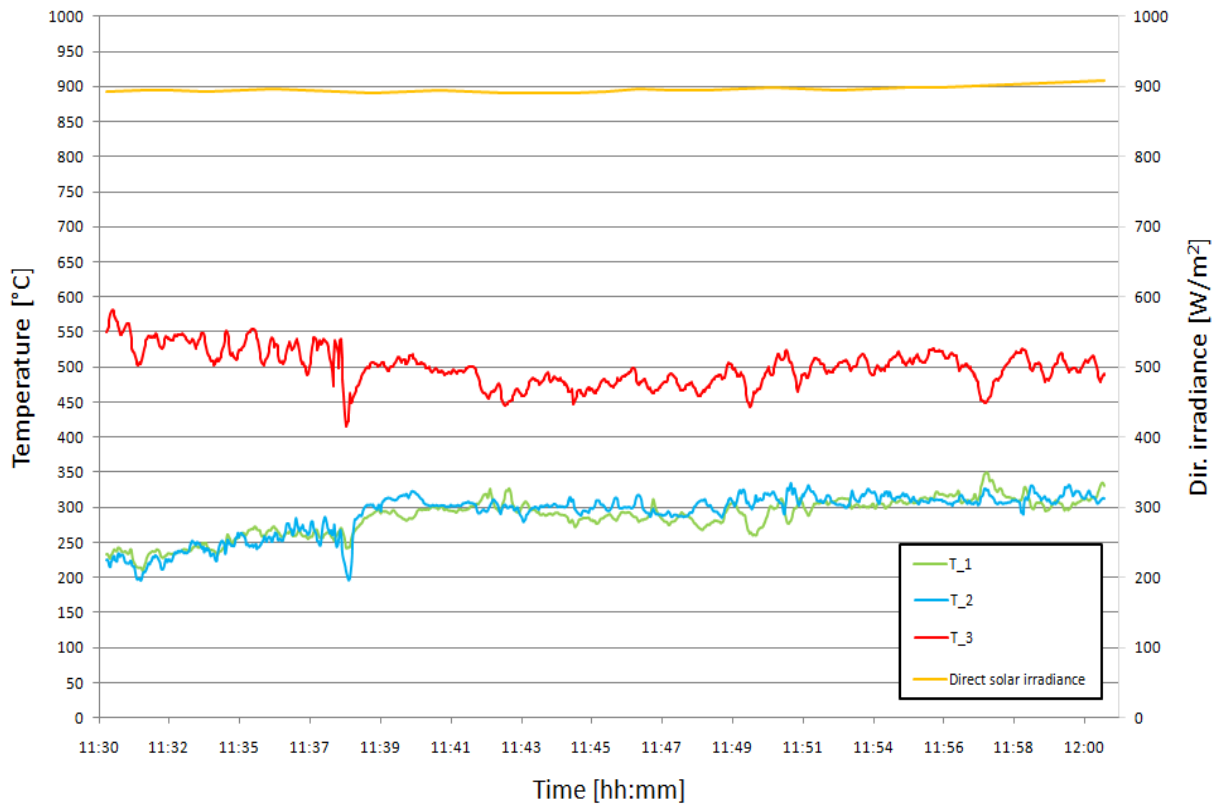


7.2.4.3 4,0 m/s

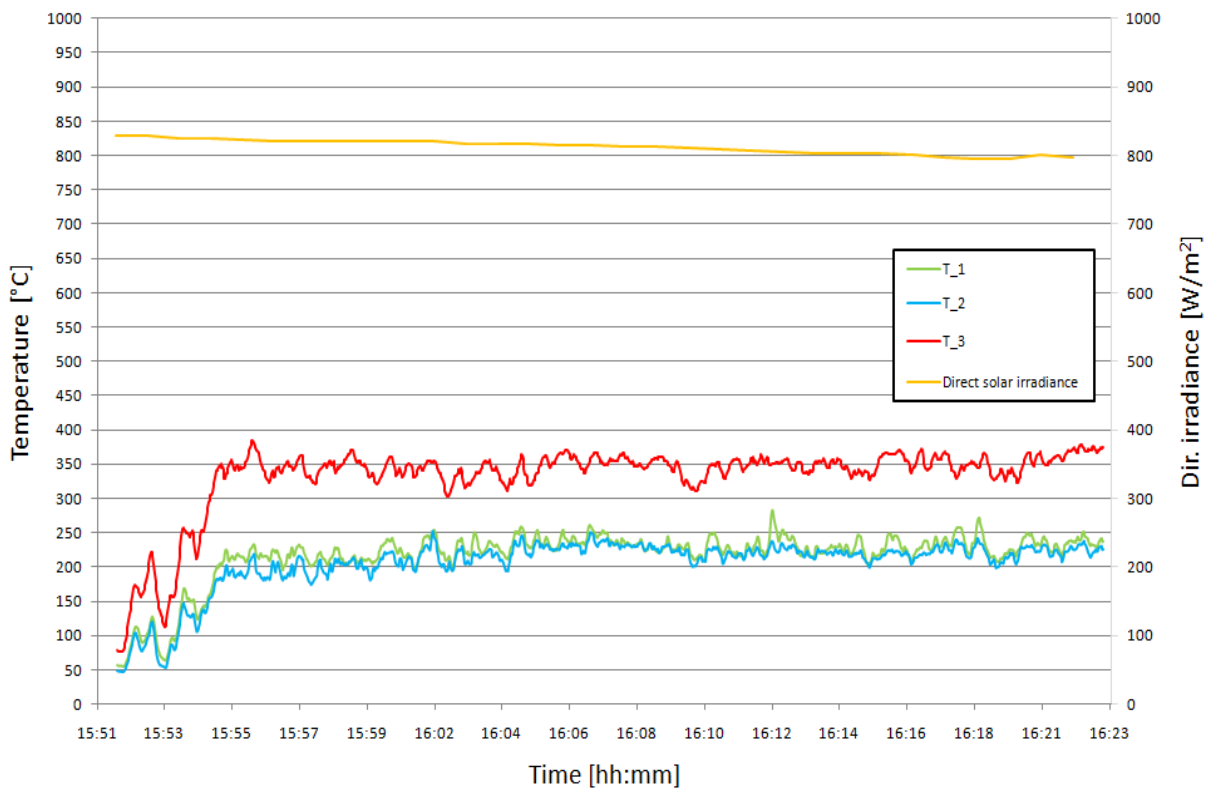


7.2.5 70 mm fiber absorber

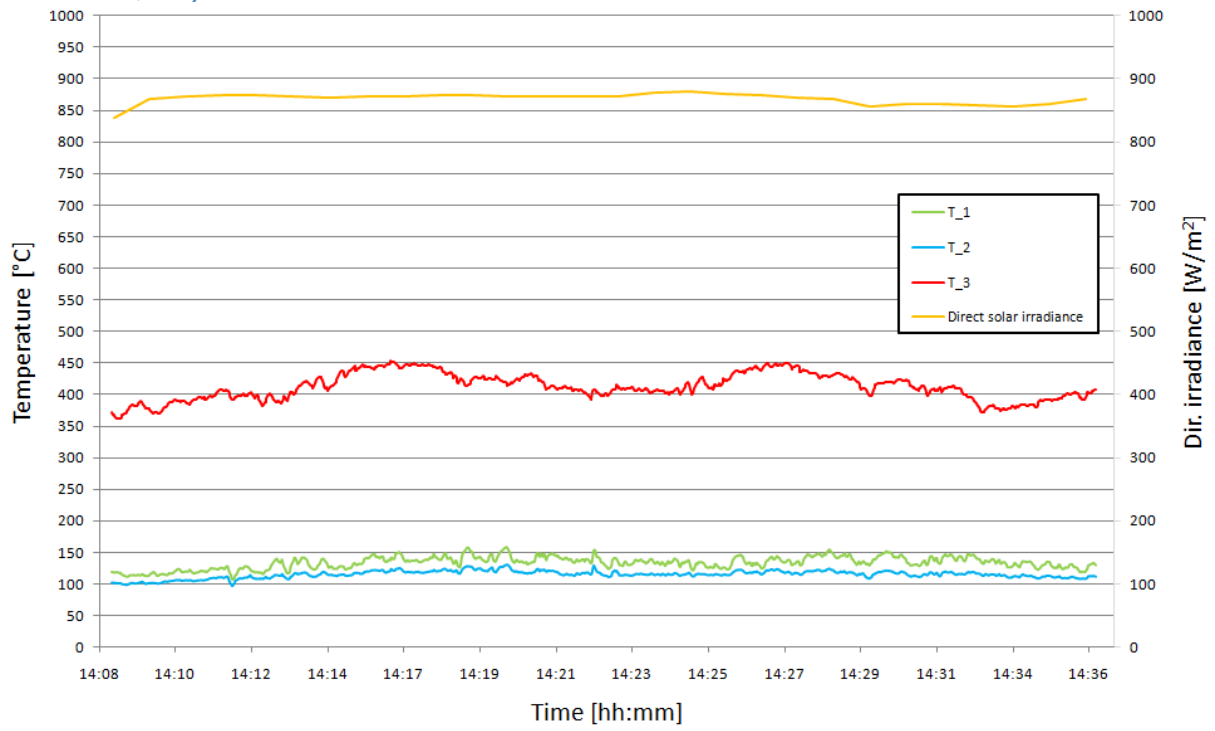
7.2.5.1 1,0 m/s



7.2.5.2 2,0 m/s



7.2.5.3 4,0 m/s



8 Appendix B

8.1.1 Calculations for Q and η

Absorber		5 cm honey	5 cm honey	5 cm honey
pipe area		$=1.96 \cdot 10^{-3}$	$=1.96 \cdot 10^{-3}$	$=1.96 \cdot 10^{-3}$
T _{air}		353	234	111
T _{surr}		20	20	20
Delta T		$=C3-C4$	$=D3-D4$	$=E3-E4$
$[\text{Avg}(t1,t2)+T_{\text{surr}}]/2$		$=((C3)+C4)/2$	$=((D3)+D4)/2$	$=((E3)+E4)/2$
cp		1056	1011	1007
rho		0.7788	0.8977	1.059
V		1	2	4
mean irradiance		908	912	893
dish area		1.07	1.07	1.07
m		$=C8 \cdot C2 \cdot C9$	$=D8 \cdot D2 \cdot D9$	$=E8 \cdot E2 \cdot E9$
Q		$=C8 \cdot C2 \cdot C9 \cdot C7 \cdot C5$	$=D8 \cdot D2 \cdot D9 \cdot D7 \cdot D5$	$=E8 \cdot E2 \cdot E9 \cdot E7 \cdot E5$
n		$=C13/(C10 \cdot C11)$	$=D13/(D10 \cdot D11)$	$=E13/(E10 \cdot E11)$

Absorber		5 cm honey	5 cm honey	5 cm honey
pipe area		0.00196	0.00196	0.00196
T _{air}		353	234	111
T _{surr}		20	20	20
Delta T		333	214	91
$[\text{Avg}(t1,t2)+T_{\text{surr}}]/2$		186.5	127	65.5
cp		1056	1011	1007
rho		0.7788	0.8977	1.059
V		1	2	4
mean irradiance		908	912	893
dish area		1.07	1.07	1.07
m		0.001526448	0.003518984	0.00830256
Q		536.7723863	761.3462643	760.8216907
n		0.552485061	0.780195795	0.796246707

Absorber	70 mmhoney	70 mm fiber
k	300	300
pipe area	0.00196	0.00196
T _{air}	312	302
T _{surr}	20	20
Delta T	=B4-B5	=C4-C5
[Avg(t1,t2)+T _{surr}]/2	=(B4+B5)/2	=(C4+C5)/2
cp	1016	1016
rho	0.815	0.815
V	1	1
mean irradiance	885	896
dish area	1.07	1.07
AV	=B10*B3*1000	=C10*C3*1000
m	=B9*B3*B10	=C9*C3*C10
Q=	=B9*B3*B10*B8*B6	=C9*C3*C10*C8*C6
n	=B15/(B12*B11)	=C15/(C12*C11)

Absorber	70 mmhoney	70 mm fiber
k	300	300
pipe area	0.00196	0.00196
T _{air}	312	302
T _{surr}	20	20
Delta T	292	282
[Avg(t1,t2)+T _{surr}]/2	166	161
cp	1016	1016
rho	0.815	0.815
V	1	1
mean irradiance	885	896
dish area	1.07	1.07
Q=	473.90	457.67
n	0.50	0.48

